RICE UNIVERSITY

**Finite Element Nonlocal Technique Based on
Superconvergent Patch Second Derivative Recovery**

by

Xiaoge Gan

A THESIS SUBMITTED
IN PARTIAL FULFILLMENT OF THE
REQUIREMENTS FOR THE DEGREE
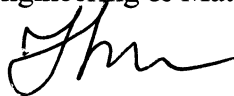
Doctor of Philosophy

APPROVED, THESIS COMMITTEE

Dr. John E. Akin, Chair
Professor of Mechanical Engineering &
Materials Science

Dr. Pol D. Spanos
Lewis B. Ryon Professor in Engineering

Dr. Jun Lou
Assistant Professor of Mechanical
Engineering & Materials Science

Dr. Ilinca Stanciulescu
Assistant Professor of Civil Engineering

HOUSTON, TEXAS
August 2011

Abstract

Finite Element Nonlocal Technique Based on Superconvergent Patch Second Derivative Recovery

by

Xiaoge Gan

This dissertation proposes a finite element procedure for evaluating the high order strain derivatives in nonlocal computational mechanics. The superconvergent second derivative recovery methods used are proven to be effective in evaluating the Laplacian of the equivalent strain based on low order (linear) elements. Current nonlocal finite element techniques with linear elements are limited to structured meshes, while the new technique can deal with unstructured meshes with various element types. Other superconvergent patch recovery (SCP) based nonlocal approaches, such as the patch projection techniques only utilize nodal based patches to evaluate the first derivatives of the strain. The SCP technique has not yet been used for recovery of higher order strain derivatives. The proposed technique is capable of evaluating the Laplacian of the equivalent strain and has the potential for even higher order derivative recovery. The same patches can be easily utilized for error estimation and adaptive meshing for nonlocal problems.

We employ two super-convergent patch options: the element based patch with all neighbors or only facing neighbors. The nonlocal strain derivatives can be recovered through either a mesh nodal averaging process or directly at the patch element quadrature points after the patch least square fitting problems are solved. Numerical examples for both strain gradient damage mechanics and strain gradient plasticity problems are given. In summary, the new finite element nonlocal computational technique based on the superconvergent second derivative recovery methods is proven to be robust in evaluating the high order strain derivatives with low order element unstructured meshes.

Acknowledgments

At this moment, I feel both blessed and grateful. Four year's PhD life might not be a long time in a human's whole life, but to me, it would be an invaluable experience that benefits my every step afterwards. Words are not enough to express my gratitude to those, without whom I would not have made a tiny little accomplishment.

First of all, I would like to sincerely thank my advisor Dr. Akin for his guidance, patience and understanding. This work will not be accomplished without his brilliant mentorship. I would also like to thank my committee member Dr. P.D. Spanos, for his timely encouragement and friendliness; thank Dr. Ilinca Stanciulescu for her fruitful discussion and help on learning FEAP; thank Dr. Jun Lou for his helpful advices and kindness. And I also want to extend my gratefulness to all the other excellent professors at Rice University who educated or helped me during my study here.

I would like to thank my lovely fellow students at Rice University: Cheng Peng, Jianxin Lu, Yue Huang, Jiangnan Zhang, Zhenjia Gao, Zhengzong Sun, Joseph Li, Philip Loya, Kenneth Davis and all those who studied by my side. Thank you all for being a memorable part of my PhD life. I would also like to thank my Air Force friends Matthew Guertin, Matt Wichmann and Brad Ward, life would be too boring without you guys around. My gratitude also goes to the Rice University alumni: Dr. Hao Lu, Dr. Tianmin Jian, Dr. Jianxin Wang, Lt. Joel S. Martin, Dr. Jonny Lee, Jianshun Shen, Dr. Kun Jiao, Dr. Milton Esteva, Dr. Yi Yang, Dr. Yu Lin, Dr. Yang Lu, Dr. Yogee Genason and Dr. Yanpeng Wu. Special thanks go to Dr. Yao Zhao, who came to Rice University MEMS department the same day as I did and also defended his PhD the same day as I did. I really appreciate the friendship between us and wish him a successful career. I also want to take this opportunity to thank my friends outside Rice University: Dr. Zhen Li, Zhao Ge and Qun Huang, Yichun Chen and Mo Fu, Tianhong Fang and Yamin Qiu. Thanks for their kindness and all the help they have given me.

For my undergraduate mentors back in Fudan University, professor Guoan Tang and professor Hanwen Song, I also want to say thank you for the education and advices they have given me.

This is also the opportunity for me thank my future supervisor Dr. Jiaqing Yu . I won't successfully finish my PhD degree at Rice University without his understanding and patience.

My family is always the source of my strength that put me through this program, I would like to thank my parents. I especially want to dedicate this dissertation to my beloved father Luping Gan. How I wished he could be here with me. The last but not the least, I want to thank my lovely wife Jiajie Dai from the bottom of my heart for her understanding and insistent supports.

Contents

List of Figures

List of Tables

Chapter 1

Introduction

The past several years may probably have witnessed some of the most devastating disasters in human's history: 2008 Sichuan earthquake (8.0 Magnitude) in China; 2011 Tohoku earthquake (9.0 Magnitude) and tsunami in Japan; 2011 Tuscaloosa tornado in U.S.A., etc.. Facing nature's rampage, our infrastructure has become unprecedentedly vulnerable. Structure safety is now a prior concern. To prevent failure and improve structure integrity, the very first step is to use effective failure analysis approaches to identify the root cause of likely failures. It has been discovered that the failure of the structures usually initiates from highly strain localized zones. The strain localization usually accompanies a softening material behavior and is studied with nonlocal continuum mechanics. Nonlocal continuum mechanics prevents the numerical difficulties caused by the loss of ellipticity and also incorporates the material length scales to bridge the material micro and macro scales. A one-dimensional benchmark problem is first given to illustrate the idea of the loss of the ellipticity.

1.1. One-dimensional benchmark problem

The simulation of materials with softening behavior, including damage mechanics, softening plasticity, etc., is generally a challenging topic. Classical continuum mechanics fails in this regard when the ellipticity of the governing equations is lost. This loss of the ellipticity of the equations results in a physically meaningless post peak unloading behavior, i.e., mesh dependent finite element results.

The loss of ellipticity is best illustrated by a one-dimensional bar tension example as in de Borst (2001). As shown in Figure 1.1, a one-dimensional bar is fixed at the left end and is pulled horizontally at the right end. The bar is divided into m elements. The stress-strain relationship is assumed to be elastic at first. When the tensile strength f_t is reached, any further loading will cause a linear decrease in the tensile strength of the material until it reaches zero.
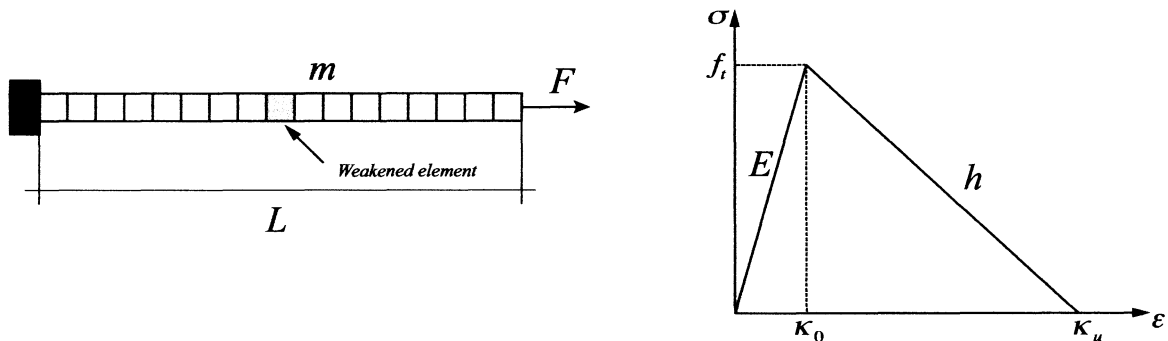
Figure 1.1 One-dimensional bar tension problem

Since it is one-dimensional, the stress-strain relationship is defined by the axial stress and strain of the bar as,

$$\sigma = \begin{cases} E\varepsilon & \varepsilon \leq \kappa_0 \\ f_t + h(\varepsilon - \kappa_0) & \kappa_0 \leq \varepsilon \leq \kappa_u \\ 0 & \kappa_u \leq \varepsilon \end{cases} \qquad (1.1)$$

where E is the Young's modulus, κ_0 is the strain corresponding to the tensile strength f_t, and κ_t is the strain when stress reaches zero. The linear hardening/softening modulus h is then expressed as,

$$h = -\frac{f_t}{\kappa_u - \kappa_0} \qquad (1.2)$$

The center element, shown in grey in Figure 1.1, is weakened by assuming a *10%* reduced tensile strength as compared to that of the other elements. The axial force along the bar needs to be balanced, which means the stress is equal among all the elements. Therefore, upon loading, the weakened element reaches its tensile strength ahead of the other elements and is the first to enter the softening stage. From Eq. 1.1, the strain in this element ε_m is obtained as,

$$\varepsilon_m = \frac{(E-h)(\sigma - f_t)}{Eh} \qquad (1.3)$$

The other *m-1* elements experience elastic unloading while the weakened element is further softened. Therefore, they have the same strain ε_{m-1} as,

$$\varepsilon_{m-1} = \frac{\sigma}{E} \qquad (1.4)$$

The average strain $\bar{\varepsilon}$ is given as

$$\bar{\varepsilon} = \frac{1}{m}\left[(m-1)\varepsilon_{m-1} + \varepsilon_m\right] = \frac{\sigma}{E} + \frac{E-h}{Eh}\frac{\sigma - f_t}{m} \qquad (1.5)$$

Equation 1.5 shows that the average strain along the bar is actually dependent on the

number of the elements in the bar. That is to say, the discretization of the bar changes the loading-displacement curve obtained for this bar tension problem. When the mesh is refined, as m goes to infinity, the area where damage or softening initiates disappears from the problem and the bar tension problem incorrectly becomes purely elastic.

$$\bar{\varepsilon} \to \frac{\sigma}{E} \quad as \quad m \to \infty \tag{1.6}$$

The result is plotted in Figure 1.2. It shows spurious post-peak mesh dependence, which is unacceptable.

The mesh dependence shown in the benchmark example here is also discovered in two-dimensional or three-dimensional problems. Mathematically speaking, this is caused by the loss of the ellipticity of the governing equations. During the post-peak stage, the slope of the stress-strain curve is usually negative. In general, the tangential stiffness is no longer positive definite but negative definite. This means the elliptical problem becomes hyperbolic. Therefore, the solution may not be unique and becomes unstable. Consequently, the classical continuum mechanics fails in this regard, showing spurious mesh dependence and giving physical meaningless solutions. As a remedy, the nonlocal approaches are introduced and proven to be mesh independent.
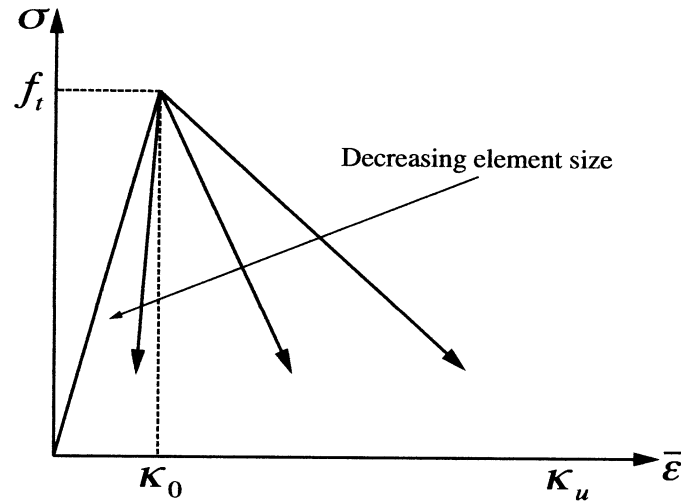
Figure 1.2 Stress against average strain curve shows mesh dependence

1.2. Literature review

Classical continuum solid mechanics usually refers to the local formulations. In continuum solid mechanics, the state variables (i.e., stress, strain, etc.) at each material point depend only on the current status and the history at that point, i.e., loading, deformation, etc. The continuity of the state variables is satisfied globally on the level of the equilibrium of the governing equations, which are derived from the underlying thermodynamics. The treatment of material as a general continuum has its limitations, since it overlooks the microscopic characteristics of the material. On the other hand, as shown in the benchmark problem, because of lacking microscopic information, the numerical implementation of the local continuum models shows spurious mesh dependence for certain softening material behaviors, which is unacceptable. The mathematical explanation for this mesh dependence is called the loss of ellipticity of the

governing differential equations.

Historically, Cosserat or micropolar continuum theories (Mindlin 1964, Eringen and Suhubi 1964a, 1964b, etc.) were among the first attempts that were introduced in the early 1980s to include information on the material micro scales. Cosserat or micropolar continuum theory is not included in the nonlocal formulations discussed in this dissertation. Discussion on this topic is reviewed in Bazant and Jirasek (2002). Most nonlocal continuum models are either of the integral types such as Bazant and Jirasek (2002) or on the gradient types such as Pamin (2005), Jirasek and Rolshoven (2009a, 2009b), etc. The review given hereafter will mainly focus on the finite element implementations for both integral and gradient type nonlocal methods.

1.2.1. Integral type nonlocal formula

In an integral type formula, the nonlocal form F(x) of a local state variable f(x) is expressed as,

$$F(x) = \int_{\Omega} \alpha(x,\xi) f(\xi) d\xi \qquad (1.7)$$

where $\alpha(x,\xi)$ is the spatial weight function defined in the three-dimensional Euclidean space Ω. It must satisfy,

$$\int_{\Omega} \alpha(x,\xi) d\xi = 1 \quad for \quad x \in \Omega \qquad (1.8)$$

This is achieved by normalizing the original weight function $\alpha_0(x,\xi)$,

$$\alpha(x,\xi) = \frac{\alpha_0(x,\xi)}{\int_\Omega \alpha_0(x,\xi)d\eta}$$

(1.9)

(1) Nonlocal stiffness matrices

Eringen and Edelen (1972) are among the pioneers who study the nonlocal elasticity theories. In those theories, a nonlocal elastic constitutive relation is developed such that the strain at any point is obtained by a weighted integral average of the strains at all the points in the body. The implementation of such theories in finite elements always involves the construction of the nonlocal stiffness matrices.

Bazant and Chang (1987), Pijaudier-Cabot and Bazant (1987) propose an imbricate finite element procedure for the simulation of the strain-softening materials. The idea is to use a set of overlapping elements, called the imbricated elements, to include the nonlocal interactions from the other elements into the current element. However, the imbricated elements can fail because of zero energy modes instability.

Addessi et al. (2002) develop a plastic nonlocal damage model that also implements the same idea of a spatial integral averaging process. Addessi and Ciampi (2006) later introduce an elastic-plastic predictor and damage-corrector process, which could be used in the incremental solution of the damage-plastic coupled problems.

Most recently, Pisano et al. (2009) implement similar nonlocal elasticity theory to inhomogeneous materials. The nonlocal stiffness matrices are obtained through a cross-

stiffness by a set of elements within an influence distance.

(2) Nonlocal yield function or loading-unloading function

Another way to implement the integral type nonlocal formula is through the introduction of a scalar nonlocal variable, i.e. nonlocal equivalent stress and strain, etc., into the yield function or the loading-unloading functions. Similarly, both de Vree et al. (1995) and Stromberg and Ristinmaa (1996) propose a way to obtain the nonlocal field through a spatial averaging process. The weighted integral is evaluated through the numerical integration of each finite element.

Similarly, Jirasek and Marfia (2005) also advocate a way to calculate the nonlocal quantity through a weighted spatial averaging process through the neighboring integration points in the mesh.

$$F(x_k) = \sum_{l=1}^{N_{GP}} w_l J_l \alpha(x_k, x_l) f(x_l) \tag{1.10}$$

With the normalized weight function evaluated as,

$$\alpha(x_k, x_l) = \frac{\alpha_0(\|x_k - x_l\|)}{\sum_{n=1}^{N_{GP}} w_n J_n \alpha_0(\|x_k - x_n\|)} \tag{1.11}$$

where w_l and J_l are the integration weights and element Jacobian at the Gauss point x_l. Theoretically, the weighted integral should consider the whole space; however, it is not realistic in practice. Then the numerical integration would take all the N_{GP} integration points in the body. To avoid that, an approximate weight function with a cut off radius needs to be used to improve the efficiency, such as,

$$\alpha_0\left(x,\xi\right) = \left(1 - \frac{r^2}{R^2}\right)^2 \quad for \quad r \leq R \tag{1.12}$$

In their study, they also choose the displacements to be nonlocal averaged instead of the commonly used strain-like quantities. However, this averaging process requires a fast distance checking algorithm to find all pairs of the integration points for larger problems.

Later, Grassl and Jirasek (2006, 2006) apply this averaging technique to concrete failure analysis with a plastic-damage model. The mesh bias problem in the concrete fracture simulations is studied in Jirasek and Grassl (2008).

Ricci and Brunig (2007) propose an integral type nonlocal damage model describing the anisotropic damage caused by the micro defects in ductile materials.

(3) Error estimations

Error estimations in integral type nonlocal finite element models are studied by Rodriguez-Ferran and Huerta (2000), who introduces a residual type error estimator. Comi and Perego (2004) also study the mesh refinement criteria for an integral type damage model by introducing energy based nonlocal error estimators.

1.2.2. Strain gradient type nonlocal formula

The strain gradient formula is also considered nonlocal, since the gradient terms generally reflect the interaction of the surrounding material points. The strain gradient

forms originally refer to the equations obtained from the Taylor expansion of a weighted averaged strain, as in Peerlings (1999). It gives the explicit or implicit forms of the nonlocal strain,

$$\text{Explicit}: \tilde{\varepsilon}(x) = \varepsilon(x) + l^2 \nabla^2 \varepsilon(x)$$

$$\text{Implicit}: \tilde{\varepsilon}(x) - l^2 \nabla^2 \tilde{\varepsilon}(x) = \varepsilon(x)$$

(1.13)

In general, any formula that involves the gradients of the state variables is considered a nonlocal strain gradient formula, such as the strain gradient enhanced plasticity, etc.

(1) Additional nodal parameter

Another branch of the research on nonlocal formulas focuses on the gradient-enhanced formula. Compared to an integral averaging type, the gradient-enhanced formula is nonlocal in a broad sense. The nonlocal interactions are brought in by the gradients of the variable field. The gradient-enhanced nonlocal methods have two types, explicit and implicit types. In explicit types, the nonlocal variable can be explicitly expressed by the local variable and its gradient terms. While in the implicit types, the nonlocal variable and its gradients satisfy a Helmholtz type equation. It is proven by Peerlings (1999) that implicit gradient type models are equivalent to the integral type models if using Green's function as the weighting function and with suitable boundary conditions.

In recent years, much attention has been given in the numerical implementation of the gradient enhanced models. One of the main reasons for introducing gradient terms into the local models is the regularization of the softening models. The gradient terms keep

the ellipticity of the governing equations and thus, no pathological mesh dependence occurs during material's post peak behavior. Other regularization tools, such as the localization limiters, have the similar ideas as to regularize the local models that are studied in Larsy and Belytschko (1988), Belytschko and Larsy (1989). De Borst (1992), de Borst and Pamin (1996) are among the first to implement gradient-enhanced formula in finite element methods. In their methods, usually a scalar nonlocal variable is treated as an additional nodal parameter. Hence, an additional equation with the appropriate boundary conditions is combined with the local governing equations to be solved as a coupled finite element formula. For plasticity problems, the additional equation usually comes from the consistent condition of a strain gradient dependent yield function. The main difficulty faced by a coupled formulation is to define an appropriate boundary condition for this additional equation. That boundary is a moving boundary, which is at the intersection between the localized plastic zones and the elastic zones. This topic is discussed in Peerlings (2006).

Much research focuses on the coupled finite element formulations of the implicit gradient types, since they are considered "true" nonlocal as the integral forms. Peerlings et al. (1996) applies the gradient-enhanced damage models to quasi-brittle materials. Ramaswamy and Aravas (1998) develop a nonlocal finite element plasticity model based on gradient dependent yield functions. Askes and Sluys (2002) later study the higher order (fourth order) derivative terms and compare them to the second order derivative terms. Zervos et al. (2002) and others argue that C^1 continuous displacement elements are needed for a gradient-enhanced formulation. While Simone et al. (2003) states that in

coupled formulations, the additional nonlocal equation is satisfied in a weighted residual sense, therefore, a C^0 continuous element suffices for the gradient formulation. Simone et al. (2004) also reports some possibilities of incorrect failure initiations predicted by both gradient and integral types nonlocal models. Other implementations of a coupled finite element formulation include: Engelen et al. (2003), Geers (2004), Cesar de Sa et al. (2005), Mediavilla et al. (2006), Dorgan and Voyiadjis (2006), Samal et al. (2008), Bui (2010) etc. They all focus on the implicit type gradient-enhanced plasticity or damage theories for a softening material behavior. D'hers S. and Dvorkin E. (2011) study the J_2 plasticity and damage coupled problems by introducing strong discontinuous modes into a coupled finite element formulation.

(2) Additional internal variable

For coupled formulations, the additional boundary condition is always hard to satisfy since it is a moving boundary; therefore, that boundary condition is usually relaxed to be set at the external boundary of the whole body, as in Simon et al. (2004). In order to overcome this difficulty, Abu Al-Rub and Voyiadjis (2005) propose a way to evaluate the nonlocal variable through a so-called super element. Their idea is to evaluate the strain gradients at each integration point by least square fitting the local strains at a structured set of neighboring integration points. A structured set of integrations points in a super element is shown in Figure 1.3.

Later, Abu Al-Rub and Voyiadjis (2009) successfully apply this technique to an anisotropic damage model for the concrete fracture analysis. However, this method is

limited to a structured mesh.
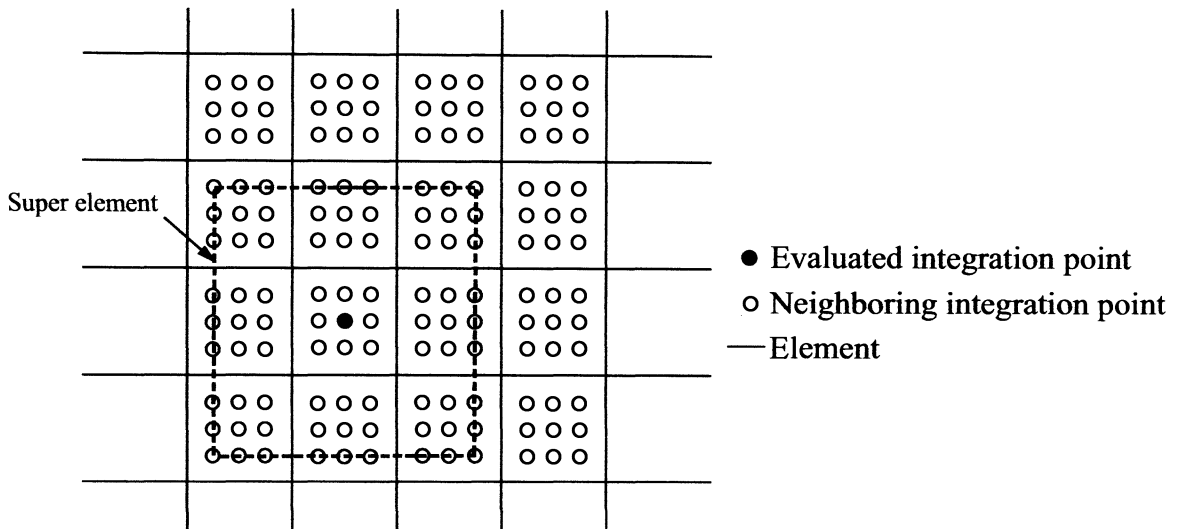
Figure 1.3 Super element based on structured mesh - Abu Al-Rub and Voyiadjis (2005)

Han et al. (2007) propose a finite element approach which can recover the derivatives of the strain tensor from nodal based patches. This patch projection technique is very close to that used in the super-convergent patch recovery methods. The patch least square fitting process is conducted to obtain the nodal nonlocal values. It is shown in Figure 1.4.

Boundary node   Inner node
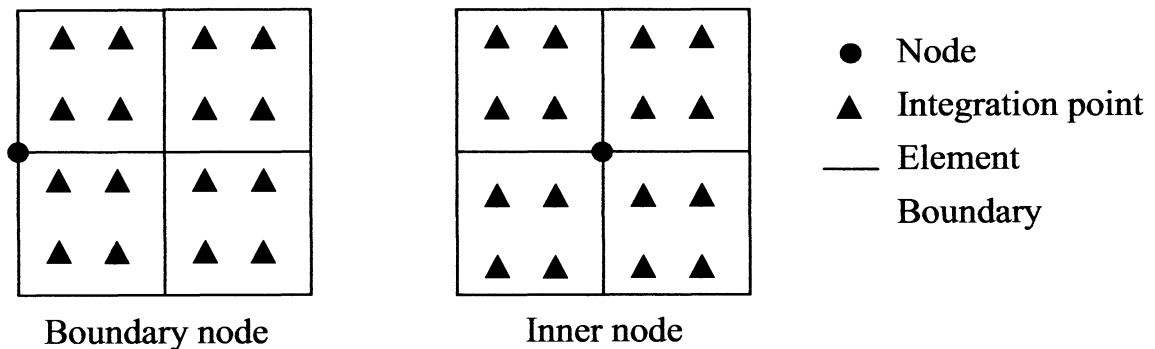
Figure 1.4 Patch projection technique – Han et al. (2007)

The benefit of this method is that it is no longer limited to structured meshes, however, only the nodal based patches are built in this method and it has so far only been utilized to evaluate the first derivatives of the strain. Also, no unstructured mesh examples are tested. However, it shows the potential of SCP technique in the implementation of nonlocal gradient-enhanced formulations.

(3) Element free method

One thing to mention here is the increased interest in the implementation of nonlocal models in the element free or meshless methods. A moving least square fitting process suggested in the element-free Galerkin method can be easily used for the evaluation of higher order gradients, which are not available from linear C^0 elements in finite element methods. Researchers in this field include: de Borst (2001), Askes and Aifantis (2002), Pamin et al. (2003), Pan and Yuan (2009, 2010), etc.

1.2.3. Material length scales

A major motivation for the development of the nonlocal continuum models is the need to incorporate the material length scales into the classical continuum models. The introduction of the length scales bridges the material micro and macro scales. Therefore, nonlocal continuum models are capable of capturing the size effects widely discovered in the experiments. For example, particulate reinforced composites show a higher strength with a decreasing particle size (Lloyd 1994; Zhu H. and Zbib H. 1995). The micro indentation tests used to measure the length scales for strain gradient plasticity theories

show that the material hardness increases with a decreasing indent size (Begley and Hutchinson 1998). Micro-bending tests also suggest that a higher bending moment is required to bend a thinner high purity nickel foil (Stölken and Evans 1998; Lou J. et al., 2006).

The material length scale is an intrinsic material property; however, its physical meaning is still not yet fully understood. Much work has been conducted on the theoretical study of the underlying relationship of the physical meaning of length scales to the strain gradients in a higher order strain gradient theory. The higher order strain derivatives are introduced in mechanism-based theories to incorporate the density of the statistically stored and geometrically necessary dislocations at the micro scale (Gao et al. 1999; Huang et al. 2000; Gurtin 2002; etc.). Those theories are based on the Taylor dislocation models (Gao and Huang 2001, Abu Al-Rub and Voyiadjis 2006), where the density of the geometrically necessary dislocations is obtained through a nonlocal integral of the strain field. Another similar idea is to incorporate the micro stresses, which depend on the higher order derivatives of the strains. The systematic development within the continuum framework in this study is given by (Gurtin and Anand 2005a, 2005b).

As reviewed in the section 1.2.1-1.2.2, the material length scales are also studied through the numerical implementations of the nonlocal continuum models. Typically, in an integral type formula, it appears as the nonlocal interaction radius R in Eq. 1.12; while in a strain gradient type formula, it is the coefficient l before the high order gradient terms

in Eq. 1.13. In order to correctly regularize the softening problems to be solved, the material length scales are usually calibrated from of the experimental results.

1.2.4. Super-convergence Patch Recovery

Han et al. (2007) show the super-convergent patch's potential as an effective tool to recover the nonlocal strain gradients. This dissertation proposes a nonlocal un-structured finite element technique that is based on the super-convergent patches. Therefore, a review on the related SCP techniques is also given below.

Zienkiewicz and Zhu (1992a, 1992b, and 1992c) are among the first to introduce the idea of obtaining a smooth variable field utilizing patches of elements in the finite element method. For each patch of elements, the discontinuous variable field is sampled at the super-convergent points inside each element and a set of local least square fit nodal variables are obtained to yield the continuous variable field. They show that this process is numerically effective in its applications in *a posteriori* estimates. Wiberg and Abudulwahab (1993), Wiberg and Li (1994), Wiberg et al. (1994) improve the SCP technique by least square fitting higher-order derivatives at the superconvergent points. They show a higher accuracy of the first derivative recovery than Zienkiewicz's approach by using one order higher polynomials.

Most recently, Jefferson (2001) and Akin (2005) further extend the SCP technique to recover the second derivatives. Various element based patches are evaluated. Error

estimations and adaptive element methods are also developed to achieve the second derivatives recovery. This method is incorporated in a Fortran90 code, MODEL, which is described in detail in Akin (2005).

1.3. Objective and outline

This thesis systematically studies the implementation of the super-convergent patch in the finite element analysis of the nonlocal continuum mechanics models. The study proposes a new nonlocal finite element technique based on the second order derivatives. A focus is given on the nonlocal strain gradient approaches only; the implementation of the integral type approaches with SCP is not yet conducted.

As mentioned before, so far, only nodal based patches have been utilized in nonlocal approaches and the order of the derivatives recovered is no higher than the first order. Thus, this study utilizes the element based patches for the derivative recovery in nonlocal approaches for the first time. It shows a robust and accurate recovery of the second derivatives of the interested variable with only C^0 elements.

The recovery procedure involved in a traditional SCP recovery process usually takes two steps. First, the least square fit results for the derivative components are stored at the element nodes. Then the interpolation of those nodal values in each element is conducted for the recovery. This procedure is also utilized for the recovery of the derivatives of the equivalent strain for the nonlocal approaches. Similarly, the least square fit results of the

equivalent strain are obtained, and then the derivatives of the equivalent strain are recovered at the element nodes, which are followed by a nodal averaging process.

This study also proposes another recovery option, which is inspired from the moving least square fit process for a mesh free method. The least square fit results for the equivalent strain are obtained first as before. Then the results are utilized to recover the strain derivatives at the integration points of the patch-centered element. For this option, no further nodal averaging process is required. Both recovery options are tested and compared herein.

The algorithm developed in this thesis is coded into a Fortran90 program library - MODEL that is originally developed by Akin (2005). The new version not only inherits the error estimators from the old MODEL, but also supplies the capability for the implementation of most strain gradient type nonlocal approaches. It is successfully applied to solve for both a nonlocal damage mechanics and a strain gradient plasticity problem. The simulations for those problems are assumed small deformation with static loadings.

The layout of the dissertation is outlined as follows,

Chapter 2 introduces the preliminary knowledge related to the nonlocal finite element technique developed in this dissertation.

Chapter 3 discusses in details about the implementation of the nonlocal finite element technique in the MODEL library.

Chapter 4 applies the newly developed algorithm to the nonlocal damage mechanics theory. Numerical results are given and compared.

Chapter 5 further applies the newly developed algorithm to the strain gradient plasticity theories. Two different strain gradient formulas are evaluated and numerical results are given and discussed.

Chapter 6 summarizes the dissertation and gives the conclusions. Future possible extensions are suggested.

Chapter 2

Nonlocal finite element technique preliminaries

2.1. Finite element method

The finite element method is now a standard numerical approach for most engineering design problems. Before we introduce the nonlocal finite element technique, a short summary on the general finite element process for a two-dimensional boundary value problem is given first. Assuming small deformation, the governing equations of a two-dimensional boundary value problem are given as follows,

$$Equilibrium\ equations: \qquad\qquad \nabla \cdot \sigma + b = 0 \quad in \quad \Omega$$

$$Traction\ (Natural) boundary\ conditions: \qquad \sigma \cdot n = \hat{t} \quad on \quad \Gamma_t \qquad (2.1)$$

$$Displacement\ (Essential) boundary\ conditions: \qquad u = \hat{u} \quad on \quad \Gamma_u$$

where Ω is the domain of computation, $\hat{t}$ is the traction applied on the natural boundary Γ_t of Ω, n is the normal of Γ_t, and $\hat{u}$ is the displacement applied on the essential boundary Γ_u

of Ω. If $\partial\Omega$ is the boundary of Ω, then $\Gamma_t \cap \Gamma_u = \emptyset$ and $\Gamma_t \cup \Gamma_u = \partial\Omega$. In Voigt notation, $\{\sigma\} = \{\sigma_x \quad \sigma_y \quad \tau_{xy}\}^T$ is a vector of the stress. Define a differential operator matrix $[L]$ as follows,

$$L = \begin{bmatrix} \dfrac{\partial}{\partial x} & 0 \\ 0 & \dfrac{\partial}{\partial y} \\ \dfrac{\partial}{\partial x} & \dfrac{\partial}{\partial y} \end{bmatrix} \tag{2.2}$$

Then, strain is also defined as a vector as $\{\varepsilon\} = \{\varepsilon_x \quad \varepsilon_y \quad \gamma_{xy}\}^T$, then, the strain-displacement relation can be expressed as,

$$\varepsilon = [L]\{u\} \tag{2.3}$$

Defining the tangent stiffness matrix as,

$$\left[D_{\text{tang}}\right] = \left[\dfrac{\partial\sigma}{\partial\varepsilon}\right] \tag{2.4}$$

In linear elastic problems, tangent stiffness matrix $[D_{\text{tang}}]$ is the same as the elastic stiffness, defined as $[D_e]$. For nonlinear material problems, the tangent stiffness matrix is usually evaluated from the rate form of the constitutive equations, which is application dependent.

Using the principle of virtual work, the equilibrium equations are satisfied in a weak sense as,

$$\int_V \{\delta\varepsilon\}^T \{\sigma\} dV = \int_{\Gamma_t} \{\delta u\}^T \{\hat{t}\} d\Gamma + \int_{\Gamma_V} \{\delta u\}^T \{b\} dV \tag{2.5}$$

The finite element displacements are approximated by the linear combination of shape

functions on the elementary levels, and so are the virtual displacements,

$$u = [N(x,y)]\{d\} \quad \delta u = [N(x,y)]\{\delta d\} \tag{2.6}$$

where $\{d\}$ and $\{\delta d\}$ are the nodal displacements and nodal virtual displacements, respectively.

Define the strain-displacement matrix as the differential operator acting on the shape functions as $[B] = [L][N(x,y)]$, and then the strain displacement relationship is

$$\{\varepsilon\} = [B]\{d\} \tag{2.7}$$

Substituting Eq. 2.6-2.7 into Eq. 2.5 gives,

$$\begin{aligned}
\int_V \{\delta d\}^T [B][D_{\text{tang}}][B]\{d\} dV = \\
\int_{\Gamma_t} \{\delta d\}^T [B]^T \{\hat{t}\} d\Gamma + \int_{\Gamma_V} \{\delta d\}^T [B]^T \{b\} dV
\end{aligned} \tag{2.8}$$

where the global stiffness matrix is obtained through the assembly process as in Akin (2005),

$$[K] = \sum_{e=1}^{n_e} \int_{V^e} \{\delta d^e\}^T [B^e]^T [D_{\text{tang}}][B^e]\{d^e\} dV \tag{2.9}$$

The global force vector is obtained in the same way as,

$$\{q\} = \sum_{e=1}^{n_e} \int_{\Gamma_t} \{\delta d^e\}^T [B^e]^T \{\hat{t}^e\} d\Gamma + \sum_{e=1}^{n_e} \int_{\Gamma_V} \{\delta d^e\}^T [B^e]^T \{b^e\} dV \tag{2.10}$$

Equation 2.5 is solved as the linear algebra problem,

$$[K]\{d\} = \{q\} \tag{2.11}$$

2.2. Two-dimensional C^0 elements

One of the benefits of the nonlocal finite element technique developed in this thesis is that, only C^0 elements are required. C^0 elements have only tangential inter-element continuous derivatives. The definitions and interpolation functions for C^0 elements are available from most FEA text books, i.e., Zienkiewicz (2000), Akin(2005), etc. Therefore, detailed discussions on C^0 elements are omitted here. Only those elements used in this study are introduced as follows.

Two-dimensional C^0 elements can be built from one-dimensional Lagrange interpolation functions. The Lagrange interpolation family in one dimension for the *i-th* node of *n* nodes is,

$$L_i^n = \frac{(r-r_1)(r-r_1)\cdots(r-r_{i-1})(r-r_{i+1})\cdots(r-r_n)}{(r_i-r_1)(r_i-r_2)\cdots(r_i-r_{i-1})(r_i-r_{i+1})\cdots(r_i-r_n)} \tag{2.12}$$

Therefore, for rectangular elements, the interpolations at node (i,j) of each element are obtained as the tensor product of these one-dimensional functions,

$$N_{ij}(r,s) = L_i^n(r)L_j^m(s) \tag{2.13}$$

where $N_{ij}(r,s)$ is the shape function associated with node *(i,j)* in local coordinate system *(r,s)*, *n* and *m* are the node numbers on each direction of the rectangular element. Interpolation functions for C^0 triangular elements are also well known, Zienkiewicz (2000), but are not be repeated here.

The elements to be used for the mesh are triangular elements (T3 and T6), quadrilateral

elements (Q4 and Q8). The patches (which will be discussed in details in Section 2.4) are built as elements that have non-zero second derivatives. Therefore, at least quadratic patches are required. In this study, the patches are either Q9 quadrilateral elements or T6 triangular elements.
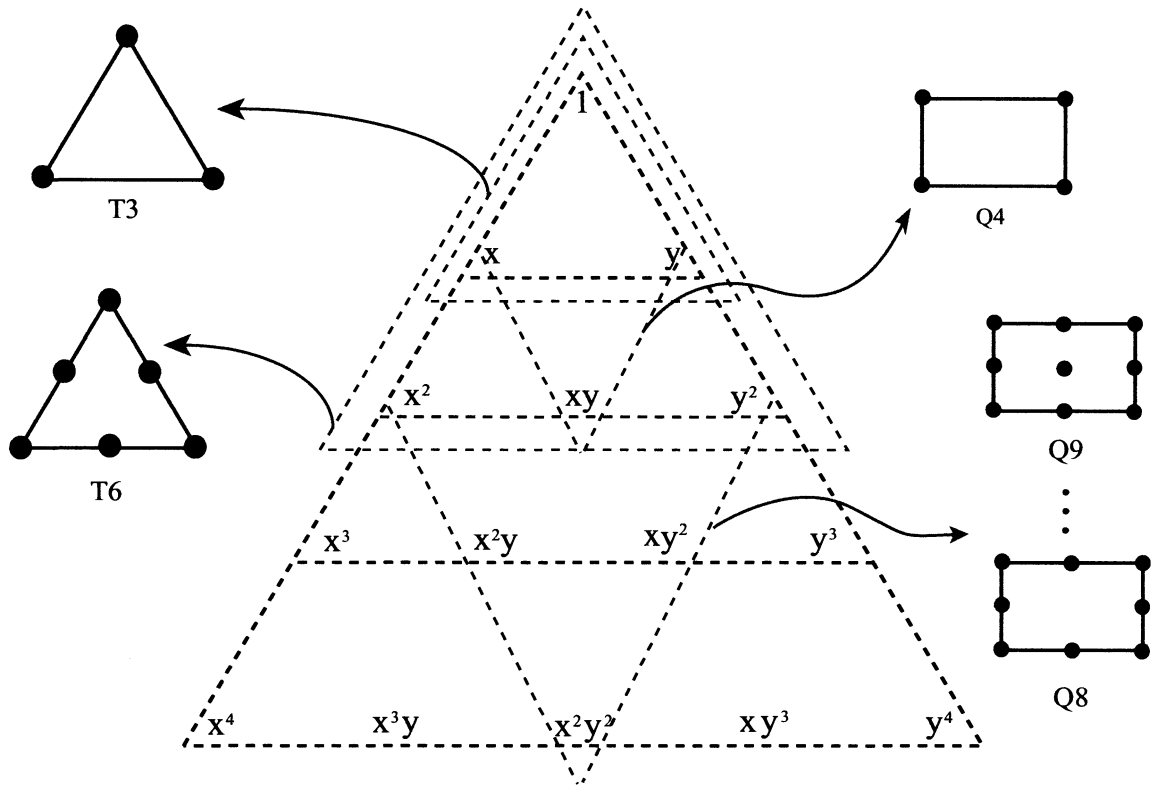
Figure 2.1 2D Pascal triangle

Figure 2.1 shows two-dimensional Pascal triangles and the interpolation polynomials for each element type. It is shown that the T6 elements give a complete second degree polynomial P_{T6} and the Q9 elements give an incomplete forth degree polynomial P_{Q9}, as shown in Eq. 2.14,

$$P_{T6} = \left\{1 \ ,x \ ,y \ ,xy \ ,x^2,y^2\right\}$$
$$P_{Q9} = \left\{1 \ ,x \ ,y \ ,xy \ ,x^2,y^2,x^2y \ ,xy^2,x^2y^2\right\}$$

(2.14)

The shape functions and their derivatives for a Q9 element are shown in Figure 2.2. The second derivatives in the Q9 elements are quadratic functions. The interpolation functions and their derivatives for a T6 element are plotted in Figure 2.3. It is shown that the second derivatives are piecewise constant in the element.
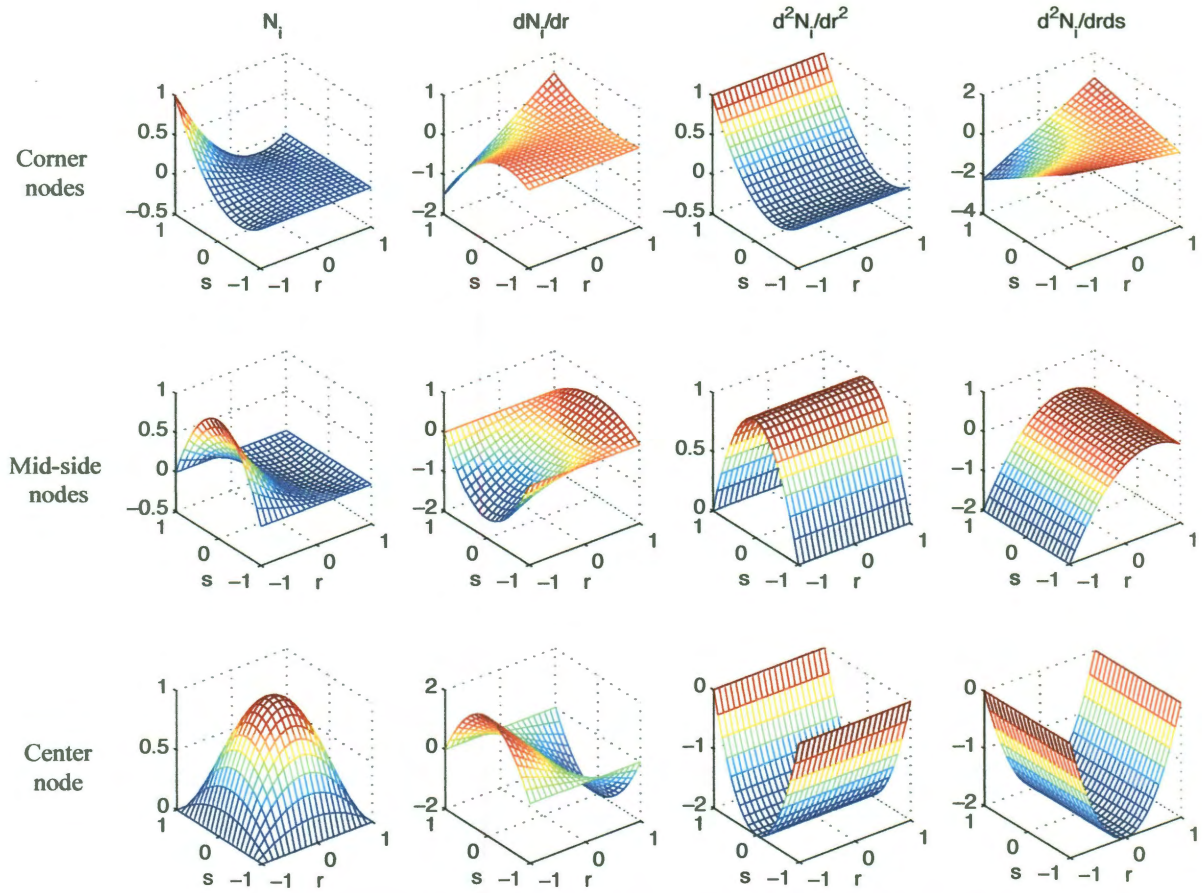
Figure 2.2 Q9 interpolation functions and their first and second derivatives
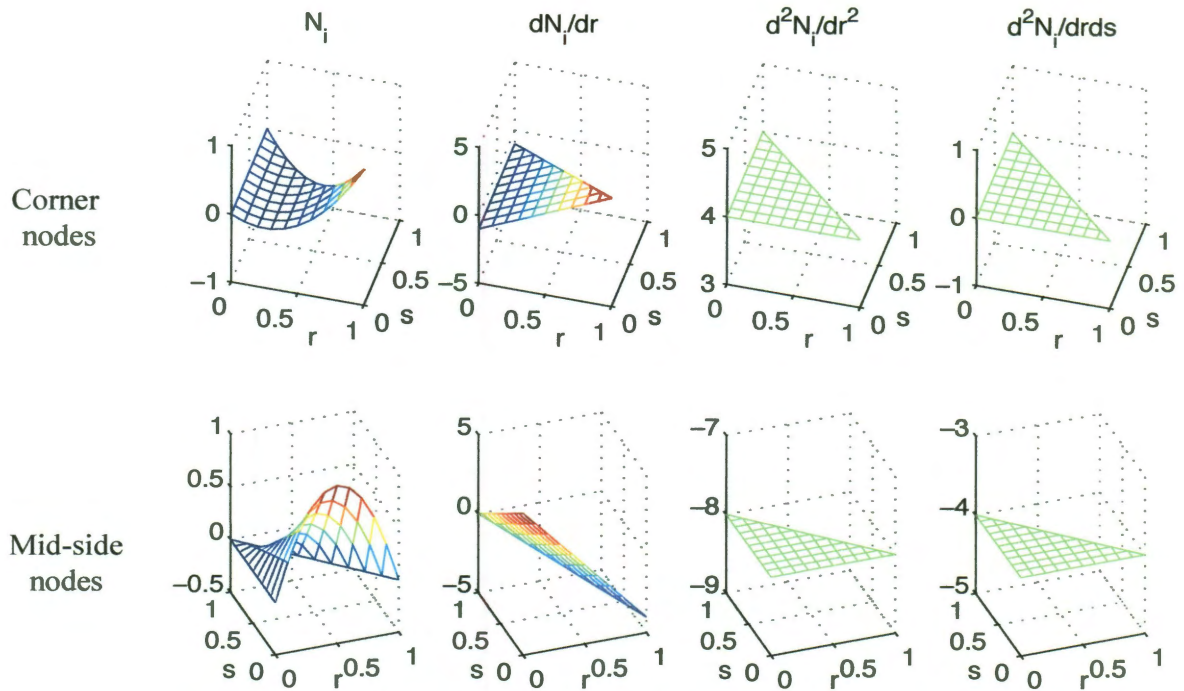
Figure 2.3 T6 interpolation functions and their first and second derivatives

2.3. Displacement control

For nonlinear material problems, an incremental-iterative Newton-Raphson (NR) solution scheme is often used. For certain problems with a softening material behavior, a force controlled NR iteration scheme can fail because of the loading limit existing in a softening material. Therefore, a displacement controlled NR iteration scheme is adopted. From a NR process as follows,

$$\{f_{\text{int}}\} + [K]\{\Delta d\} = \{f_{ext}\} \qquad (2.15)$$

$$\{d^{n+1}\} = \{d^n\} + \{\Delta d\} \qquad (2.16)$$

$$[K]\{d^{n+1}\} = \{f_{ext}\} - \{f_{\text{int}}\} - [K]\{d^n\} \qquad (2.17)$$

$$\{q\} = \{f_{ext}\} - \{f_{\text{int}}\} - [K]\{d^n\} \qquad (2.18)$$

where $[K]$ is the global stiffness matrix. $\{d^n\}$ is the nodal solution vector of interation n while $\{d^{n+1}\}$ is for the next iteration n+1. $\{f_{int}\}$ is the internal force vector and $\{f_{ext}\}$ is the external force vector. Omitting the superscript, the final equations to be solved in each iteration is the same as Eq. 2.11 for an elastic system,

$$[K]\{d\} = \{q\}$$

Partition the global stiffness equations into two parts as follows,

$$\begin{bmatrix} K_{ff} & K_{fp} \\ K_{pf} & K_{pp} \end{bmatrix} \begin{Bmatrix} d_f \\ d_p \end{Bmatrix} = \begin{Bmatrix} q_f \\ q_p \end{Bmatrix} \qquad (2.19)$$

where subscript f means 'free' and subscript p means 'prescribed'. Prescribed displacements are referring to the nodes on the essential boundaries, where displacement is known as $\{d_p\}$. Therefore Eq. 2.19 is reformulated as

$$\begin{bmatrix} K_{ff} & 0 \\ 0 & I \end{bmatrix} \begin{Bmatrix} d_f \\ d_p \end{Bmatrix} = \begin{Bmatrix} q_f - K_{fp} d_p \\ d_p \end{Bmatrix} \qquad (2.20)$$

In Eq. 2.20, the blocks in the stiffness matrix corresponding to the prescribed displacements are set to be identity matrix I, diagonal blocks are set to zeros, and the loading vector is modified to include the prescribed displacement. If reaction forces are desired, then the lower partition of Eq. 2.20 must be saved before enforcing the prescribed displacements.

The Newton-Raphson scheme can achieve a quadratic convergence rate given that the initial guess is close enough to the solution. When a NR scheme fails to converge for the displacement controlled softening problem, we can either turn to path-following schemes,

such as arc-length technique, or simply use an incremental scheme and solve the problem in an explicit way. If the incremental scheme is used, a small enough step length should be set to ensure the accuracy of the solution.

2.4. Construction of a patch element

The underlying idea of the nonlocal approaches in continuum mechanics is that the state variables at any material point are also dependent on those of the neighboring points. Therefore, for the numerical implementations of the nonlocal approaches, how to correctly incorporate the information from neighboring points is critical to its finite element implementation. One option to implement nonlocal approaches is to use higher order inter-element continuity, such as C^1 (inter-element continuous first derivative) or C^2 (inter-element continuous second derivative) elements. In this way, one could directly estimate the higher order derivatives at the element level.

The second option is to recover the state variables from a group of neighboring elements from a least square fitting process. In this regard, C^0 elements suffice. A group of neighboring elements is gathered to construct a patch or a patch 'element', since the patch has its own interpolation functions and nodes, just like a larger size element. This patch idea is utilized in the super-convergent patch recovery technique as in Zienkiewicz and Zhu (1992), Akin (2005), etc. Zienkiewicz and Zhu (1992) verify that the above mentioned least square fit process gives a first derivative estimation that is accurate at

least to the order of $O\left(h^{p+1}\right)$, where h is the size of the element and p is the order of the interpolation function. Therefore, this patch recovery process is widely known as the super-convergent patch recovery. The patches can be constructed based on nodes as well as on elements. Figure 2.4 shows the three types of Q4 element groups that can be used to construct a patch.

The selection of the patch element shape is based on the shape of the parent element of the current patch. For example, if the element is a 4 node quadrilateral element, its patch is bounded by a quadrilateral and with at least 9 nodes (bi-quadratic). If the element is a three node triangular element, its patch is bounded by a triangular and with six nodes. This idea is shown in Figure 2.5.

The patches are constructed such that their local coordinate systems are parallel to the global coordinate system. For example, as shown in Figure 2.5, the sides of the quadrilateral patch are parallel to the global axis x and y respectively. Such an alignment of the patch elements offers a linear mapping between the local coordinates and the global coordinates. The patch Jacobian is constant and diagonal in that case.

Parent element of this patch
Parent node of this patch

(a) Unstructured inite element mesh

(b) Element-based patch

(c) Face-based patch
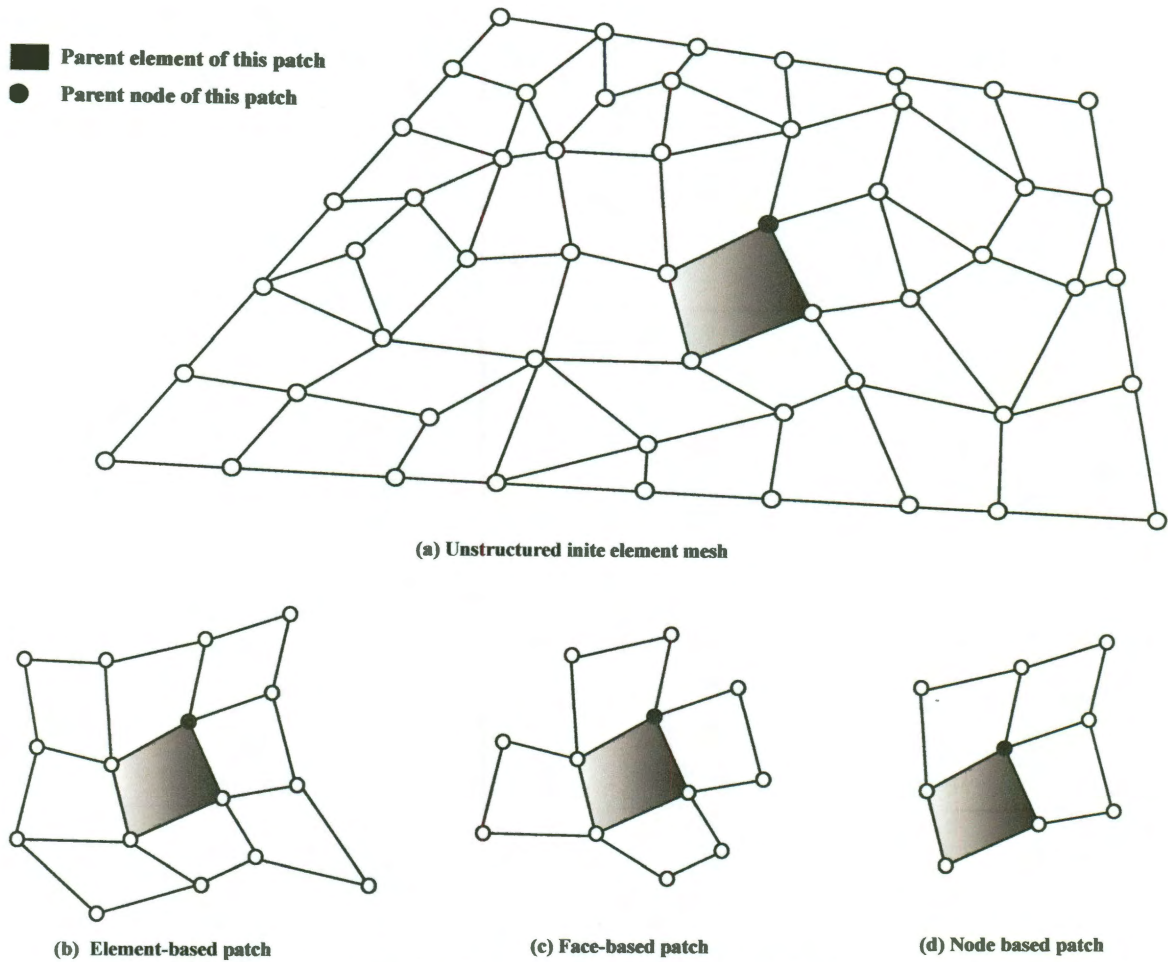
(d) Node based patch

Figure 2.4 Element and node based patches

2.5. Patch least square fit

A local least square fit process of the stress σ is introduced as follows. Assume a patch is constructed on a group of elements as shown in Figure 2.4. A polynomial approximation in two-dimensional spaces is as follows,

$$\{\sigma^*\} = \{P(\xi,\eta)\}[a] \tag{2.21}$$

where $\{\sigma^*\}$ is the smoothed stress from the approximation. ξ and η are the non-

dimensional coordinates. Here $[a]$ is a rectangular array with as many columns as components in $\{\sigma^*\}$. $\{P(\xi, \eta)\}$ is the polynomial used for the patch, Here, a triangular patch uses the same polynomials as in a T6 element, a quadrilateral patch uses the same ones as in a Q9 element.

If Eq. 2.21 is rewritten to be expressed with the interpolation of the values evaluated at the patch nodes, it is as follows,

$$\{\sigma^*\} = \left[H(\xi,\eta)\right][d] = \left[\begin{array}{ccc} H_1(\xi,\eta) & \cdots & H_n(\xi,\eta) \end{array}\right][d] \tag{2.22}$$

where $H_i(\xi, \eta)$ $(i = 1 \ldots n)$ are the patch shape functions associated with the patch nodes and n is the number of nodes of the patch. Here $[d]$ is the rectangular array that contains the patch nodal values of the stress components. Suppose $\{\hat{\sigma}\}$ is the sampled stress in the patch, which are calculated at several different internal points in the patch, usually at the quadrature points of all the elements inside the patch. For example, assume $\{\hat{\sigma}\}$ is proportional to the strains that are evaluated from the physical derivatives of elementary nodal solution $\{u^e\}$ as

$$\{\hat{\sigma}\}^T = \left[D_{\text{tang}}\right]\left[B^e\right]\{u^e\} \tag{2.23}$$

To get the smoothed solution $\{\sigma^*\}$ from the associated nodal values $[d]$, we want to minimize the function written as Eq. 2.24,
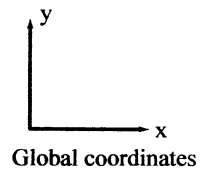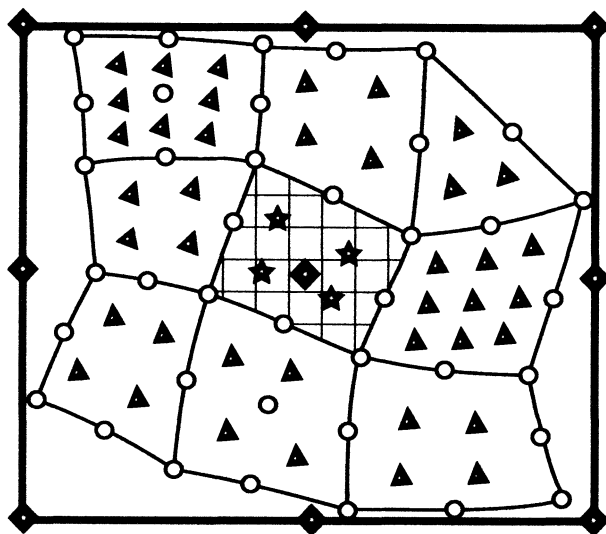
(a) 9-node quadrilateral patch

y

x

Global coordinates
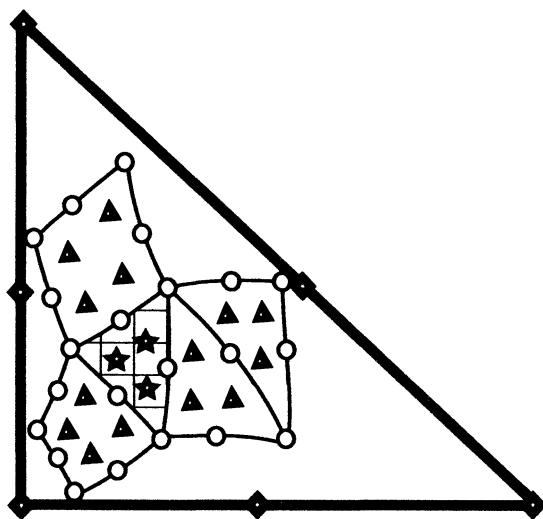
O - Element nodes

★ - Quadrature points of patch parent element

▲ - Quadrature points of patch elements

◆ - Patch nodes

▨▨▨▨ - Element based patch

⬚⬚ - Patch parent element

(b) 6-node triangular patch

Figure 2.5 Construction of an element based patch

$$F([d]) = \sum_{j=1}^{M} \left(\{\sigma^*\}_j - \{\hat{\sigma}\}_j \right)^T \left(\{\sigma^*\}_j - \{\hat{\sigma}\}_j \right)$$ (2.24)

where M is the total number of the quadrature points or the super-convergent points in the patch, and the subscript j refers to the value sampled at the j-th point.

For a patch of total n_{pe} elements with n_q quadrature points each, substituting Eq. 2.22-2.23 into Eq. 2.24 gives,

$$F([d]) =$$

$$\sum_{e=1}^{n_{pe}} \sum_{j=1}^{n_q} \left([H]_j [d] - \{u^e\}_j^T [B^e]_j^T [D_{tang}]_e \right)^T \left([H]_j [d] - \{u^e\}_j^T [B^e]_j^T [D_{tang}]_e \right) \qquad (2.25)$$

Equation 2.25 shows that we seek a least square fit by $M = n_{pe} \times n_q$ sampling points in a two-dimensional patch area. To get the patch nodal solutions, it is required that the number of the sampling points must be no less than the number of the patch nodes. The standard least square minimization reduces Eq. 2.25 into a linear algebraic problem as in Eq. 2.26,

$$[S][D] = [C] \qquad (2.26)$$

where,

$$[S] = \sum_{e=1}^{n_{pe}} \sum_{j=1}^{n_q} \left([H(\xi_j, \eta_j)]^T [H(\xi_j, \eta_j)] \right)$$

$$[C] = \sum_{e=1}^{n_{pe}} \sum_{j=1}^{n_q} [H(\xi_j, \eta_j)]^T \{u^e\}^T [B^e]_j^T [D_{tang}]_e$$

The equations are solved for every local patch. We adopt the constant Jacobian patch element that is discussed in the next paragraph. This is critical to an efficient and reliable mapping from the physical coordinates to the non-dimensional coordinates of a location in the patch. The constant Jacobian implemented actually employs a diagonal Jacobian matrix, which also benefits the second derivative recovery process discussed in the next paragraph.

2.6. Hessian matrix

For nonlocal strain gradient approaches, the derivatives of the local strains are recovered by the least square fitting process. In general, for a two-dimensional space, the Laplacian of the local scalar equivalent strain is usually of interest. This indicates that the smoothed approximation of the equivalent strain obtained from the least square fit should be at least quadratic to give the information on the second derivatives. To calculate the second derivatives from a patch, we need to calculate the Hessian matrix. In a two-dimensional space, the relations between the first parametric derivatives and the first physical derivatives are obtained as,

$$
\left\{ \begin{array}{c} \dfrac{\partial}{\partial \xi} \\[2mm] \dfrac{\partial}{\partial \eta} \end{array} \right\} = \left[\begin{array}{cc} \dfrac{\partial x}{\partial \xi} & \dfrac{\partial y}{\partial \xi} \\[2mm] \dfrac{\partial x}{\partial \eta} & \dfrac{\partial y}{\partial \eta} \end{array} \right] \left\{ \begin{array}{c} \dfrac{\partial}{\partial x} \\[2mm] \dfrac{\partial}{\partial y} \end{array} \right\}
\tag{2.27}
$$

where (ξ, η) are the coordinates for the parametric space and (x, y) are those for the physical space. The Jacobian is

$$
J = \left[\begin{array}{cc} \dfrac{\partial x}{\partial \xi} & \dfrac{\partial y}{\partial \xi} \\[2mm] \dfrac{\partial x}{\partial \eta} & \dfrac{\partial y}{\partial \eta} \end{array} \right]
\tag{2.28}
$$

Take one more derivative of Eq. 2.27 to get the relationship between the second parametric derivatives to the second physical derivatives,

$$\left\{ \begin{array}{c} \dfrac{\partial^2}{\partial \xi^2} \\[3mm] \dfrac{\partial^2}{\partial \eta^2} \\[3mm] \dfrac{\partial^2}{\partial \xi \partial \eta} \end{array} \right\} = \left[\begin{array}{cc} \dfrac{\partial^2 x}{\partial \xi^2} & \dfrac{\partial^2 y}{\partial \xi^2} \\[3mm] \dfrac{\partial^2 x}{\partial \eta^2} & \dfrac{\partial^2 y}{\partial \eta^2} \\[3mm] \dfrac{\partial^2 x}{\partial \xi \partial \eta} & \dfrac{\partial^2 y}{\partial \xi \partial \eta} \end{array} \right] \left\{ \begin{array}{c} \dfrac{\partial}{\partial x} \\[3mm] \dfrac{\partial}{\partial y} \end{array} \right\} + \left[\begin{array}{ccc} \left(\dfrac{\partial x}{\partial \xi}\right)^2 & \left(\dfrac{\partial y}{\partial \xi}\right)^2 & 2\dfrac{\partial x}{\partial \xi}\dfrac{\partial y}{\partial \xi} \\[3mm] \left(\dfrac{\partial x}{\partial \eta}\right)^2 & \left(\dfrac{\partial y}{\partial \eta}\right)^2 & 2\dfrac{\partial x}{\partial \eta}\dfrac{\partial y}{\partial \eta} \\[3mm] \dfrac{\partial x}{\partial \xi}\dfrac{\partial x}{\partial \eta} & \dfrac{\partial y}{\partial \xi}\dfrac{\partial y}{\partial \eta} & \dfrac{\partial x}{\partial \eta}\dfrac{\partial y}{\partial \xi} + \dfrac{\partial x}{\partial \xi}\dfrac{\partial y}{\partial \eta} \end{array} \right] \left\{ \begin{array}{c} \dfrac{\partial^2}{\partial x^2} \\[3mm] \dfrac{\partial^2}{\partial y^2} \\[3mm] \dfrac{\partial^2}{\partial x \partial y} \end{array} \right\} \qquad (2.29)$$

From Eq. 2.29, it is seen that the Hessian matrix is usually nonsymmetrical. If the patch has a constant Jacobian, the first rectangular matrix on the right hand side is zero. If in addition, the Jacobian is diagonal, then,

$$\frac{\partial x}{\partial \eta} = \frac{\partial y}{\partial \xi} = 0 \qquad (2.30)$$

In that case, Equation 2.29 is simplified as follows,

$$\left\{ \begin{array}{c} \dfrac{\partial^2}{\partial \xi^2} \\[3mm] \dfrac{\partial^2}{\partial \eta^2} \\[3mm] \dfrac{\partial^2}{\partial \xi \partial \eta} \end{array} \right\} = \left[\begin{array}{ccc} \left(\dfrac{\partial x}{\partial \xi}\right)^2 & 0 & 0 \\[3mm] 0 & \left(\dfrac{\partial y}{\partial \eta}\right)^2 & 0 \\[3mm] 0 & 0 & \dfrac{\partial x}{\partial \xi}\dfrac{\partial y}{\partial \eta} \end{array} \right] \left\{ \begin{array}{c} \dfrac{\partial^2}{\partial x^2} \\[3mm] \dfrac{\partial^2}{\partial y^2} \\[3mm] \dfrac{\partial^2}{\partial x \partial y} \end{array} \right\} \qquad (2.31)$$

Then, we just need to calculate the inverse of the diagonal square matrix on the right hand side to obtain the physical second derivatives. Since we are interested in obtaining the Laplacian and the patches are constructed as shown in Figure 2.5 in order to be able to utilize Equation 2.31. The computation of the Hessian matrix is finally simplified as,

$$\left\{ \begin{array}{c} \dfrac{\partial^2}{\partial x^2} \\[2mm] \dfrac{\partial^2}{\partial y^2} \end{array} \right\} = \left[\begin{array}{cc} \left(\dfrac{\partial x}{\partial \xi}\right)^{-2} & 0 \\[4mm] 0 & \left(\dfrac{\partial y}{\partial \eta}\right)^{-2} \end{array} \right] \left\{ \begin{array}{c} \dfrac{\partial^2}{\partial \xi^2} \\[2mm] \dfrac{\partial^2}{\partial \eta^2} \end{array} \right\} \tag{2.32}$$

Chapter 3

Nonlocal finite element implementation

3.1. Introduction

The super-convergent patch recovery process is now a routine procedure for several commercial finite element codes. Useful and robust SCP algorithms serve as the fundamental tools for error estimations, h-adaptive and p-adaptive finite element methods, etc.

The present work in this thesis establishes a new nonlocal finite element technique that is based on the SCP recovery technique for the second order derivatives. The algorithm is implemented in an F90 program – library MODEL, Akin (2005). The MODEL library was originally developed to include the super-convergent patch recovery process and the error estimators. The current version developed here inherits the functionalities of the above mentioned versions of MODEL library and is modified to have the new capability of the nonlocal strain gradients recovery. All the new nonlocal capabilities are enabled by the newly developed subroutines and additional keyword inputs into the MODEL

code. They will be introduced in detail in this chapter. Input control keywords are usually *italic lower-case* and subroutines are named in UPPER-CASE. Arrays, matrices and binary data files are in **BOLD UPPER_CASE**. Integers and real numbers are in ***ITALIC BOLD UPPERCASE***.

Two second order derivative recovery options are available for the nonlocal finite element technique based on the SCP process.

(1) Recovery by mesh nodal averaged equivalent strain derivatives (Nodal averages)

(2) Recovery by least square fitted equivalent strain derivatives at the patch-centered element (LSF)

The two recovery options are introduced in Section 3.2.3. Their performances are compared and discussed for the numerical examples in Chapter 4 and Chapter 5.

3.2. Super-convergent patch recovery of the nonlocal strain gradients

The SCP recovery method implemented in the MODEL library is actually the third version of the SCP algorithm as compared to Wilberg (1994), Zienkiewicz and Zhu (1992). Most of the available SCP recovery algorithms are limited to a single element type. The MODEL library is written in a modular fashion that allows unstructured meshes with a mixture of different element shapes with interpolation functions of different polynomial degrees, i.e., linear, quadratic, or cubic.

The new version of MODEL is developed to include the capability for the implementation of strain gradient type nonlocal methods. The second derivatives of the scalar equivalent strain are recovered from the same super-convergent patches built for the error estimation. The recovery technique introduced in this thesis allows an unstructured mesh with arbitrary element types and arbitrary, but compatible patch degrees.

3.2.1. Implementation of the element patches

The main idea of this dissertation is to recover the nonlocal strain derivatives through the local groups of the finite elements, or the so called patches. Usually, the patches are defined as groups of neighboring elements who share a common internal node or are adjacent to a boundary node in the mesh. Our choices of the element based patches are previously defined in Section 2.4. The same patches are proven to be efficient in the evaluation of the second or even higher order derivative recoveries (Jefferson and Akin 2001), which is also implemented in MODEL. Three types of the element patches are implemented and the user choice can be made by using different keyword inputs as listed in Table 3.1 on the next page.

In the current MODEL, element-based patches are kept as the default option if the strain gradient recovery is required for the task. For each type of the patch selected, a list of the neighboring elements is required. Establishing such neighboring lists can be expensive for large problems, however, it is beneficial to have those lists since they can be used for

multiple purposes, including the SCP process error estimations. Furthermore, they are only built once before at the preliminary stage for the problem to be solved. The number of the elements in each neighboring list may vary, for example, an interior patch may have more neighboring elements than one at the boundaries. For research purposes, we choose to store the entire neighboring lists as a rectangular array for increased speed, but at the cost of memory storage space. Other data structures such as linked lists could be considered for larger problems.

Keyword	Patch type	Definition
scp_neigh_pt	Node-based patch	Elements sharing a particular node. (Most widely used in SCP techniques)
scp_neigh_el	Element-based patch	All elements sharing any of the nodes of a particular element.
scp_neigh_face	Face-based patch	A subset of the element-based patch. In two-dimensional, they are the elements share a common edge with a particular element. In three-dimensional, they are the elements share a common face with a particular element.

Table 3.1 Keyword inputs for element patches

A patch element (as shown in Figure 2.5) is considered as a larger element with the interpolation polynomial P. The degree of the patch polynomial can be chosen to be the same as the elements or one to two orders higher than the element polynomial. Even higher order patches can also be set in the code but their accuracy is not yet studied. If the implementation of a nonlocal method involves the recovery of the Laplacian of the strains, then at least a quadratic patch polynomial is required. The patch polynomial degree is set as the same as that of the elements by default. To invoke higher degree patch polynomials, keyword *scp_deg_inc* is to be used.

Element patches are built to have a constant and diagonal Jacobian (as shown in Figure 2.5) which means their local axes are parallel to the global axes. This is done by obtaining the maximum and minimum coordinate components of the nodes of the all the elements in the neighboring list. This is achieved by the subroutine named DETERMINE_SCP_BOUNDS. In practice, a *1%* margin is added to the maximum and minimum coordinates to avoid ill-shaped patches. As introduced in Section 2.6, the constant Jacobian is diagonal and greatly simplifies the evaluation of the second derivatives of the equivalent strains.

3.2.2. Patch recovery options

So far, the patch element shape and interpolation polynomials are all set. We need to make one more choice of how the derivatives of the equivalent strains are recovered after solving the patch least square fitting problem. This version of MODEL gives the users two least square fitting options for the second derivative recovery.

(1) Recovery by mesh nodal averaged equivalent strain derivatives (Nodal averages)

This is a process similar to the SCP error estimation process where the recovery of the smoothed strains from the local strains is conducted during the post processing element loop after all the patches are processed. After the patch loop, each mesh node would receive multiple smoothed strain values which need to be averaged before being used for other purposes. This is also true for the nonlocal strain gradient recovery

process if the nodal averaging recovery option for higher derivatives is selected. The difference is that at all mesh nodes the derivatives of the strains are to be smoothed instead of strains. A global rectangular array **SCP_AVERAGES** is built to receive the nodal values of the equivalent strain derivatives from the patch least square fit loop.

Generally, during the patch loop, three main tasks are performed as follows,

1) Solve the local least square fitting problem to obtain the patch nodal equivalent strain results

2) Evaluate the gradients at each element's node inside the patch, by using the derivatives of the patch interpolation function and the patch nodal equivalent strain results.

3) Add the recovered element nodal equivalent strain gradients to the rectangular array **SCP_AVERAGES**, increase each integer counter by one.

After looping over all the patches, average the accumulated element nodal equivalent strain derivatives, i.e., divide each row of the rectangular array **SCP_AVERAGES** by the integer counter of the number of elements connected to that node.

To recover the equivalent strain derivatives from the nodal averaged ones at the element quadrature points, there are also two options available,

1) Evaluate the strain derivatives at the nodes of all the elements in this patch, this is the default option, no keyword required.

2) Evaluate the strain derivatives at the nodes of the parent element only, use

keyword *scp_center_only*.

Generally, the second option is preferred in the analysis of a nonlocal problem, since the recovery of gradients at all the nodes tends to give a smoother and more averaged result. This usually will over-smooth the higher derivatives needed in the nonlocal model.

The rectangular array **SCP_AVERAGES** has the following structure. The first four columns of the **SCP_AVERAGES** are reserved for error estimation purposes. Therefore, the nonlocal derivatives are stored in the later columns. The element nodal results are retrieved from the **SCP_AVERAGES** through location vector **ELEM_NODES** as,

$$\text{SCP\_AVERAGES (ELEM\_NODES, } i), (i = 5, 6, 7, 8)$$

For two-dimensional nonlocal strain gradient problems, the terms of interest are $\partial^2\_/\partial x^2$, $\partial^2\_/\partial y^2$, $\partial\_/\partial x$ and $\partial\_/\partial y$. They are stored from the fifth column to the eighth column of **SCP_AVERAGES**. However, the gradient terms to be recovered are not limited to the above four terms. Additional gradient terms such as $\partial^2\_/\partial x\partial y$ and $\partial^2\_/\partial y\partial x$ can be included.

(2) Recovery by least square fitted equivalent strain derivatives at the patch-centered element (LSF)

The second option is to directly recover the derivatives of the equivalent strain, within a patch, at the quadrature points of the parent element. A smoothed equivalent

strain field is obtained for each patch after the least square fitting process. The strain derivatives are evaluated directly at the quadrature points of the parent element in the patch using the above mentioned smoothed equivalent strain fields. This option is similar to the moving least square fitting process used in the mesh free methods. The difference is that the approach implemented here recovers the strain derivatives at all the quadrature points of the parent element at once instead of later averaging them at the nodes and interpolating back to the quadrature points.

Generally, for this option, there are also three tasks performed during the patch loop as follows,

1) Solve the local least square fitting problem to obtain patch nodal equivalent strain results

2) Evaluate the derivatives of the equivalent strains at the quadrature point, by using the derivatives of the patch interpolation functions and the patch nodal results.

3) Store the strain derivatives at quadrature points for updating the state variable in the following element loop

Compared to the recovery option by nodal averages, this option does not require further averaging process after the patch loop, since each quadrature point of the mesh only receives strain derivative results once during the loop. However, this option requires a random access data structure to store the equivalent strain derivative results for later use.

3.2.3. Data preparation and transfer

The nonlocal strain evaluation process will generally require three loops over the elements and one loop over the patches. The first loop is the element loop for constructing the stiffness matrix. After solving for the nodal solutions, the second element loop is required for obtaining the derivatives or the local strains from the nodal displacements. The third loop is the patch loop for evaluating the nonlocal strain derivatives from the local strains. The last loop is the element loop for updating the state variables using the nonlocal strains. The reuse of certain data at the integration points or the element levels is frequent among the loops. Therefore, to save computational cost and increase efficiency, certain data should be properly stored and transferred among them.

During the patch loop, the local least square fitting processes are conducted. Therefore, data are sampled within the patch, usually at the element integration points. In the SCP process, those points are very close to the super-convergent points in each element where the derivatives are most accurate for a certain polynomial degree. Therefore, SCP recovery usually takes the minimum required quadrature points in each element for the locations to evaluate the derivatives of the strains. It is reasonable to also use Gaussian quadrature points as the sampling locations for the recovery of the nonlocal strain derivatives.

While we loop over all the elements to build the element stiffness matrices, we need to store the information from those quadrature points for later access. For the stress analysis

with the implementation of the nonlocal strain gradient methods, information that are frequently needed are listed in Table 3.2 ,

Variable	Definition	Purpose
XYZ	Quadrature point's physical location	Evaluate interpolation functions, element Jacobian
B	Quadrature point's differential operator matrix	Obtain derivatives from element nodal solutions
E	Element constitutive matrix	Evaluate stress increments
LT_QP	Quadrature point counts for this element	Quadrature point loops

Table 3.2 Frequently used data for nonlocal strain gradient recovery

The information in Table 3.2 could be recorded in a sequential file in the element loop, which means that information is also read in the same sequence. For an unstructured mesh, the number of the elements in the list for each patch is a random number. Therefore, the local strains are sampled in a random style depending on the elements defining that patch. After the displacement solution, the strain derivatives obtained are also stored in a random style, which indicates a random access file is needed to store them.

For this purpose, two different data files are declared, the sequential file *U_FLUX* and the random access file *U_SCPR*. All the data are stored in binary format to minimize storage. In order to access the data unit for a specific quadrature point, the user needs to find the record number indicating the location for that piece of data, then followed by the other actions such as read, write or rewrite. The length of each data record will also need to be declared. Since a record length is hardware dependent, we use the Fortran90 intrinsic function INQUIRE (IOLENGTH) to compute the length for each data record.

Finally, the general outline of the data structure building and transfer process for the nonlocal strain gradient problems, are given in Figure 3.1. The element loop at the preliminary stage to build the element neighboring lists is also included, the logic of the patch loop shown in Figure 3.1 is discussed in the next section.

3.2.4. Nonlocal strain gradient recovery via SCP

The implementation of the nonlocal strain derivative recovery using the super-convergent patches is incorporated into an extension of the prior subroutine for obtaining smoother local strains: CALC_NONLOCAL_STRAIN_GRADIENTS. This subroutine loops over all the patches in the mesh. It is called to find the neighboring elements and construct the patch, then to solve the local least square fitting problem by singular values decomposition method. Subroutine CALC_NONLOCAL_STRAIN_GRADIENTS calls EVAL_GRADIENTS_AT_PATCH_NODES to recover the derivatives at all the element nodes in this patch. Then, subroutine EVAL_GRADIENTS_AT_PATCH_NODES calls EVAL_PT_GRADIENTS_IN_PATCH to recover the strain derivatives at the quadrature points of the parent element. Eventually, the resultant smoothed field of the equivalent strain is used to recover the nonlocal strain derivatives either by a nodal averaging process or directly through the least square fitted equivalent strains at the quadrature points within that patch.

The logic of the subroutine CALC_NONLOCAL_STRAIN_GRADIENTS is outlined in

Figure 3.2. Figure 3.2 gives the main flowchart of the subroutine, depending on the choices of the recovery option. Two subsidiary flowcharts of the recovery processes given in Figure 3.3 and Figure 3.4 are called separately.

Element loop: Preliminary
- Build lists of element neighbors
- Open the sequential file unit *U_FLUX*
- Open the random access file unit *U_SCPR*
- Estimate record length for *U_SCPR*

Element loop: Stiffness matrices
- Save element **LT_QP** to *U_FLUX*
  QP loop:
  - Save **XYZ**, **E** and **B** to *U_FLUX*

Rewind *U_FLUX*

Element loop: Calculate local strains
- Read **LT_QP** from *U_FLUX*
- Recover element type
- Gather nodal DOFs of this element
  QP loop:
  - Read **XYZ**, **E** and **B** from *U_FLUX*
  - Calculate local strains or other derivatives
  - Save the above results to *U_SCPR*

Rewind *U_FLUX*

Patch loop: Calculate strain gradients
  Element loop:
  - Read **LT_QP** from *U_FLUX*
  - Recover element type
  - Gather nodal DOFs of this element
    QP loop:
    - Read **XYZ**, **E** and **B** from *U_FLUX*
    - *If Nodal averages*
        Save strain gradients to **SCP_AVERAGES**
      else if Direct LSF
        Save strain gradients to *U_SCPR*
    end

Element loop: Update state variables
- Read **LT_QP** from *U_FLUX*
- Recover element type
- Gather nodal DOFs of this element
  QP loop:
  - Read **XYZ**, **E** and **B** from *U_FLUX*
  - *If Nodal averages*
      Read strain gradients to **SCP_AVERAGES**
    else if Direct LSF
      Read strain gradients to *U_SCPR*
    end
- Update state variables

Figure 3.1 Data structure building and data transfer between element and patch loops

SUBROUTINE: CALC_NONLOCAL_STRAIN_GRADIENTS

Loop: Element-based patches:

Gather information and construct the patch:

I.   Extract its element neighbors to define the patch
II.   Find the spatial boundaries for this patch
III. Find the total number of quadrature points in this patch
IV.   Determine the parent element type and thus the patch element type
V.   Allocate storage for the least square fit arrays
VI.   Set fit matrices row number to zero

Loop: Elements in this patch:

Find the element type and quadrature rules for this element

Loop: Quadrature points in this element:

Prepare data for the least square fitting, assemble $[S][D]=[C]$ (Eq. 2.28):

I.   Increment the row number of Eq. 2.28 by one
II. Recover the random record number for this quadrature point
     (Use function SCP_RECORD_NUMBER)
III. Read the physical corrdinates and the equivalent strain from random access
     file U_SCPR by that recorde number
IV. Use the constant Jacobian of the patch to convert the physical location to the
     corresponding non-dimensional coordinates in the patch
V.   Evaluate the patch interpolation polynomial at the local point. Insert it into
     the left hand side of this row of the coefficient matrix $[S]$.
VI. Substitue the equivalent strain into the right hand side data matrix $[C]$, in the
     same row.

End Loop: Quadrature points in this element

End Loop: Elements in this patch

Solve $[S][D]=[C]$ (Eq. 2.28) by SVD

IF to be recovered by the nodal averaging process (Nodal averages)
    THEN goto Box 3.2(b)
ELSE IF to be directly at the quadrature points of the parent element (LSF)
    THEN goto Box 3.2(c)
END IF

End Loop: Element-based patches

IF to be recovered by the nodal averaging process (Nodal averages)
    Averaging the nodal equivalent strain gradients by using the integer counter
END IF

Figure 3.2 Logic of subroutine CALC_NONLOCAL_STRAIN_GRADIENTS

Box 3.2 (b) - / EVAL_STRAIN_GRADIENTS_AT_PATCH_NODES /

Loop: Element nodes in this patch:

I.   Use the constant patch Jacobian to convert the node coordinates
     to non-dimensional coordinates of the patch

II. Evaluate the patch interpolation matrix **SCP_H** at each node points

III. **IF** First gradients of the flux are to be recovered
        THEN
             Calculate the first derivatives of the patch interpolation matrix **SCP_DLH**
             Use patch Jacobian to convert it to its physical coordinates **SCP_DGH**
        END IF

IV. **IF** The Laplacian of the equivalent strain is to be recovered
        THEN
             Calculate the second derivatives of the patch interpolation matrix **SCP_D2LH**
             Use patch Jacobian to convert it to its physical coordinates **SCP_D2GH**

V.   Compute the gradients of the equivalent strain at the node by the matrix product of
     SCP_DGH and **SCP_D2GH** seperately with the continuous gradients at the patch
     node *[D]*.

VI. Increment the nodal counter for patch contributions by one and scatter the equivalent
     strain gradients to the rectangular system nodal array **SCP_AVERAGES**.

└─ **End Loop: Element nodes in this patch**

Figure 3. 3 Logic of recovery by nodal averaging process

Box 3.2 (c) - / EVAL_PT_GRADIENTS_IN_PATCH /

Loop: Quadrature points of the parent element:

I.   Retrieve the record number for writing to *U_SCPR*

II. Use the constant patch Jacobian to convert the physical coordinates to non-dimensional
     coordinates of the patch

III. Evaluate the patch interpolation matrix **SCP_H** at the quadrature points.

IV. **IF** First gradients of the equivalent strain are to be recovered
        THEN
             Calculate the first derivatives of the patch interpolation matrix **SCP_DLH**
             Use patch Jacobian to convert it to its physical coordinates **SCP_DGH**
        END IF

V.   **IF** The Laplacian of the equivalent strain is to be recovered
        THEN
             Calculate the second derivatives of the patch interpolation matrix **SCP_D2LH**
             Use patch Jacobian to convert it to its physical coordinates **SCP_D2GH**
        END IF

VI. Compute the gradients of the equivalent strains at the quadrature point by the matrix
     product of **SCP_DGH** and **SCP_D2GH** separately with the continuous gradients at
     the patch node *[D]*.

VII. Rewrite the recovered equivalent strain gradients to the same location of *U_SCPR*

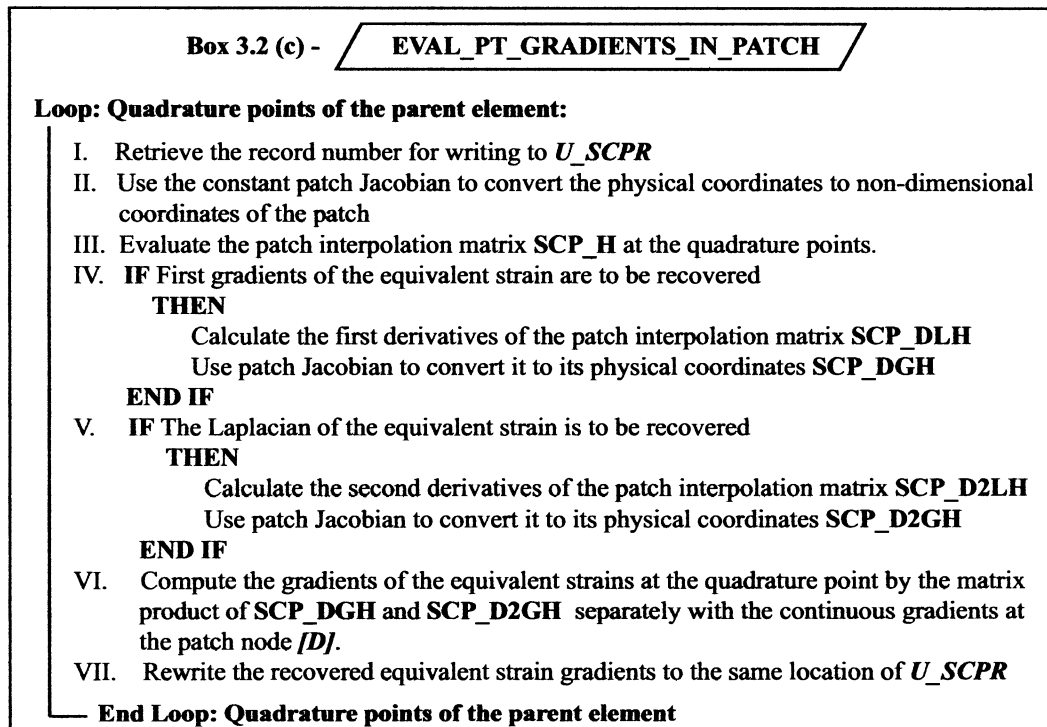└─ **End Loop: Quadrature points of the parent element**

Figure 3.4 Logic of recovery directly by least square fitted equivalent strains

3.3. Discussion of the recovery process

The recovery procedure of the strain derivatives based on the super-convergent patch recovery technique is introduced. Here are some comments on its implementation. To solve the local least square fitting problem for each patch and to avoid the possible numerical ill-conditioning, we choose to use an equivalent but more powerful process called singular value decomposition (SVD). The SVD process first factorizes the patch least square fitting matrix into the multiplication of two rectangular matrices and a diagonal matrix of the singular values (in subroutine SVDC_FACTOR), and then recovers the rectangular array of local continuous patch nodal flux values (in subroutine SVDC_BACK_SUBT). The solution of this algorithm gives us the patch nodal values. We use the patch interpolation functions to interpolate from the patch nodal values back to the element nodal values or directly to the quadrature points within the current patch center element.

Generally, the patches are overlapping each other in the mesh; each node may receive multiple nodal equivalent strain gradients after processing all the patches. Therefore, a logical way to get the final unique flux and flux gradients at each node should be decided. In MODEL, this is achieved by simply mathematical averaging calculation at each node. The times each node receives a equivalent strain gradient estimates are recorded in an integer counter. The final results are saved in **SCP_AVERAGES** for the later usage.

For nonlinear softening material problems, such as nonlocal damage mechanics and strain gradient enhanced elasto-plasticity, the nonlocality is usually introduced by including the

gradients of a scalar equivalent strain into a scalar type equation, i.e., yield function, loading-unloading functions, etc. The gradient dependent consistency conditions obtained from those equations are evaluated in a least square fitting sense in the above mentioned procedure for each patch. A scalar equivalent strain is used as the local fluxes to be fitted. In a Newton-Raphson solution scheme, this recovery procedure is conducted at every incremental or iterative step.

Chapter 4

Nonlocal damage mechanics via SCP

4.1. Review on local damage mechanics

Considering an isotropic damage model for a typical softening continuum, the stress-strain relationship is defined as,

$$\sigma = (1-\omega)D_e : \varepsilon \tag{4.1}$$

where σ is the stress tensor, ε is the strain tensor, D_e is the elastic stiffness tensor. ω is the damage density, which is a never decreasing variable ranging from 0 (undamaged) to 1 (totally damaged). The growth of the damage density ω is expressed as a damage law,

$$\omega = g(\kappa) \tag{4.2}$$

The loading function is

$$f(\varepsilon,\kappa) = \varepsilon_{eq}(\varepsilon) - \kappa \tag{4.3}$$

where $g(\kappa)$ is the damage evolution function, ε_{eq} is a scalar type equivalent strain. κ is called the damage threshold which is an internal variable usually representing the maximum equivalent strain level reached in the loading history.

$$\kappa = \max\left(\varepsilon_{eq}\right) \tag{4.4}$$

Whether there is a further damage growth or not is controlled by the loading-unloading conditions,

$$f(\varepsilon,\kappa) \leq 0 \quad \dot{\kappa} \geq 0 \quad f(\varepsilon,\kappa)\dot{\kappa} = 0 \tag{4.5}$$

For quasi-brittle material, the equivalent strain ε_{eq} can be defined as in Mazar (1984), which assumes damage occurs more easily under a tension state rather than a compression state.

$$\varepsilon_{eq} = \sqrt{\sum_{I=1}^{3}\langle\varepsilon_I\rangle^2} \tag{4.6}$$

where, $\varepsilon_I (I = 1,2,3)$ are the principle strains, the positive operator $\langle\varepsilon_I\rangle$ is defined to only use the positive part of ε,

$$\langle\varepsilon_I\rangle = \frac{\varepsilon_I + |\varepsilon_I|}{2} \tag{4.7}$$

The damage evolution function $g(\kappa)$ can be directly identified from the uniaxial stress-strain curves. It can represent a linear softening behavior as,

$$g(\kappa) = \begin{cases} 0 & \kappa \leq \varepsilon_0 \\ \dfrac{\varepsilon_f}{\varepsilon_f - \varepsilon_0}\left(1 - \dfrac{\varepsilon_0}{\kappa}\right) & \varepsilon_0 \leq \kappa \leq \varepsilon_f \\ 1 & \varepsilon_f \leq \kappa \end{cases} \tag{4.8}$$

or an exponential softening behavior as,

$$g(\kappa) = \begin{cases} 0 & \kappa \le \varepsilon_0 \\ 1 - \dfrac{\varepsilon_0}{\kappa} \exp\left(-\dfrac{\kappa - \varepsilon_0}{\varepsilon_f - \varepsilon_0} \right) & \varepsilon_0 \le \kappa \le \varepsilon_f \end{cases} \tag{4.9}$$

A softening problem needs to be solved iteratively through a Newton-Raphson process. Therefore, the rate form of constitutive law is to be developed.

$$\dot{\sigma} = (1-\omega)D_e : \dot{\varepsilon} - (D_e : \varepsilon)\dot{\omega} \tag{4.10}$$

$$\dot{\omega} = \frac{dg}{d\kappa}\dot{\kappa} = g'(\kappa)\dot{\kappa} \tag{4.11}$$

If there is a damage growth, then

$$\dot{\kappa} = \dot{\varepsilon} \tag{4.12}$$

The rate form of the stress-strain relationship is obtained as,

$$\dot{\sigma} = (1-\omega)D_e : \dot{\varepsilon} - (D_e : \varepsilon)g'(\kappa)\dot{\varepsilon} \tag{4.13}$$

The integration of the rate constitutive equation from t_n to $t_{n+1} = t_n + \Delta t$ is conducted to develop a time discretization algorithm as

$$\Delta\sigma = \int_{t_n}^{t_{n+1}} \dot{\sigma}dt \quad \Delta\varepsilon = \int_{t_n}^{t_{n+1}} \dot{\varepsilon}dt \tag{4.14}$$

It gives incremental form of the constitutive law for the elasto-damage mechanics as

$$\Delta\sigma = (1-\omega)D_e : \Delta\varepsilon - (D_e : \varepsilon)g'(\kappa)\Delta\varepsilon \tag{4.15}$$

4.2. Review on nonlocal damage mechanics

So far, we have developed the constitutive laws for the classical or local damage mechanics approach. The nonlocal damage mechanics model is developed by introducing

the nonlocal equivalent strain into the loading function (Eq. 4.5). The integral type of the equivalent strain is defined as a weighted spatial average of the local ones as

$$\tilde{\varepsilon}_{eq}(x) = \int_V \alpha(x,\xi)\varepsilon_{eq}(\xi)d\xi \qquad (4.16)$$

where the weighting function $\alpha(x,\xi)$ is only dependent on the distance between a source point x and a target point ξ in the infinite Euclidean space. To keep the uniform field unaltered by this spatial weighted averaging process, the weighting function is normalized as

$$\alpha(x,\xi) = \frac{\alpha_0(\|x-\xi\|)}{\int_V \alpha_0(\|x-\eta\|)d\eta} \qquad (4.17)$$

The weighting function can be chosen to be the Gaussian function, a bell shaped quartic polynomial approximating the Gaussian function, or a Green's function such as

$$\alpha_0(x,\xi) = G(x,\xi) = \frac{1}{2l}\exp\left(-\frac{\|x-\xi\|}{l}\right) \qquad (4.18)$$

where l is the material length scale describing the material microscopic structure.

The gradient type of the nonlocal equivalent strain can be obtained either from an explicit form,

$$\tilde{\varepsilon}_{eq}(x) = \varepsilon_{eq}(x) + l^2\nabla^2\varepsilon_{eq}(x) \qquad (4.19)$$

or an implicit form,

$$\tilde{\varepsilon}_{eq}(x) - l^2\nabla^2\tilde{\varepsilon}_{eq}(x) = \varepsilon_{eq}(x) \qquad (4.20)$$

It has been proven in Peerlings (1999) that, the solution to the Helmholtz-type differential equation (Eq. 4.20) with a boundary condition

$$n \cdot \nabla \varepsilon_{eq}(x) = 0 \tag{4.21}$$

set on the entire boundary Γ of the whole domain V, is exactly the integral type Eq. 4.16 with the Green's weighting function Eq. 4.18. Substituting the nonlocal equivalent strain $\tilde{\varepsilon}_{eq}(x)$ into the loading function and the loading-unloading conditions gives,

$$f(\varepsilon, \kappa) = \tilde{\varepsilon}_{eq}(x) - \kappa \tag{4.22}$$

$$\tilde{\varepsilon}_{eq}(x) - \kappa \leq 0 \quad \dot{\kappa} \geq 0 \quad \left[\tilde{\varepsilon}_{eq}(x) - \kappa \right] \dot{\kappa} = 0 \tag{4.23}$$

For the numerical implementation, Eq. 4.19 and Eq. 4.20 are more useful in their incremental forms for the Newton-Raphson process. The incremental explicit and implicit nonlocal strain gradient forms are

Explicit form:

$$\Delta \tilde{\varepsilon}_{eq}(x) = \Delta \varepsilon_{eq}(x) + l^2 \nabla^2 \Delta \varepsilon_{eq}(x) \tag{4.24}$$

Implicit form:

$$\Delta \tilde{\varepsilon}_{eq}(x) - l^2 \nabla^2 \Delta \tilde{\varepsilon}_{eq}(x) = \Delta \varepsilon_{eq}(x) \tag{4.25}$$

4.3. Evaluation of the strain gradients at SCP

The gradient type nonlocal damage mechanics involves the evaluation of the second derivatives (Laplacian) of the equivalent strain. Here, it is obtained through the same patch recovery process as proposed in Chapter 3. The patches are constructed based on a group of neighboring elements. For each patch, a local least square fitting problem is solved either for the explicit form or the implicit form,

$$\min \left\| \Delta \tilde{\varepsilon}_{eq}(x) - \Delta \varepsilon_{eq}(x) - l^2 \nabla^2 \Delta \varepsilon_{eq}(x) \right\|$$

$$or \qquad\qquad\qquad (4.26)$$

$$\min \left\| \Delta \tilde{\varepsilon}_{eq}(x) - \Delta \tilde{\varepsilon}_{eq}(x) - l^2 \nabla^2 \Delta \varepsilon_{eq}(x) \right\|$$

The incremental nonlocal equivalent strain $\Delta \tilde{\varepsilon}_{eq}(x)$ is approximated from the polynomials of the patch element. However, this recovery process will yield an over-smoothed result for the nonlocal equivalent strain, which is not able to initialize a localized behavior. Therefore, the least square fitting process is only used to evaluate the derivatives of the local equivalent strain. For example, in a two-dimensional problem, the patches are utilized to construct an smooth surface $\Delta \hat{\varepsilon}_{eq}(x, y)$ fitting the local equivalent strains by approximating the continuous equivalent strain field from the patch interpolation functions $[H(x,y)]$ times its nodal values $\{d\}$ of the patch fitted equivalent strain increments,

$$\Delta \hat{\varepsilon}_{eq} = \left[H(x,y) \right] \{d\} \qquad\qquad (4.27)$$

Therefore, instead of Eq. 4.26, the local least square fitting problem to be solved is

$$\min \left\| \Delta \hat{\varepsilon}_{eq} - \Delta \varepsilon_{eq} \right\| \qquad\qquad (4.28)$$

The local equivalent strain increments are sampled at all the quadrature points in the patch as

$$\Delta \varepsilon_{eq} = \{a\} = \left\{ \Delta \varepsilon_{eq}^1, \cdots, \Delta \varepsilon_{eq}^{n_{qp}} \right\}^T \qquad\qquad (4.29)$$

The local equivalent strain increments $\Delta \varepsilon_{eq}^q$ $(q = 1 \ldots n_{qp})$ are calculated and recorded in the *U_SCPR* random file.

Substituting Eq. 4.27 and Eq. 4.29 into Eq.4.28, the normal equations can be developed as,

$$\int_{\Omega}\left(\left[H(x,y)\right]^{T}\left[H(x,y)\right]\right)\{d\}d\Omega = \int_{\Omega}\left[H(x,y)\right]^{T}\{a\}d\Omega \qquad (4.30)$$

or it can be expressed as the summation over the quadrature points in the patch,

$$\left(\sum_{q=1}^{q=n_{qp}}\left[H(x_{q},y_{q})\right]^{T}\left[H(x_{q},y_{q})\right]\right)\{d\} = \left(\sum_{q=1}^{q=n_{qp}}\left[H(x_{q},y_{q})\right]^{T}a_{q}\right) \qquad (4.31)$$

And the patch nodal solution is obtained as,

$$\{d\} = \left(\sum_{q=1}^{q=n_{qp}}\left[H(x_{q},y_{q})\right]^{T}\left[H(x_{q},y_{q})\right]\right)^{-1}\left(\sum_{q=1}^{q=n_{qp}}\left[H(x_{q},y_{q})\right]^{T}a_{q}\right) \qquad (4.32)$$

This part of the calculation is done in the subroutine POST_PROCESS_GRADS and in LIST_ELEM_FLUXES. This process implies that the local and nonlocal Laplacian $\nabla^{2}\Delta\varepsilon_{eq}(x)$ and $\nabla^{2}\Delta\tilde{\varepsilon}_{eq}(x)$ are evaluated from the continuous surface obtained from the patch least square fit of the local equivalent strain increments. Since the local equivalent strain increments are identical for both the implicit and explicit forms for each loading increment, the fitted surface is the same for both forms. Therefore, the least square fitting process is the same for the implicit and explicit forms at each local patch. That is to say, for each patch,

$$\nabla^{2}\Delta\tilde{\varepsilon}_{eq} = \nabla^{2}\Delta\varepsilon_{eq} = \nabla^{2}\Delta\hat{\varepsilon}_{eq} = \left[\nabla^{2}H(x,y)\right]\{d\} \qquad (4.33)$$

where

$$\left[\nabla^{2}H(x,y)\right] = \left[\frac{\partial^{2}H(x,y)}{\partial x^{2}} + \frac{\partial^{2}H(x,y)}{\partial y^{2}}\right] \qquad (4.34)$$

The second derivatives of the equivalent strain calculated from the patch loop are stored through one of the two recovery options available in MODEL. To calculate the Laplacian, two second partial derivatives are required and thus saved, they are

$$\frac{\partial^2 \Delta \hat{\varepsilon}_{eq}}{\partial x^2} = \left[\frac{\partial^2 H(x,y)}{\partial x^2}\right]\{d\} \quad \text{and} \quad \frac{\partial^2 \Delta \hat{\varepsilon}_{eq}}{\partial y^2} = \left[\frac{\partial^2 H(x,y)}{\partial y^2}\right]\{d\} \qquad (4.35)$$

For recovery by nodal averaging approaches, the two second derivative components are saved in the rectangular matrix **SCP_AVERAGES** containing all the nodal values of the second derivative components. During the post processing element loop, the strain derivatives are recovered by the element interpolation function, [*N(x,y)*], multiplying the nodal vectors of this element in **SCP_AVERAGES (ELEM_NODES,** 5) and **SCP_AVERAGES (ELEM_NODES,** 6), which are retrieved from the global matrix **SCP_AVERAGES** (See Section 3.2.3). Therefore,

$$\nabla^2 \Delta \hat{\varepsilon}_{eq} = \frac{\partial^2 \Delta \hat{\varepsilon}_{eq}}{\partial x^2} + \frac{\partial^2 \Delta \hat{\varepsilon}_{eq}}{\partial y^2} \qquad (4.36)$$

with

$$\frac{\partial^2 \Delta \hat{\varepsilon}_{eq}}{\partial x^2} = \left[N(x,y)\right]\left\{\text{SCP\_AVERAGES}\left(\text{ELEM\_NODES} , 5 \right)\right\}$$

$$\frac{\partial^2 \Delta \hat{\varepsilon}_{eq}}{\partial y^2} = \left[N(x,y)\right]\left\{\text{SCP\_AVERAGES}\left(\text{ELEM\_NODES} , 6 \right)\right\}$$

Then, the Laplacian of the equivalent strain increments is calculated and added to the local equivalent strain increments to get the nonlocal equivalent strain increments according to Eq.4.24.

For the second recovery option, the two second derivative components Eq. 4.35 are stored directly at the quadrature points of the parent element of each patch, which means they are stored into the corresponding locations in the *U_SCPR* file. Then, during the post processing loop, the second derivative components are recovered by reading the *U_SCPR* file. The rest of the steps are the same as for the other recover option.

Finally, for each loading increment or iteration, the flow chart for the above mentioned recovery process of the nonlocal equivalent strain increments is plotted in Figure 4.1.
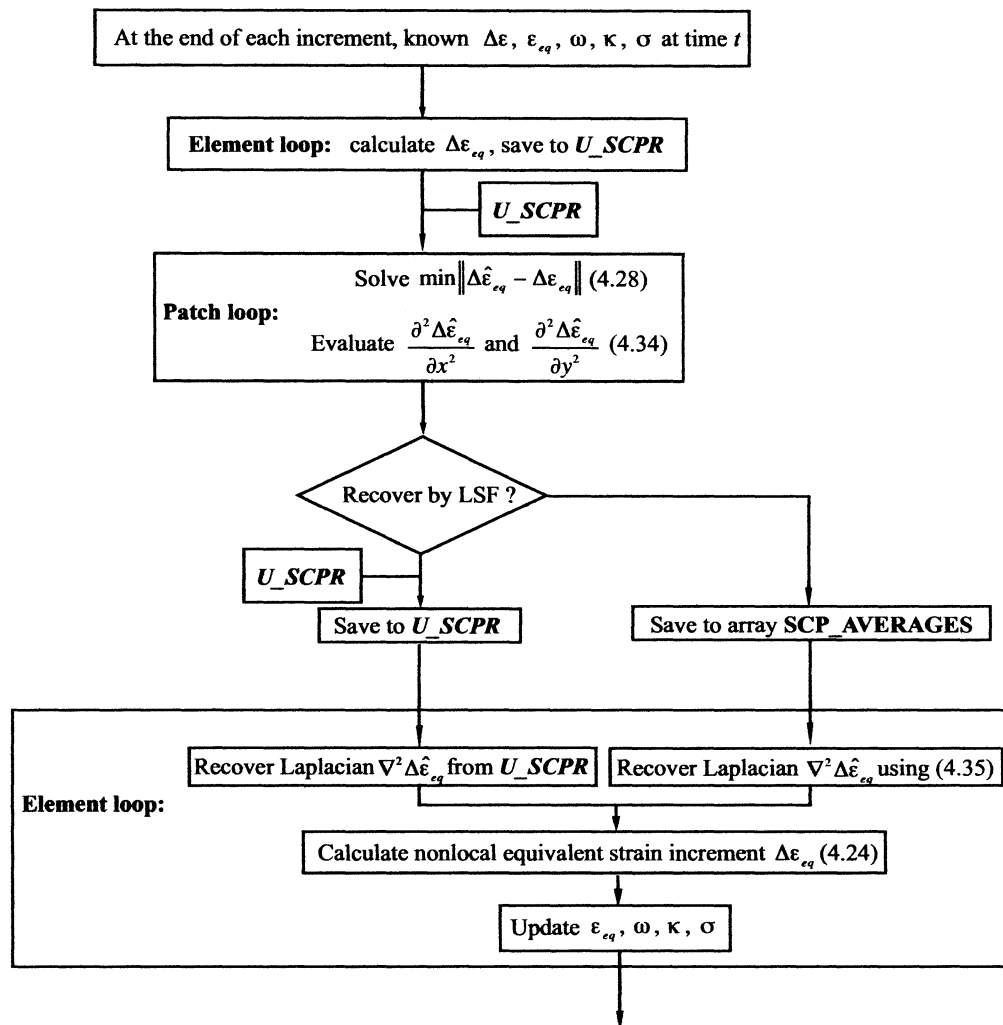
Figure 4.1 Flow chart for nonlocal equivalent strain recovery process

4.4. Three point bending of a beam

To test the new nonlocal finite element technique, a nonlocal damage mechanics problems is solved. The same example is analyzed by Jirasek (2007) with an integral type nonlocal damage mechanics model. Here, the problem is solved with the current strain gradient type model instead of Jirasek's integral model.

The simulation is conducted on the three point bending test of a concrete beam with and without a notch. The beam tested has a square cross section area of *100×100 mm*. The span of the beam is *450 mm*. The notch is set at the center of the beam throughout the beam thickness. The notch is *5 mm* wide and *50 mm* deep into the beam. Figure 4.2 shows the two-dimensional plane stress model used for the simulation. The Young's modulus *E = 20 GPa* and Poisson's ratio γ = *0.2*. Assume an exponential softening material with a stress strain curve that is defined in Eq. 4.9 with parameters ε_0 = *1.2e-4* and ε_f = *7e-3*.

4.4.1. Local damage mechanics

The bending test simulations are first run on the notched beam case. Three different meshes with the element size of *5 mm*, *2.5 mm* and *1.6 mm* are built. The element type used is the bi-linear four node quadrilateral element (Q4) with a standard *2x2* Gauss quadrature rule. The meshes are shown in Figure 4.3(a). The unnotched beam is also simulated with the same element type. Again, meshes with three different element sizes are built as *15 mm*, *7.5 mm* and *5 mm*. The meshes are shown in Figure 4.3(b). The

meshes for both cases are all constructed in an unstructured fashion and the meshes are refined around the middle region for both beams.

$L = 450mm$

$h = 100mm$

$d = 5mm$

$E = 20GPa$

$\gamma = 0.2$

$\varepsilon_0 = 120 \times 10^{-6}$

$\varepsilon_f = 7 \times 10^{-3}$
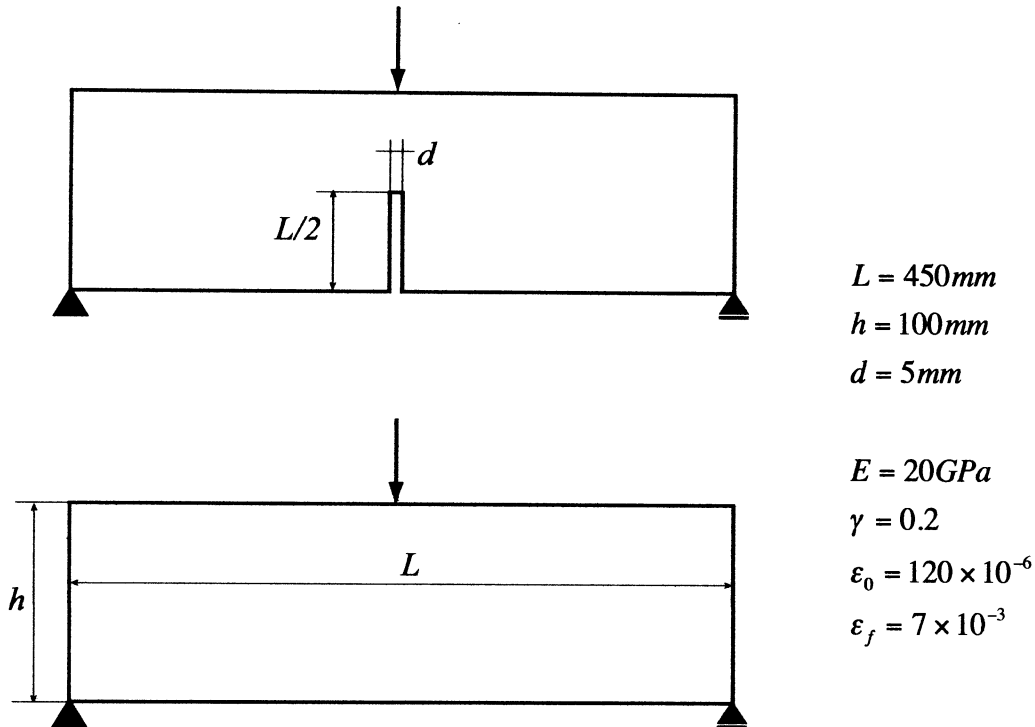
Figure 4.2 Three point bending of notched and unnotched beam

As expected, the results obtained from the local damage mechanics model show spurious mesh dependence in the post-peak stage of the simulation for both cases. The loading displacement curves for the notched beam and the unnotched beam are plotted in Figure 4.4 and Figure 4.5. It is shown that for a set of the fixed material properties, if the element size gets smaller, the loading peak reached is lower and so is the total dissipation energy (areas under the loading displacement curve). The post-peak behavior is totally mesh dependent and physically meaningless for both the notched beam and unnotched beam. For the notched beam test, the coarse mesh (5 mm) results show a loading-displacement curve that is closest to the experimental results.

(a) Mesh facts of notched beam
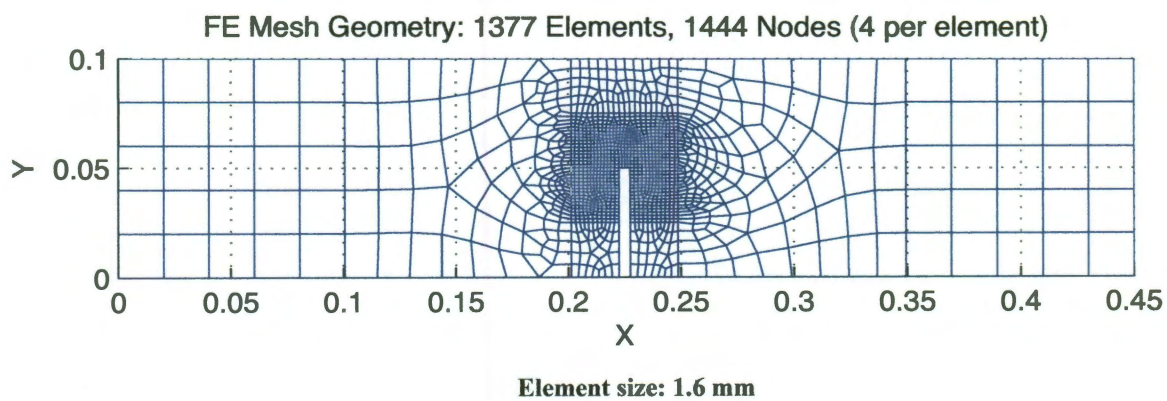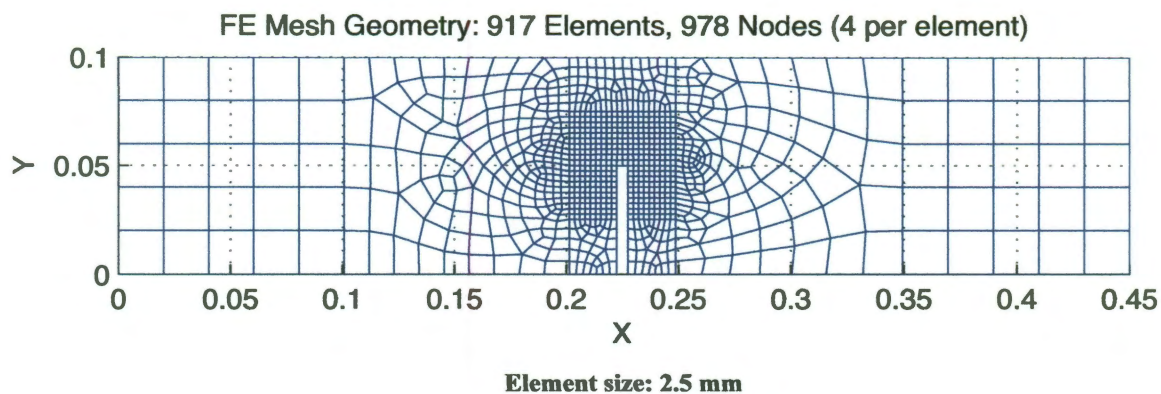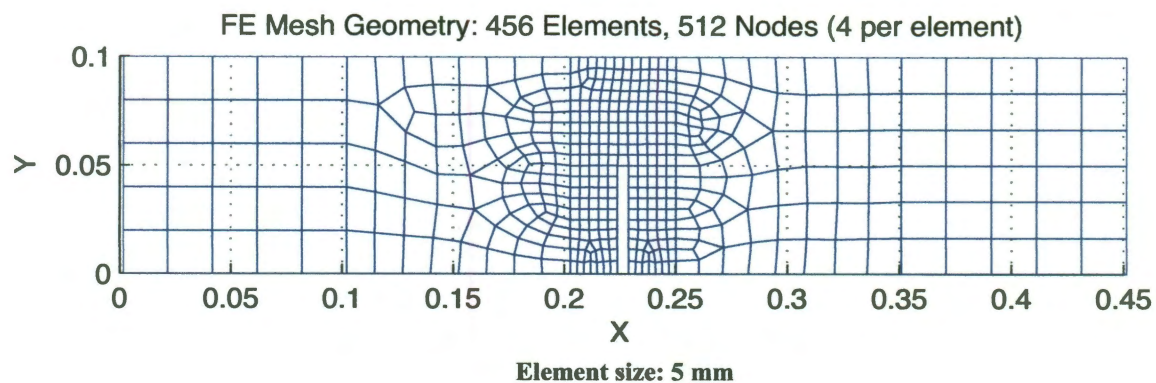
FE Mesh Geometry: 456 Elements, 512 Nodes (4 per element)

Element size: 5 mm

FE Mesh Geometry: 917 Elements, 978 Nodes (4 per element)

Element size: 2.5 mm

FE Mesh Geometry: 1377 Elements, 1444 Nodes (4 per element)

Element size: 1.6 mm

Figure 4.3 Beam unstructured Q4 mesh with different minimum element sizes, (a) Notched, (b) Unnotched

(b) Mesh facts of unnotched beam

FE Mesh Geometry: 157 Elements, 187 Nodes (4 per element)

Element size: 15 mm

FE Mesh Geometry: 426 Elements, 472 Nodes (4 per element)

Element size: 7.5 mm

FE Mesh Geometry: 752 Elements, 811 Nodes (4 per element)

Element size: 5 mm

Figure 4.3 Beam unstructured Q4 mesh with different minimum element sizes, (a) Notched, (b) Unnotched (Contd.)
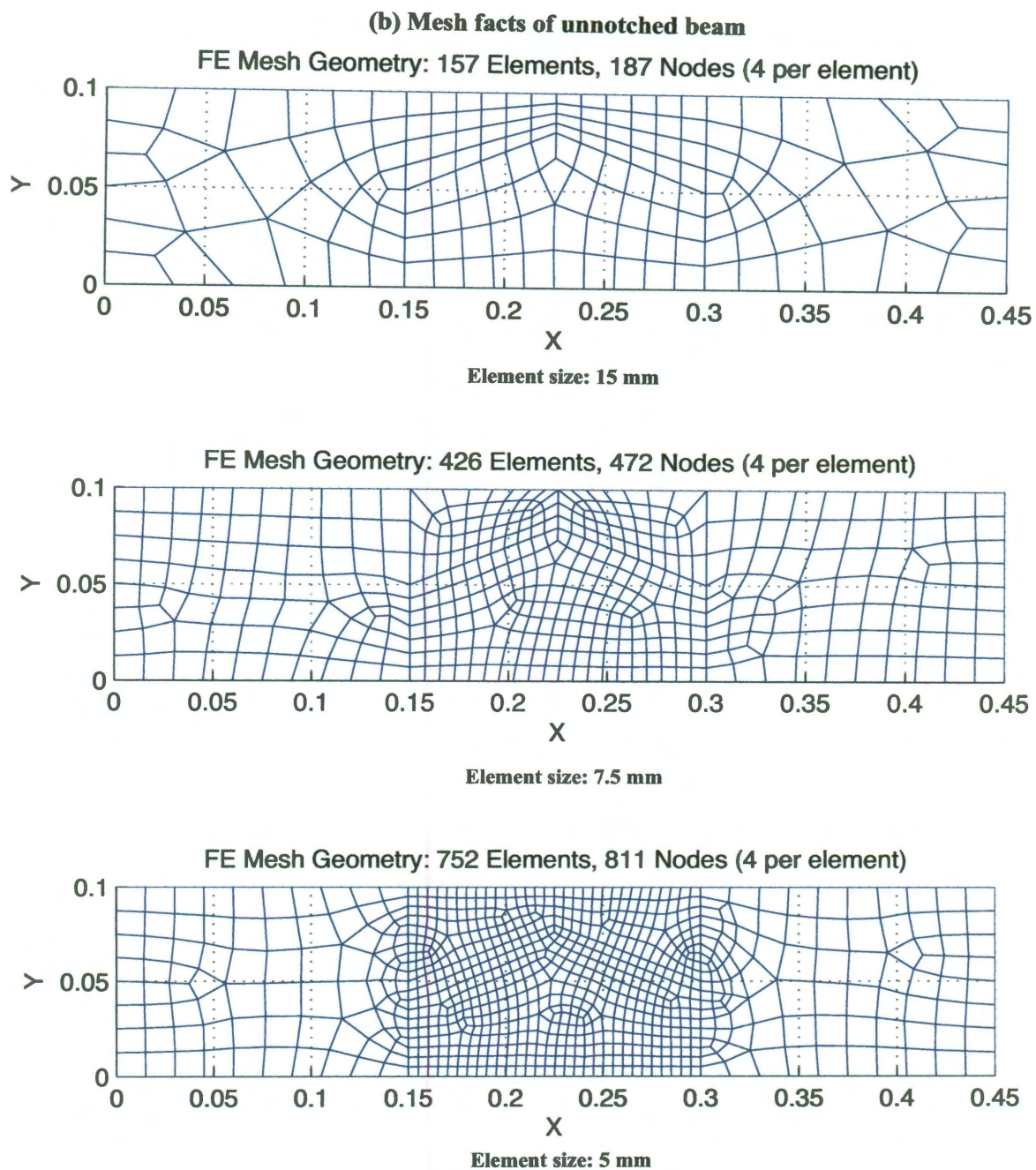
Loading – displacement curve for notched beam (Local)
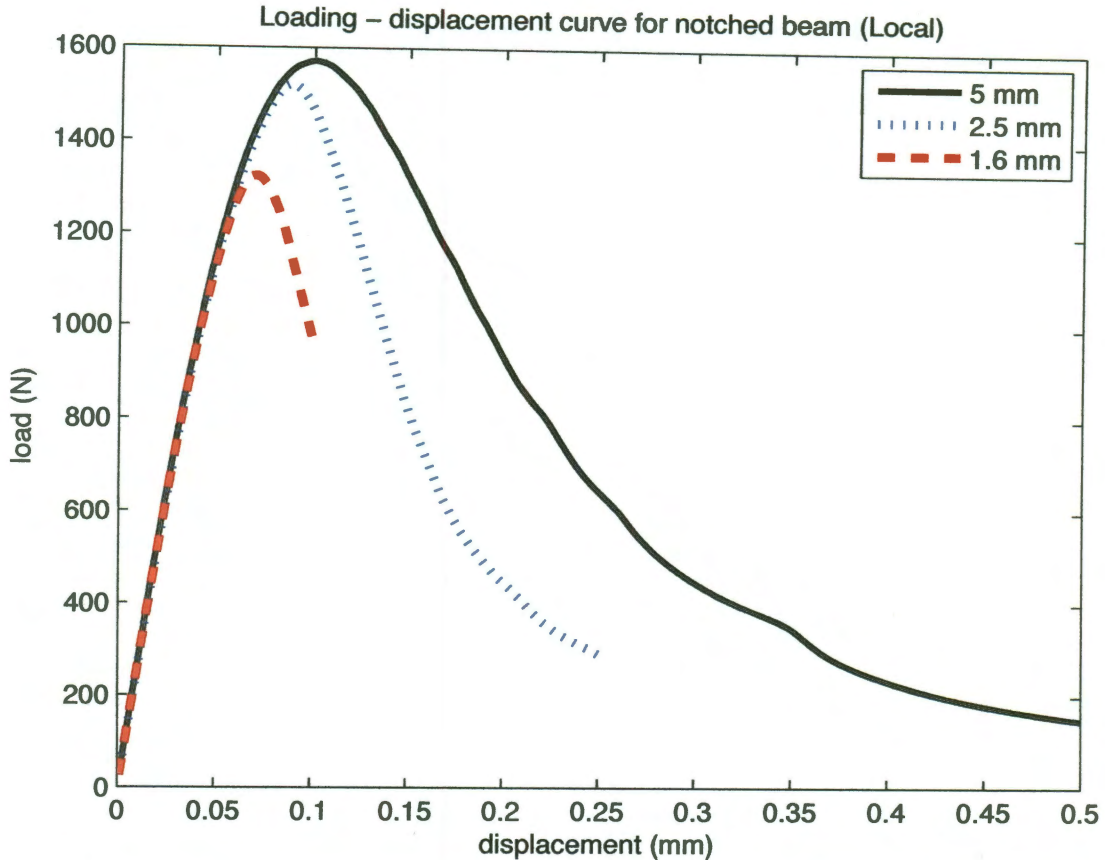
Figure 4.4 Loading-displacement curves of notched beam obtained from the local damage mechanics model

4.4.2. Nonlocal damage mechanics

The same three point bending experiments of the notched and unnotched beams are then simulated with the nonlocal formulation. The nonlocal formulation uses a strain gradient form as introduced in Section 4.2. The nonlocal equivalent strain is calculated and updated as in Figure 4.1. The exponential damage law used in the nonlocal tests is modified to calibrate the numerical results to the experimental results. Therefore, the fitted parameters are $\varepsilon_0 = 9.0e\text{-}5$ and $\varepsilon_f = 7e\text{-}3$. Since the strain gradient methods are used instead of the integral type methods, the length scales used are different from those

used by Jirasek. For integral type methods, the length scale is given as the cut-off radius R of the spatial weighting function. According to Jirasek (2007), it is assumed that $R = 4$ mm for the notched beam and $R = 8\ mm$ for the unnotched beam. In this study, the length scale l as defined in Eq.4.24 and Eq. 4.25, is set to be $2\ mm$ for the notched beam and $8\ mm$ for the unnotched beam. The choice of the material length scale l is made based on the calibration with the experimental results. Since this study focuses on showing the robustness and efficiency of the proposed technique in the implementation of nonlocal formulations, the question of the physical meanings of the length scales is not further discussed in this dissertation.
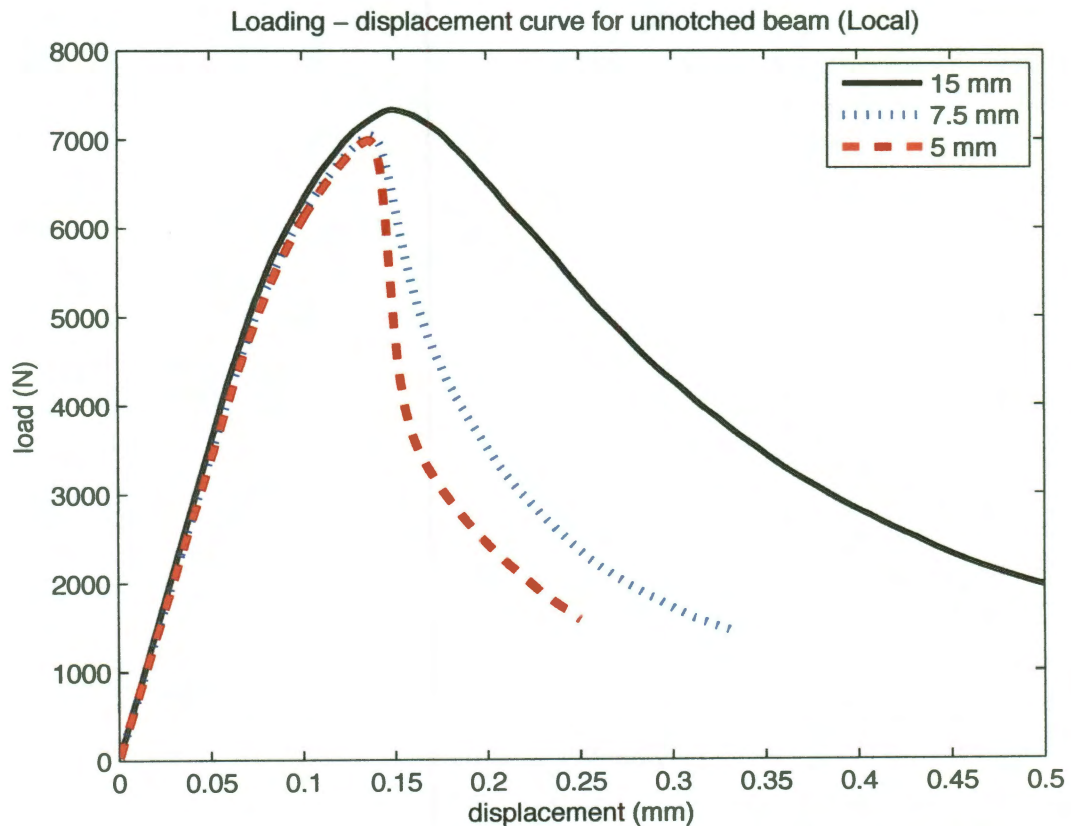
Figure 4.5 Loading-displacement curves of unnotched beam obtained from the local damage mechanics model

In the MODEL library, the elements used are set to be Q4 bilinear quadrilateral elements, therefore, the patches are constructed as bi-quadratic Q9 quadrilateral elements (user control *scp_deg_inc* 1). The gradient recovery method is chosen to be the nodal averaging process. The averages are only saved at the nodes of the parent element in each patch (user control *scp_center_only*).

Finally, the loading-displacement curves obtained from the nonlocal tests are plotted in Figure 4.6 for the notched beam case. The experimental results and Jirasek's result are also plotted in the same figure. It is seen that the regularized loading displacement curves behave similarly during post peak stage, the peak loads reached are almost the same regardless of the mesh sizes and are all converged to center area of the experimental results. The dissipation energy is also conserved for different mesh results. Compared to the experiments, the results obtained from this study are closer to the experimental data than Jirasek's result.

The unnotched beam's loading-displacement curves obtained from the nonlocal tests are plotted in Figure 4.7. The length scale $l = 8$ *mm* used for the strain gradient formulation is kept the same as the cut-off radius R used in Jirasek (2007). Again, the patch smoothed nonlocal finite element technique implemented in this study successfully presents a mesh independent loading-displacement curve for the unnotched beam simulation. As compared to the nonlocal integral formula, the strain gradient formula implemented here shows the similar results. However, as compared to Jirasek's result,

the simulation gives a higher peak loading value for the same length scale, but for different mesh refinements, the loading-displacement curves are quite uniform.
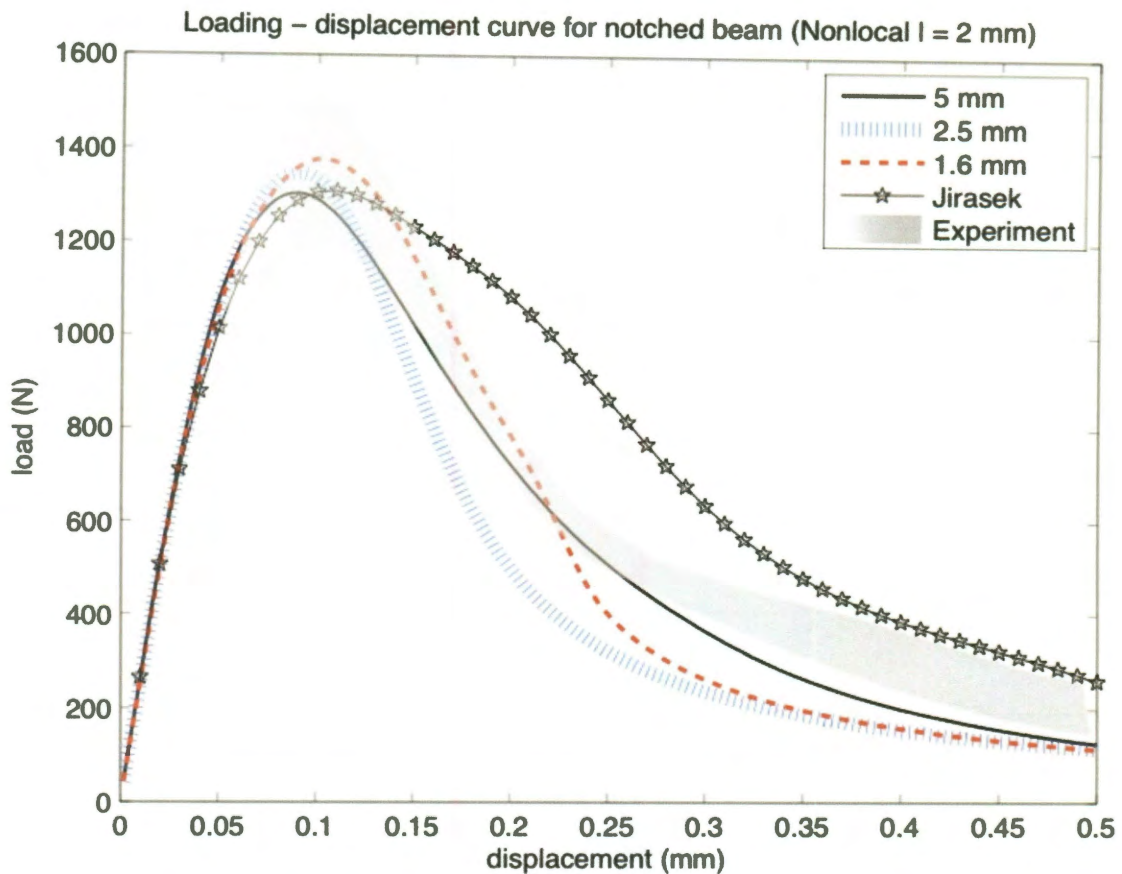
Figure 4.6 Loading-displacement curves of notched beam from the nonlocal damage mechanics model (*l = 2mm*)

4.4.1. Comparison of the local and nonlocal damage contours

The exaggerated deformed meshes are plotted in Figure 4.8 for the notched beam and in Figure 4.9 for the unnotched beam. It is seen that the nonlocal strain gradient models implemented give a proper localized deformation for both beams. The final damage

contour at the middle area of the notched and unnotched beams, shown as the dashed box

in Figure 4.8 and Figure 4.9, are plotted through Figure 4.10 to Figure 4.15.
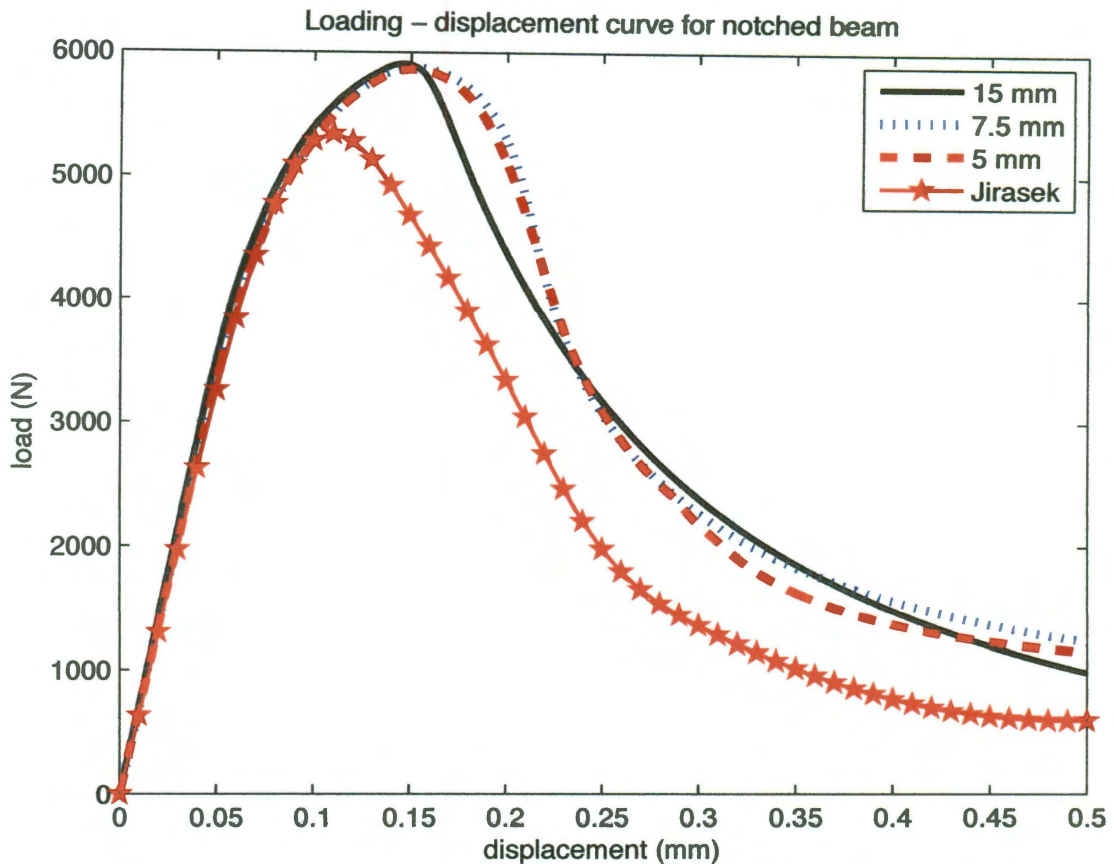
Figure 4.7 Loading-displacement curves of the unnotched beam from the nonlocal damage mechanics model ($l = 8mm$)

The damage density contours of the notched beams for the three different meshes are

shown in Figure 4.10-4.12. The contour plots on the left are from the local model while

the contour plots on the right are from the nonlocal model. It is seen that the evolution of

the damage density is localized to single elements in the mesh for the local model. The

damage area initiates from the stress concentration point at the notch and is restricted to a

narrow strip, of which the width is limited to the size of a single element. The damage area can not propagate properly to adjacent elements when using a local formulation.

The same damage density contour plots for the unnotched beam are plotted in Figure 4.13-4.15. Again, the damage density contours obtained from the local model are plotted on the left and those from the nonlocal model are on the right. For unnotched beams, the damage initiates at the bottom edge of the beam and is localized into a strip-like area that is limited to the size of a single element from the local damage model. The loss of the ellipticity again causes the localized damage area to fail to propagate properly, which explains the occurrence of the mesh dependent loading-displacement curves shown in Figure 4.4 and Figure 4.5.

Next consider the final damage density contours obtained from the nonlocal model as shown on the right in Figure 4.10-4.12 for the notched beam and Figure 4.13-4.15 for the unnotched beam. The final damage areas obtained are all very similar for difference mesh sizes. The damage area is no longer localized to the size of a single element size but is now localized to certain areas of a similar size.

4.4.2. Recovered strain gradient results

The Laplacian of the equivalent strain can be easily visualized with the nodal averaged results. It would be helpful to see the one-dimensional case before plotting the Laplacian surface in two-dimensional space. In one-dimensional case, as shown in

Figure 4.16, a spike shaped continuous function $f(x)$ is shown in solid line, while its Laplacian is obtained as the dashed line. Typically, the Laplacian is negative at the peak of the spike and is positive at the diminishing bounds of the spike.
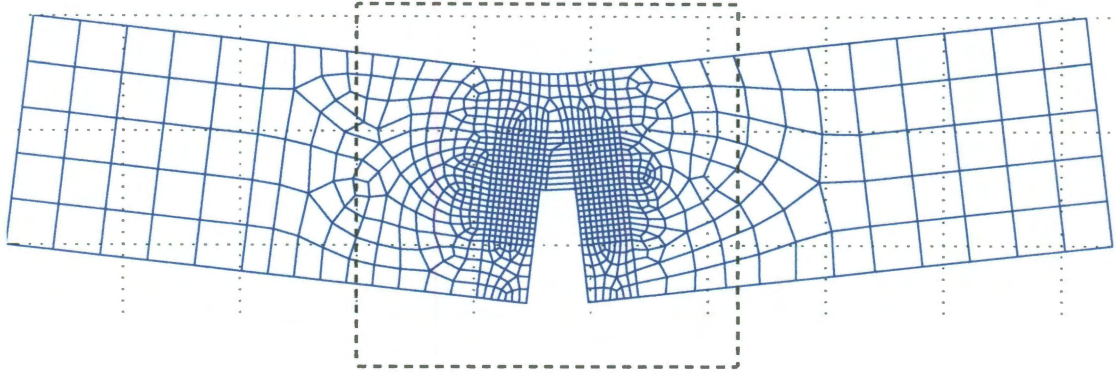
Figure 4.8 Exaggerated deformed mesh - notched beam from nonlocal model
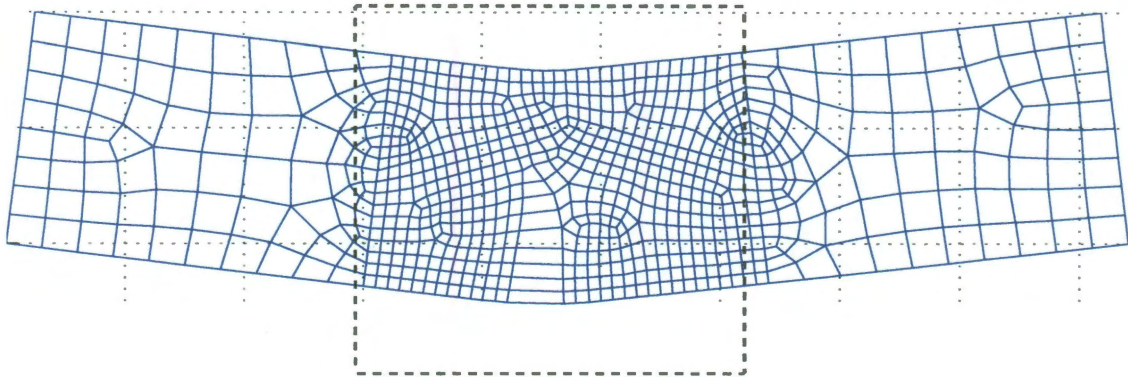
Figure 4.9 Exaggerated deformed mesh - unnotched beam from nonlocal model

For the nodal averaging recovery method, the recovered Laplacian of the equivalent strain increment is plotted in Figure 4.17 for the final loading stage. To avoid redundancy, the recovered Laplacian is plotted in only one mesh resolution for each case.

The contours of the localized normal strains in the x-direction are also plotted. As indicated from a one-dimensional case, it is noted as expected that the Laplacian is positive at the edge and is negative at the center of the localized strain zone. The SCP nodal averaging process used to recover the second derivatives of the equivalent strain creates a good approximation to the Laplacian profile, thus helps the proper propagation of the localized zone and keeps the ellipticity of the original problem.
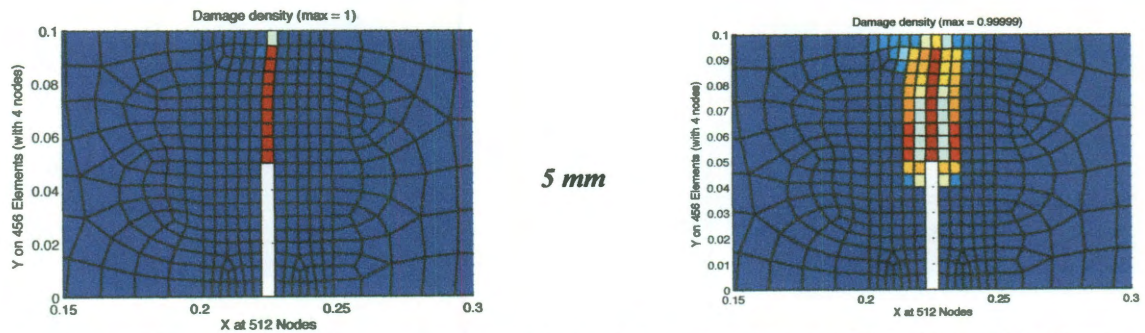
Figure 4.10 Notched beam damage contour (element size = 5mm): local (left), nonlocal *l* = 2mm (right)
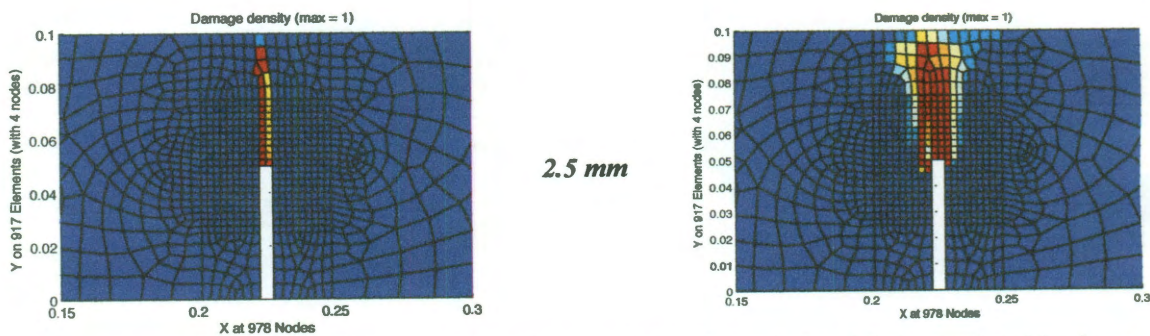
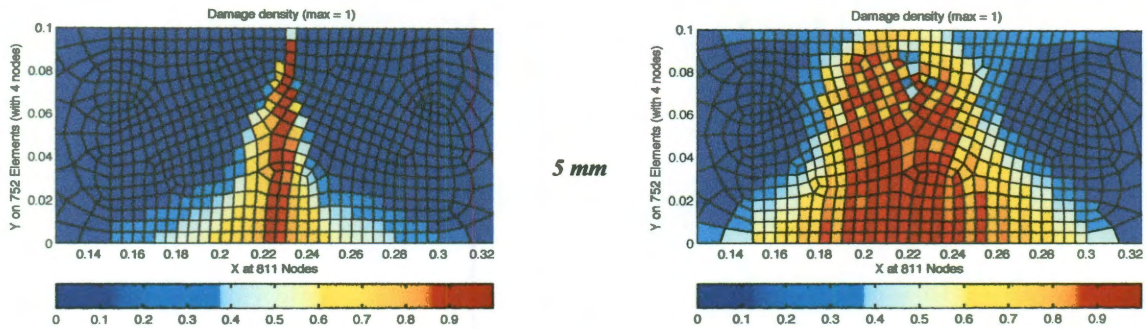**Figure 4.11 Notched beam damage contour (element size = *2.5mm*): local (left), nonlocal *l* = *2mm* (right)**
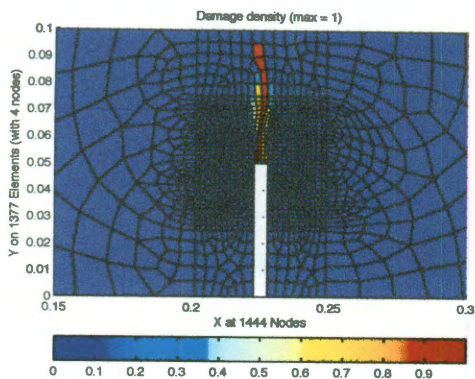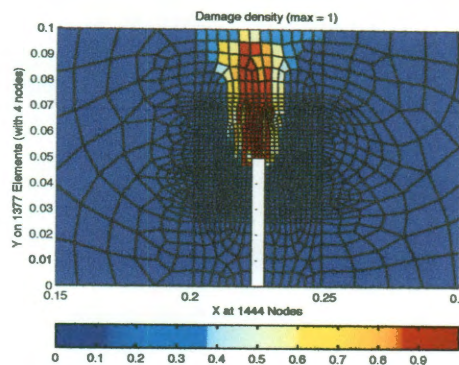
Figure 4.12 Notched beam damage contour (element size = *1.6mm*): local (left), nonlocal *l* = *2mm* (right)
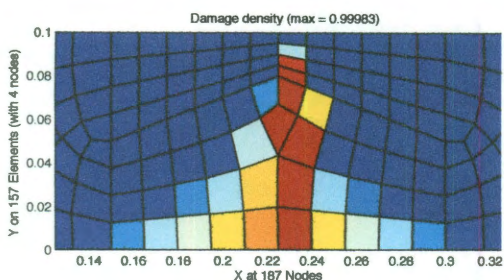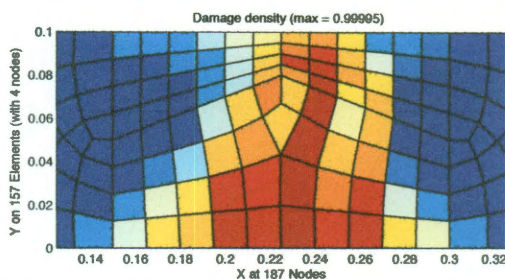
Figure 4.13 Unnotched beam damage contour (element size = 15mm): local (left), nonlocal *l* = 8mm (right)
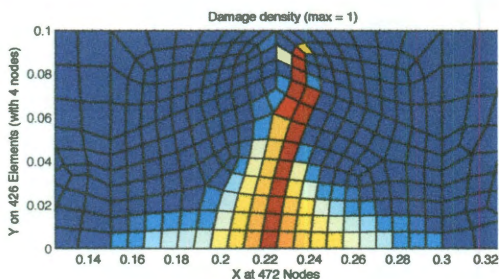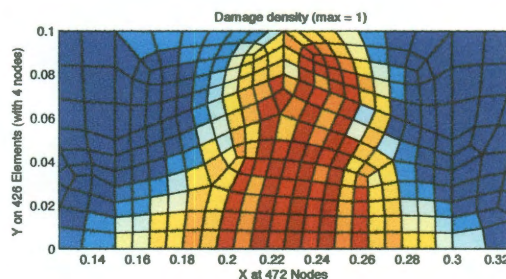
Figure 4.14 Unnotched beam damage contour (element size = 7.5mm): local (left), nonlocal *l* = 8mm (right)

Figure 4.15 Unnotched beam damage contour (element size = 5mm): local (left), nonlocal l = 8mm (right)

4.4.3. Choices of the recovery options

So far, the equivalent strain derivatives recovered from the SCP process are all evaluated from the first recovery option, which is the recovery by the nodal averages. In next example the equivalent strain derivatives are recovered only at the parent element of each patch. This choice is regarded as the most efficient and reliable way to recover the strain gradients for the nonlocal damage mechanics problem simulated here. It avoids the over smoothing caused by the nodal averaging process and also supplies a legitimate estimation of the Laplacian required.
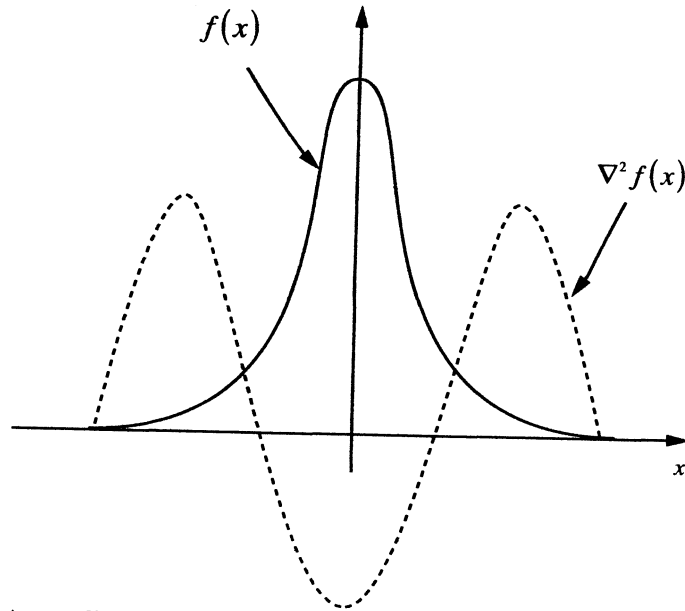
Figure 4.16 A one-dimensional continuous function and its Laplacian (Dorgan 2006)

However, remember from Chapter 3, a second recovery option is also proposed as to recover the equivalent strain derivatives directly at the quadrature points of the parent elements from the least square fit. This option is also tested here. For the notched beam, for the same mesh size, the two options give similar loading-displacement curves as shown in Figure 4.17. While for the unnotched beam test of the same mesh size (*15mm*), the second option shows a loading-displacement curve with a more gradual slope as shown in Figure 4.18. This indicates that the direct recovery by LSF method may introduce an over-smoothed gradient recovery process for a regular geometric problem without any stress concentration point. This might be caused by using a too coarse mesh for a regular domain where no stress concentration points exist for damage initiation. That also explains why the two recovery options give similar results for the bending of a notched beam while different ones for the bending of an unnotched beam. Therefore, the nodal averages method seems to be more reliable even when the mesh is coarse.

However, the choices of the recovery options are problem dependent. A further study on the LSF method is conducted in Chapter 5 for the strain gradient type plasticity problems.
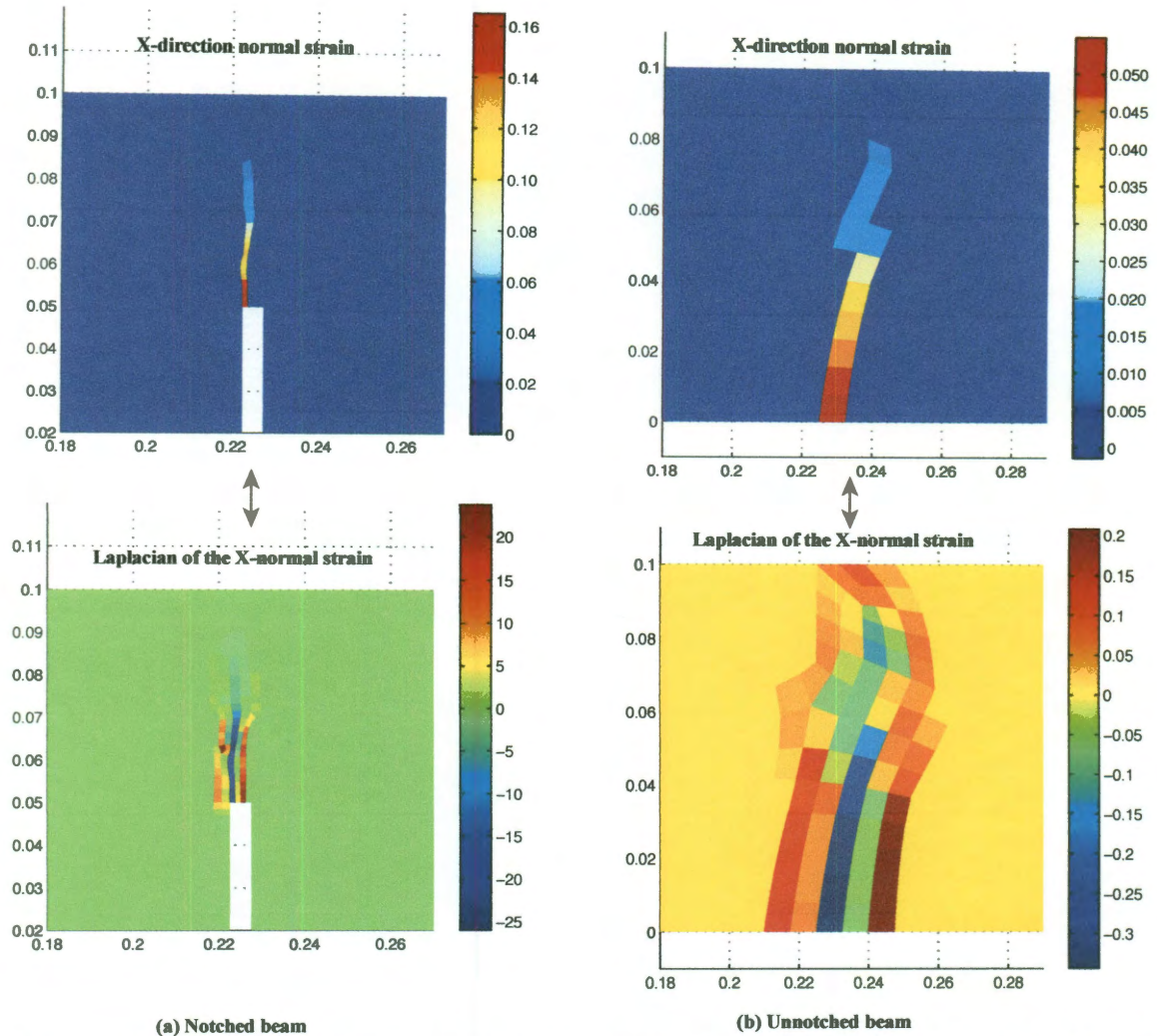

(a) Notched beam   (b) Unnotched beam

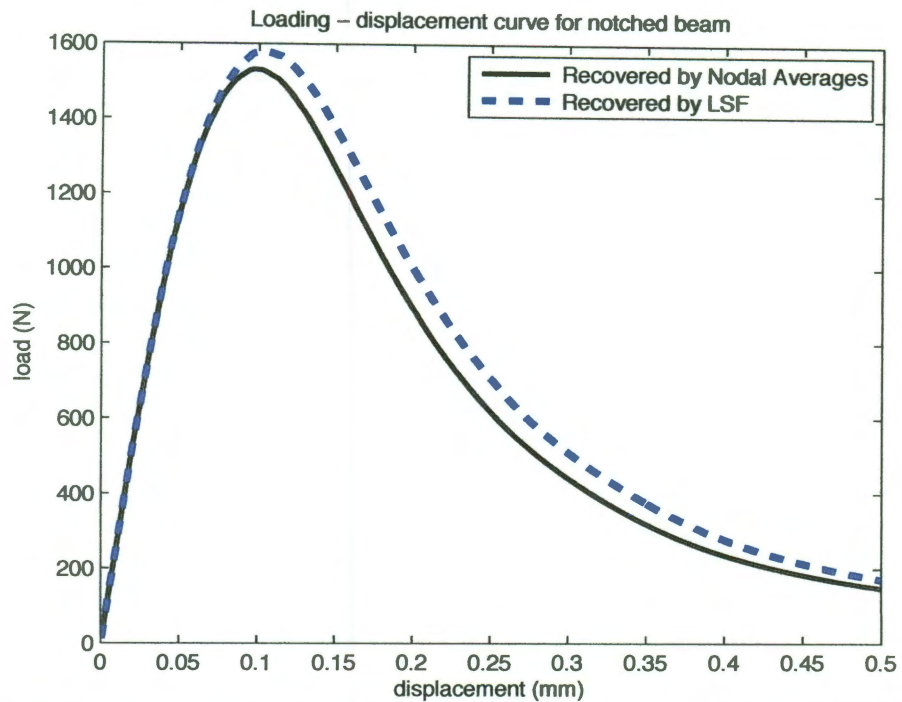**Figure 4.17 Equivalent strain and its recovered Laplacians: (a) Notched beam (b) Unnotched beam**

Figure 4.18 Load-displacement curves obtained from nodal averaged and direct least square fit recoveries – notched beam
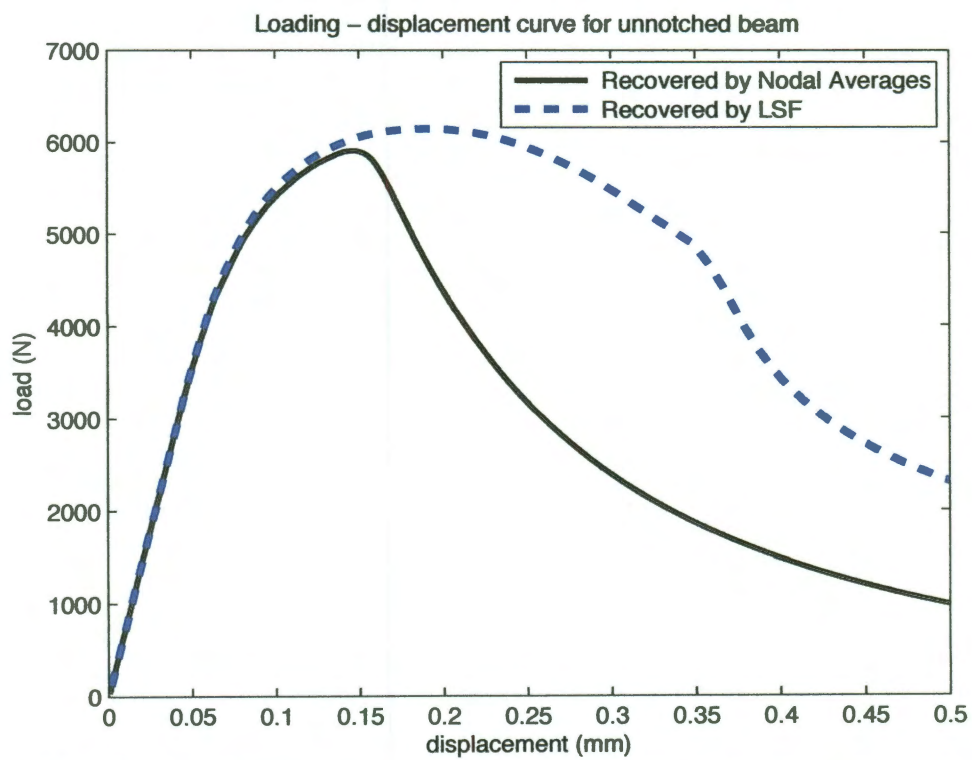

Figure 4.19 Loading-displacement curves obtained from nodal averaged and direct least square fit recoveries - unnotched beam

4.1. Discussion

The algorithm for the implementation of a strain gradient type nonlocal damage mechanics was developed and tested. Unstructured meshes were constructed and tested. The effectiveness of the SCP patches for the recovery of the second derivatives of the equivalent strains was proven. The numerical results for a three point bending problem for both a notched and unnotched beam were obtained from the proposed algorithm and compared to the experimental results as well as Jirasek's results. The nonlocal models implemented yield mesh independent loading-displacement curves. The dissipation energy or the areas under the loading-displacement curves are quite uniform regardless of the mesh resolution tested. The peak stress values obtained are all within the experimental range. The unnotched beam shows a more mesh independent result than that of the notched beam.

The nonlocal damage models evaluated only involve the recovery of the second derivatives of the equivalent strain. Also, the unstructured mesh consists of only one type of element, the linear quadrilateral elements (Q4). Multiple types of elements and higher order C^0 elements are not tested for the algorithm. These tests will be conducted in the Chapter 5 for the strain gradient plasticity problems.

For the nonlocal damage mechanics model, the recovery by the LSF method shows overly smoothed effects, judging from the loading-displacement curves, when the mesh is too coarse and no stress concentration points exist to initiate damage. The performance

of the two recovery options, Nodal Averages and LSF, is not fully compared here and further studies are conducted in Chapter 5.

Chapter 5

Nonlocal strain gradient plasticity via SCP

5.1. Review on nonlocal strain gradient plasticity

5.1.1. Local softening plasticity

The rate-independent elasto-plastic problem is first reviewed in this section assuming a linear isotropic softening behavior, where the tangential modulus $h < 0$. The rate form of the stress-strain relationship is given first then is integrated to obtain the incremental form for the numerical implementation.

Applying the standard additive decomposition of the total strain rate $\dot{\varepsilon}$ into its elastic part $\dot{\varepsilon}_e$ and the plastic part $\dot{\varepsilon}_p$, the Cauchy stress rate $\dot{\sigma}$ is given as

$$\dot{\sigma} = D_e : \dot{\varepsilon}_e = D_e : \left(\dot{\varepsilon} - \dot{\varepsilon}_p \right) \tag{5.1}$$

Integrate Eq. 5.1 from time t_n to t_{n+1} gives the incremental constitutive equation as

$$\Delta\sigma = D_e : \Delta\varepsilon_e = D_e : \left(\Delta\varepsilon - \Delta\varepsilon_p\right) \qquad (5.2)$$

where $\Delta\sigma = \int_{t_n}^{t_{n+1}} \dot{\sigma} dt$, D_e is the elastic stiffness tensor. The yield function is defined as a

Von-Mises ($J2$) type as,

$$f = \sqrt{3J_2} - Y = 0 \qquad (5.3)$$

with $J_2 = \dfrac{1}{2}\tau : \tau$, where τ is the deviatoric part of the Cauchy stress tensor

$$\tau = \sigma - pI \; , \; p = \frac{1}{3}\left(\sigma_{11} + \sigma_{22} + \sigma_{33}\right) \qquad (5.4)$$

Here, Y is the yield strength that is a function of the initial yield strength σ_0 with a linear

isotropic softening behavior,

$$Y = \sigma_0 + hp \qquad (5.5)$$

where $h < 0$ is the softening modulus, and p is the total equivalent plastic strain.

$$p = \frac{1}{2}\varepsilon_p : \varepsilon_p \qquad (5.6)$$

The flow rule assumed is the associate plasticity,

$$\dot{\varepsilon}_p = \dot{\lambda}n, \; n = \frac{\partial f}{\partial \sigma} \qquad (5.7)$$

where n is the normal direction of the yield surface f. The growth of the plastic strain

satisfies the Kuhn-Tucker conditions as

$$\dot{\lambda} \geq 0 \quad f \leq 0 \quad \dot{\lambda}f = 0 \qquad (5.8)$$

In Voigt notation, the incremental consistency condition is given as

$$\Delta f = \{n\}^T \{\Delta\sigma\} - h\Delta\lambda = 0 \qquad (5.9)$$

with $\Delta\varepsilon_p = \Delta\lambda$, substituting Eq.5.2 into Eq.5.9 gives,

$$\Delta\lambda = \frac{\{n\}\{n\}^T[D_e]}{h+\{n\}^T[D_e]\{n\}}\{\Delta\varepsilon\} \tag{5.10}$$

Therefore, substituting Eq.5.10 into Eq.5.2 gives,

$$\{\Delta\sigma\} = [D_{ep}]\{\Delta\varepsilon\} \tag{5.11}$$

where $[D_{ep}]$ is the consistent constitutive matrix,

$$[D_{ep}] = [D_e] - \frac{[D_e]\{n\}\{n\}^T[D_e]}{h+\{n\}^T[D_e]\{n\}} \tag{5.12}$$

5.1.2. Nonlocal strain gradient plasticity

The local form of a linear isotropic softening elasto-plasticity model is introduced. Next, the strain gradient enhanced softening elasto-plasticity model is developed. The general idea of strain gradient enhancement is to introduce the gradient terms of the equivalent plastic strain into the yield function. This has been regarded as the most efficient and convenient way to regularize the softening problem. The strain gradient terms automatically disappear in a homogeneous field but they have a huge influence in the areas where high strain gradients are present. Numerically speaking, for each incremental or iterative step, a gradient dependent consistency equation is solved which requires the evaluation of the strain derivatives. Two gradient dependent plasticity theories are introduced below.

The first kind of the strain gradient enhanced plasticity models suggests that the strain gradient dependent plasticity model should incorporate the implicit averaged strain. Therefore, the Laplacian of the plastic strain is introduced into the yield function. De Borst (1996) and Engelen (2003) are among the pioneers for the research on this type of model. De Borst's strain gradient model is introduced as below. The gradient dependent yield function is

$$f = \sqrt{3J_2} - \sigma_0 - h\tilde{p} \tag{5.13}$$

where $\tilde{p}$ is the nonlocal equivalent plastic strain. The consistency condition is obtained as

$$\Delta f = \{n\}^T \{\Delta\sigma\} - h\Delta\tilde{\lambda} = 0 \tag{5.14}$$

where, $\Delta\tilde{\lambda}$ is the nonlocal effective plastic strain multiplier. The first kind of gradient plasticity model is developed to explicitly express $\Delta\tilde{\lambda}$ as

$$\Delta\tilde{\lambda} = \Delta\lambda + l^2 \nabla^2 \Delta\lambda \tag{5.15}$$

Substitute Eq. 5.2 and Eq.5.15 into Eq. 5.14, it gives,

$$\Delta\lambda + \left(\frac{hl^2}{\{n\}^T[D_e]\{n\}}\right)\nabla^2\Delta\lambda = \left(\frac{\{n\}^T[D_e]}{\{n\}^T[D_e]\{n\}+h}\right)\{\Delta\varepsilon\} \tag{5.16}$$

The second kind of the gradient enhanced plasticity models is summarized as those developed by Aifantis (1984). He similarly advocates that the yield function greatly depends on gradients of the equivalent plastic strain. However, he introduces not only the Laplacian but also the first derivatives of the plastic strain. The nonlocal strain gradient plastic strain multiplier $\Delta\tilde{\lambda}$ is expressed as

$$\Delta\tilde{\lambda} = \Delta\lambda + l|\nabla\Delta\lambda| + l^2\nabla^2\Delta\lambda \tag{5.17}$$

Substituting Eq.5.17 into Eq.5.14 gives,

$$\Delta\lambda + \left(\frac{hl}{\{n\}^T[D_e]\{n\}}\right)|\nabla\Delta\lambda| + \left(\frac{hl^2}{\{n\}^T[D_e]\{n\}}\right)\nabla^2\Delta\lambda = \left(\frac{\{n\}^T[D_e]}{\{n\}^T[D_e]\{n\}+h}\right)\{\Delta\varepsilon\}$$

(5.18)

5.2. Strain gradient evaluation from SCP

The implementation of the strain gradient type plasticity models with the super-convergent patches is quite similar to that is discussed for the nonlocal damage mechanics (Chapter 4). Two issues need to be clarified here. First, it should be noticed that Eq. 5.16 and Eq. 5.18 are both implicit type equations. As discussed in the last chapter, a patch least square fitting process for the equivalent strain gives the identical strain derivative evaluations for both implicit forms and explicit forms. Therefore, Eq.5.16 and Eq.5.18 can be solved explicitly in a least square fit sense, and then the nodal solutions for the equivalent strains are utilized to evaluate the strain derivatives. The equivalent strains to be sampled at the quadrature points are the right hand sides of the Eq.5.16 and Eq.5.18 as in a general sense,

$$\Delta\hat{\varepsilon} = \left(\frac{\{n\}^T[D_e]}{\{n\}^T[D_e]\{n\}+h}\right)\{\Delta\varepsilon\}$$

(5.19)

The local fluxes are approximated by the patch element as

$$\Delta\lambda = [H(x,y)]\{d\}$$

(5.20)

where $\{d\}$ is obtained from the local least square fit,

$$\min\|\Delta\lambda - \Delta\hat{\varepsilon}\|$$

(5.21)

After the nodal solutions of the equivalent strain $\{d\}$ are obtained, the norm of the first order strain derivatives is evaluated as

$$|\nabla\Delta\lambda| = \left|\left(\left[\frac{\partial H(x,y)}{\partial x}\right]+\left[\frac{\partial H(x,y)}{\partial y}\right]\right)\{d\}\right|$$

(5.22)

The second derivatives are obtained as

$$\nabla^2\Delta\lambda = \left[\nabla^2 H(x,y)\right]\{d\}$$

(5.23)

where, $\left[\nabla^2 H(x,y)\right]$ is defined in Eq. 4.34.

Again, the local equivalent strain defined in Eq.5.19 are calculated and stored through subroutines POST_PROCESS_GRADS and LIST_ELEM_FLUXES in the random access file *U_SCPR*. The length scale used to recover the nonlocal strains are equivalent to the coefficients appearing in Eq.5.16 and Eq.5.18 as follows,

De Borst:

$$\Delta\lambda + \tilde{l}\nabla^2\Delta\lambda = \left(\frac{\{n\}^T[D_e]}{\{n\}^T[D_e]\{n\}+h}\right)\{\Delta\varepsilon\}$$

(5. 24)

with $\tilde{l} = \left(\frac{hl^2}{\{n\}^T[D_e]\{n\}}\right)$

Aifantis:

$$\Delta\lambda + l_1|\nabla\Delta\lambda| + l_2\nabla^2\Delta\lambda = \left(\frac{\{n\}^T[D_e]}{\{n\}^T[D_e]\{n\}+h}\right)\{\Delta\varepsilon\}$$

(5. 25)

with $l_1 = \left(\dfrac{hl}{\{n\}^T [D_e]\{n\}} \right)$ and $l_2 = \left(\dfrac{hl^2}{\{n\}^T [D_e]\{n\}} \right)$

The difference between the two strain gradient enhanced plasticity models is whether the first derivative terms of the plastic strain multiplier is to be recovered. In the MODEL code, this choice is achieved by the input control keyword *aifantis*, which refers to the models where the first derivative terms are also need to be recovered. The MODEL code by default only considers the Laplacian of the plastic multiplier. The flow chart for the nonlocal strain gradient type plasticity problem is developed in Figure 5.1.

5.3. Shear band simulation

A shear band is known as a highly localized plastic zone that generally follows a straight line. This problem is one of the most studied cases for the strain gradient plasticity theory. To illustrate the robustness and efficiency of the strain gradient SCP recovery technique in its application to a nonlocal strain gradient plasticity problem, a shear band compression problem is again studied here.

A two-dimensional plane strain problem of a concrete plate in axial compression is simulated. The plate is compressed by two smooth rigid planes. One point on either the upper edge or the bottom edge was fixed to avoid rigid body motion in the horizontal direction. The plate geometry, boundary conditions and material properties are shown in Figure 5.2. A weakened area with slightly lower yield strength is assigned at the right

bottom corner of the plate to initiate the shear band from that location. A vertical

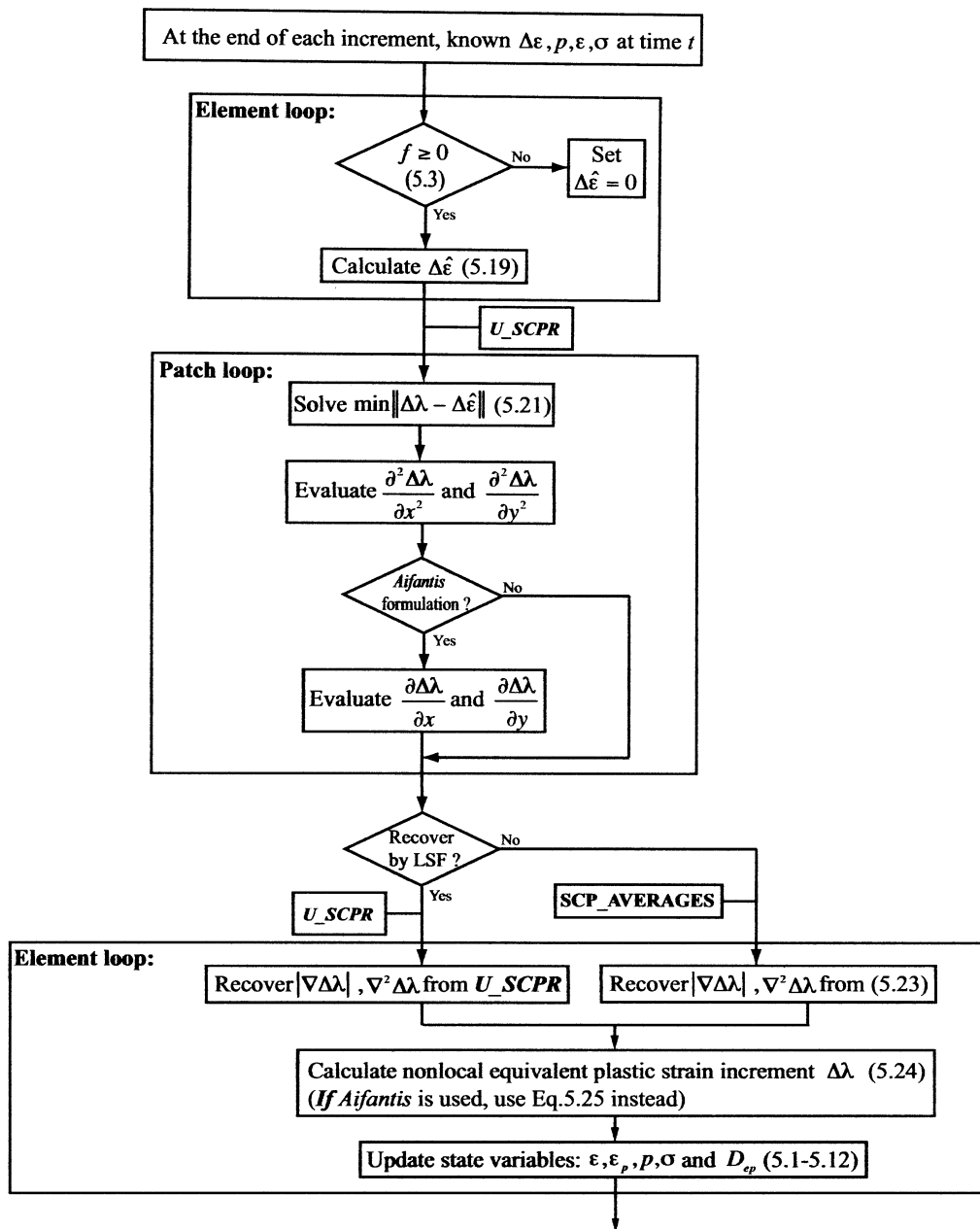displacement is applied on the top edge of the plate of $v = 0.15$ mm.

Figure 5.1 Flow chart of strain gradient plasticity via SCP

5.3.1. Analysis with linear C^0 elements

The elements simulated first were linear T3 triangular elements, which have zero second derivatives. The patches constructed have one order higher interpolations, and thus are complete quadratic T6 triangular elements. In order to get enough sampling points for the SCP process, three quadrature points are used for each element. Two structured meshes with 24×48 (coarse), 60×120 (fine) elements, as shown in Figure 5.3, are investigated.

$v = 0.15\ mm$

$B = 60\ mm$

$H = 120\ mm$

Thickness: T = 1 mm

Weakened square W = 10 mm

Young's modulus:
$$E = 2.0 \times 10^{10}\,Pa$$
Poisson's ratio:
$$v = 0.49$$
Initial yield stress:
$$\sigma_{y0} = 2.0 \times 10^{7}\,Pa$$
Initial yield stress:
$$h = -2.0 \times 10^{9}\,Pa$$

Weakened area:
$$\sigma_{y0} = 1.8 \times 10^{7}\,Pa$$
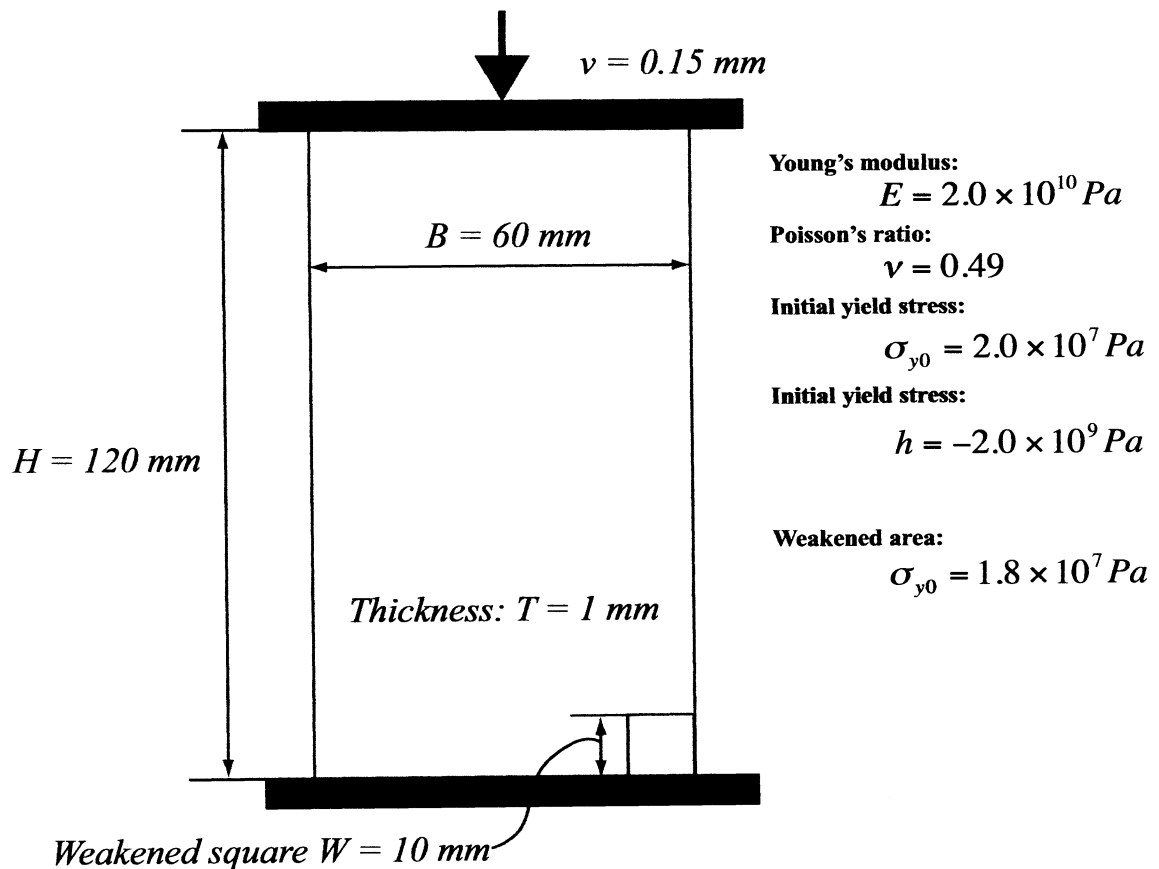
Figure 5.2 A plate in axial compression

The amplified deformed mesh obtained from the local plasticity models are plotted in Figure 5.4 on the next page. It is seen that the shear band takes as small an area as possible in the mesh, and is limited to the element size. The results are mesh dependent and thus are of little value to us.
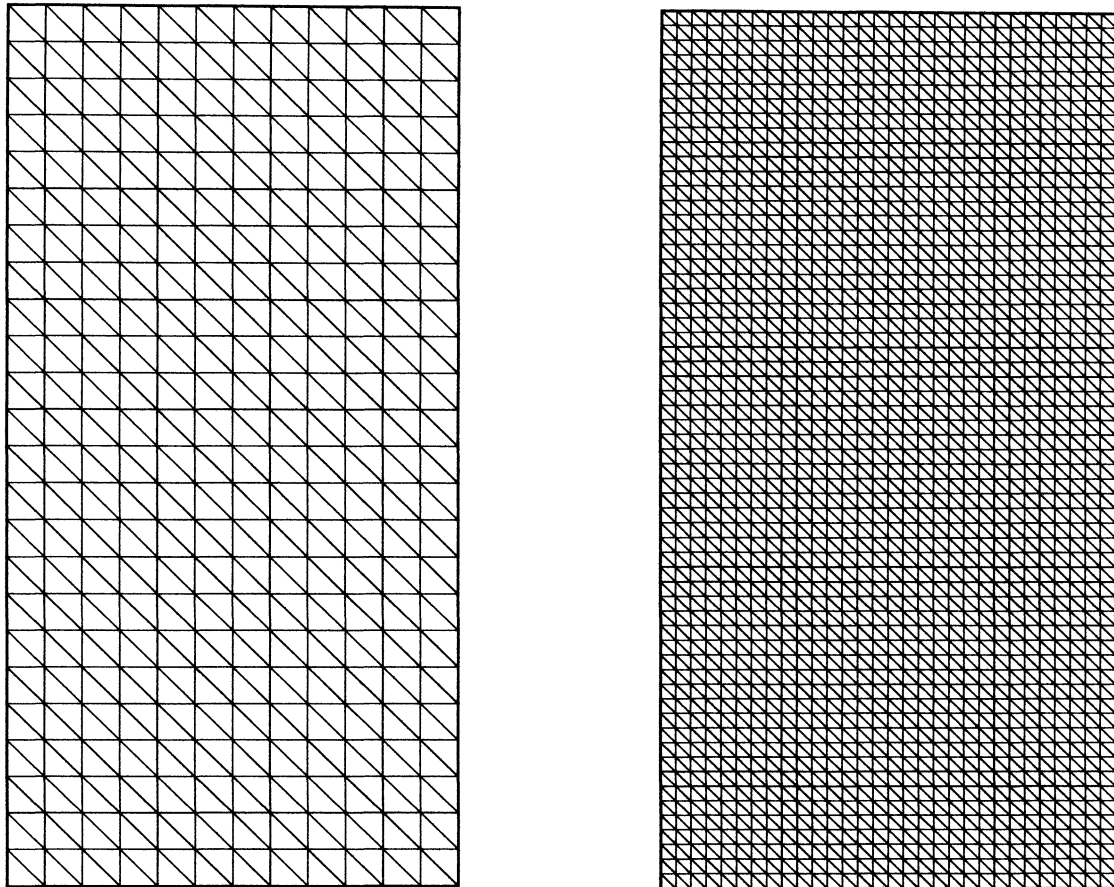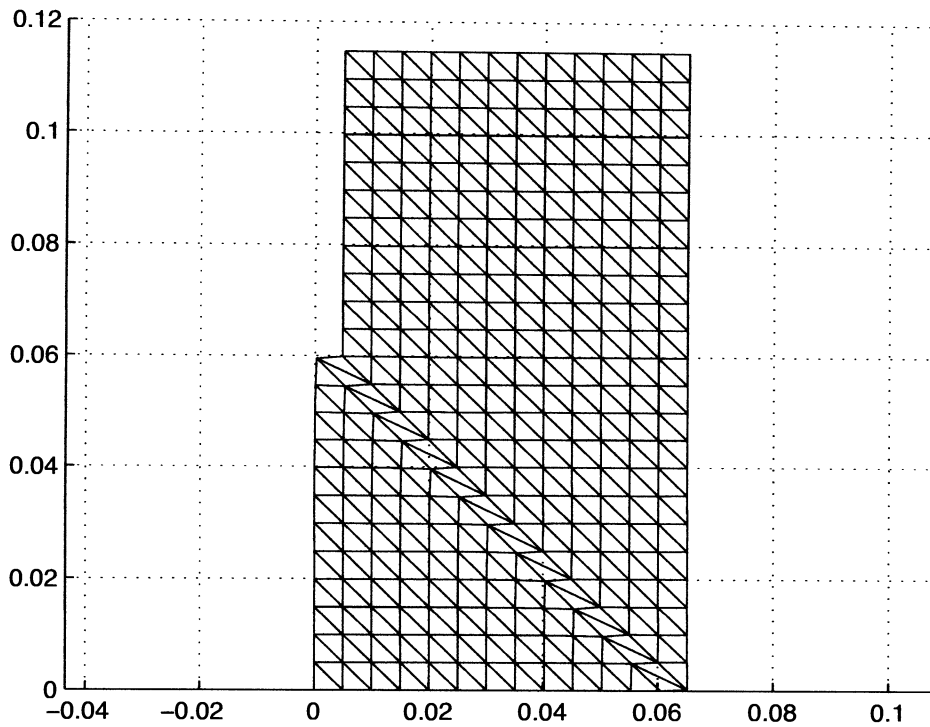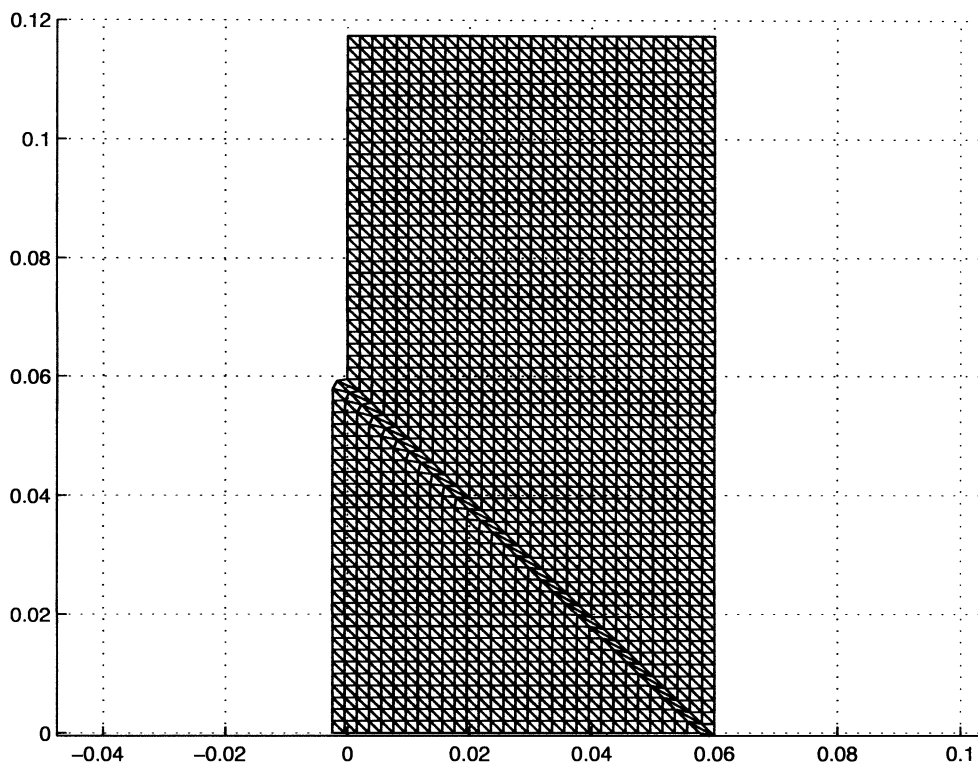

Figure 5.3 Coarse (24x48) and fine (60x120) T3 meshes

(1) De Borst's nonlocal model

Next, the same problem is studied utilizing nonlocal models. The first nonlocal strain gradient plasticity model evaluated only includes the Laplacian of the strain in the yield function, which is same as the model developed by de Borst (1996). The SCP is

(a) Deformed coarse mesh

(b) Deformed fine mesh

Figure 5.4 Deformed mesh obtained from local plasticity model: (a) coarse mesh and (b) fine mesh

only utilized to recover the second derivatives of the equivalent strain, as are used previously for the nonlocal damage models.

Both second derivative recovery methods are investigated. The direct recovery by least square fit of the equivalent strain at the integration points within the patch shows better results. Compared to the local model results, the shear band is no longer localized to a single element in the mesh, but localized to a finite width that is highly coupled to the length scale l. The length scales used are calibrated from the experimental results from Pamin (1994), where the material length scale of concrete is around *2 mm* to *5 mm*. Therefore, in order to show the size effects controlled by the length scales, shear bands are simulated for the same fine mesh, but with the length scales varying from *2 mm*, *3 mm* to *4 mm*. Figure 5.5 shows the equivalent plastic strain contour obtained from the directly recovery of the strain derivatives by least square fit. It shows that the width of the shear band also varies in the same trend as the length scale does.

The nodal averages of the equivalent strain recovery option were also evaluated. The final shear bands obtained for that option are plotted in Figure 5.6 for both the coarse and fine meshes. The length scale $l = 5$ *mm* is kept the same for both meshes. It also shows a shear band with a finite bandwidth. The equivalent strain contour of the fine mesh shows an oscillating contour profile that would be expected from a plasticity model that includes the Laplacian terms, see Figure 4.16 for the one-dimensional case. The final Laplacian of the plastic strain multiplier recovered by the nodal averaging process is plotted in Figure

5.7. The Laplacian of the plastic strain multiplier becomes more oscillatory when the mesh is refined.
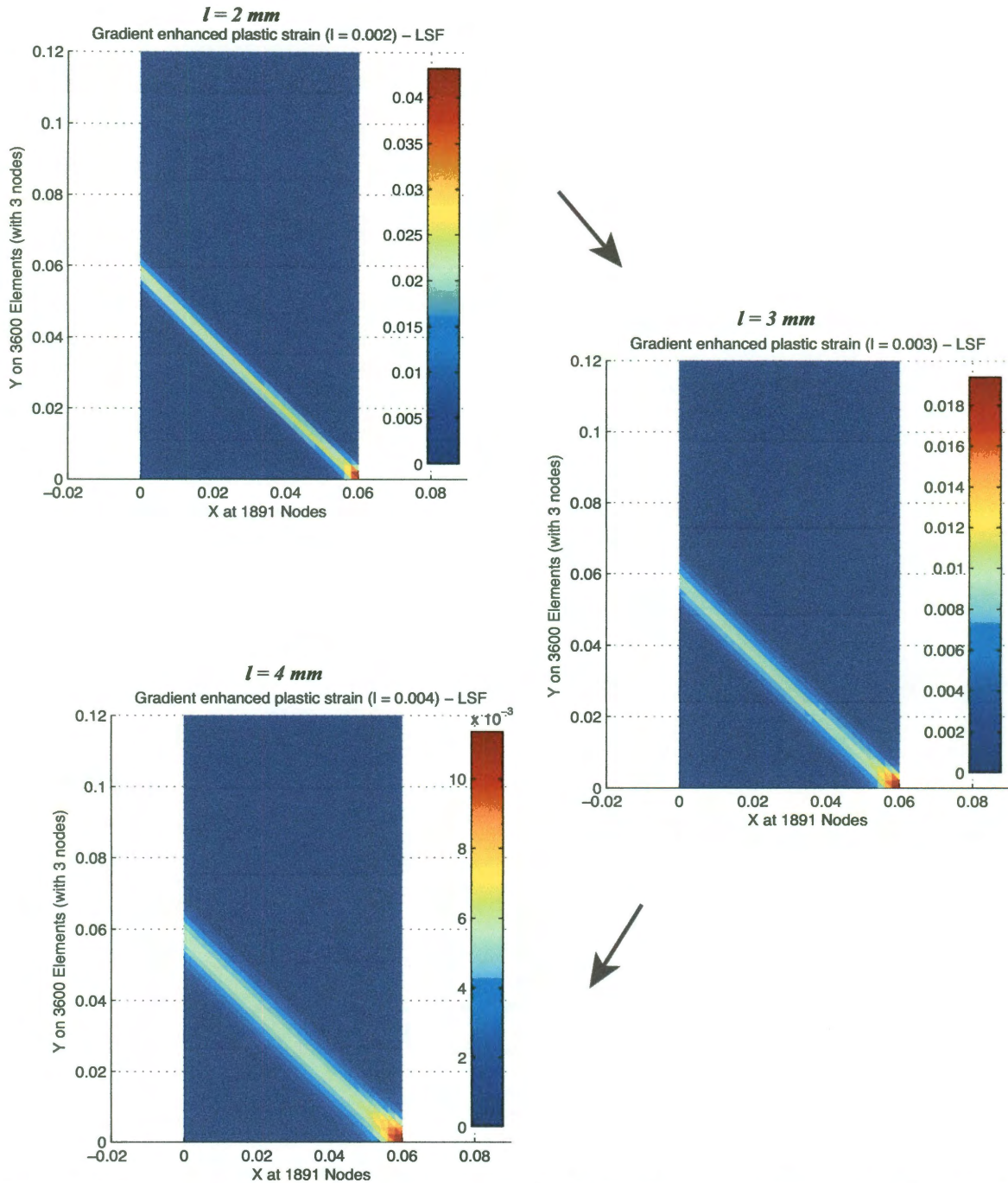

Figure 5.5 Shear bands for different length scales on the fine mesh, recovered by strain gradient least square fit (de Borst's model)
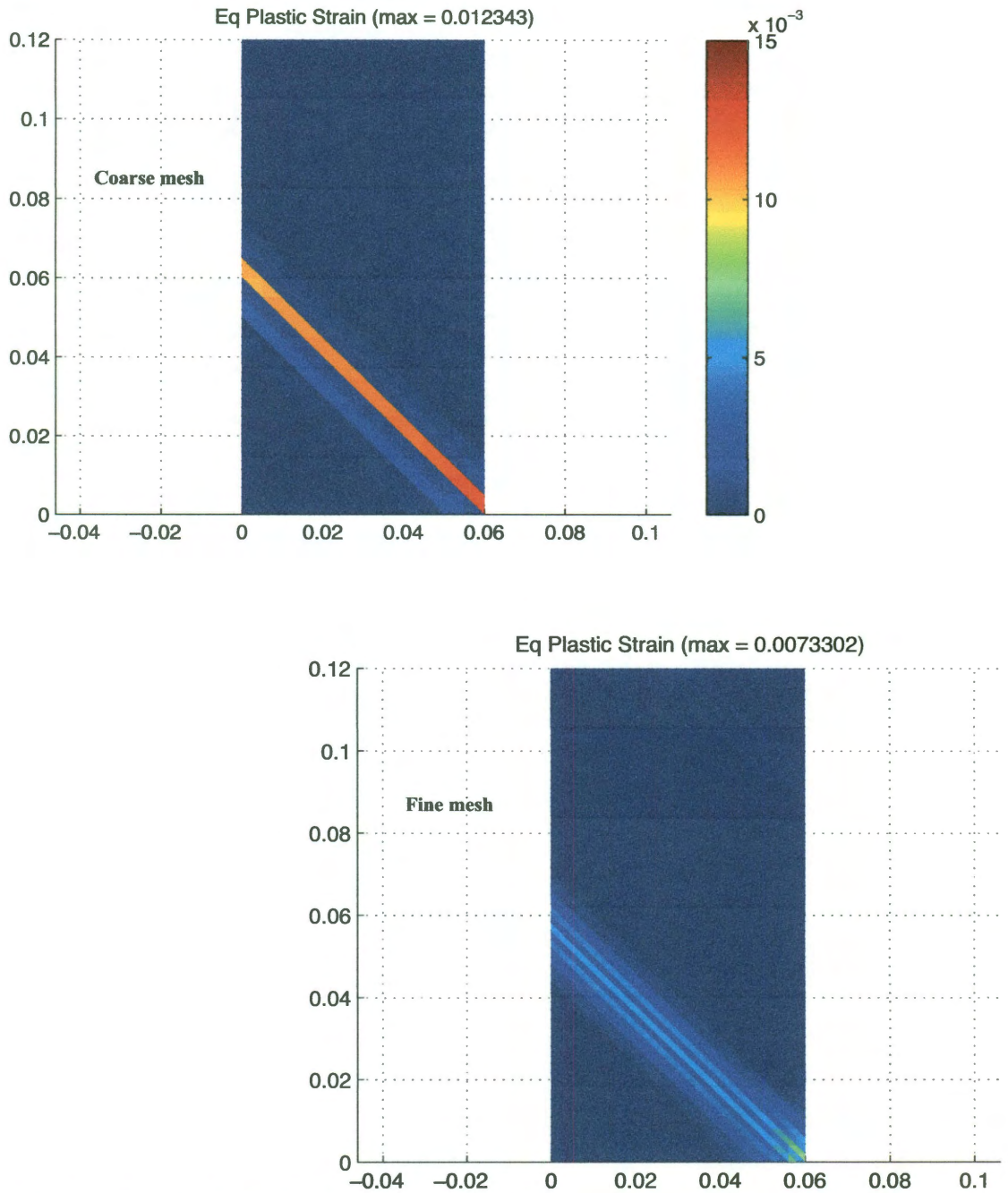
Figure 5.6 Recovered effective plastic strain by nodal averaged method ($l = 5$mm): coarse mesh (upper left) and fine mesh (lower right)

As we saw in the last paragraph, the recovery of the Laplacian of the plastic strain multiplier obtained by direct least square fit outperforms that obtained from the nodal averaging process. Although the shear band bandwidth obtained for both recovery methods is very close for the same length scale used, the nodal averaging process gives a shear band profile that is oscillating. The true second derivatives at a localized area usually change signs, i.e., positive at the edge and negative at the center as shown in Figure 4.16. Therefore, the SCP recovered second derivatives of the plastic strain multiplier should also oscillate around the strain localized zone.

(1) Aifantis' nonlocal model

Next, we will illustrate an enhanced Aifantis' strain gradient model, which also introduces the first derivatives into the yield function. How the introduction of the first derivatives affects the recovery options are evaluated. The equivalent plastic strain contours are plotted in Figure 5.8. The shear band obtained from Aifantis' model is less oscillatory because of the introduction of the first order derivatives. It shows that plastic strain obtained from the nodal averaged recovery of the plastic strain gradients shows less oscillation along the shear band. That is because of the introduction of the norm of the first derivatives of the plastic strain multiplier as in Eq. 5.18. The norm of the first derivatives and the Laplacian of the plastic strain multiplier are plotted in Figure 5.9 for both coarse and fine meshes.
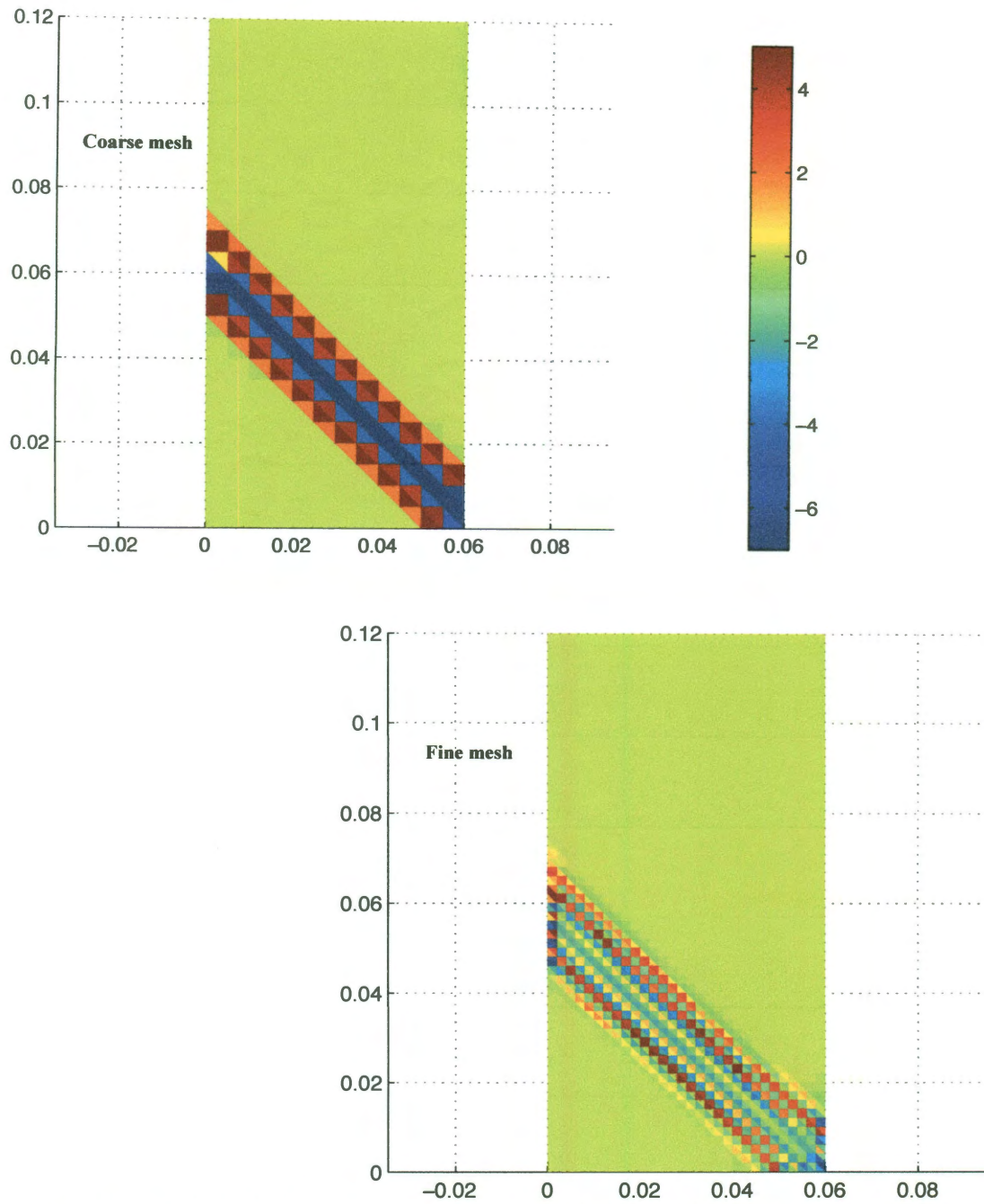
Figure 5.7 Recovered Laplacian of the effective plastic strain ($l = 5$mm): coarse mesh(upper left) and fine mesh (lower right)

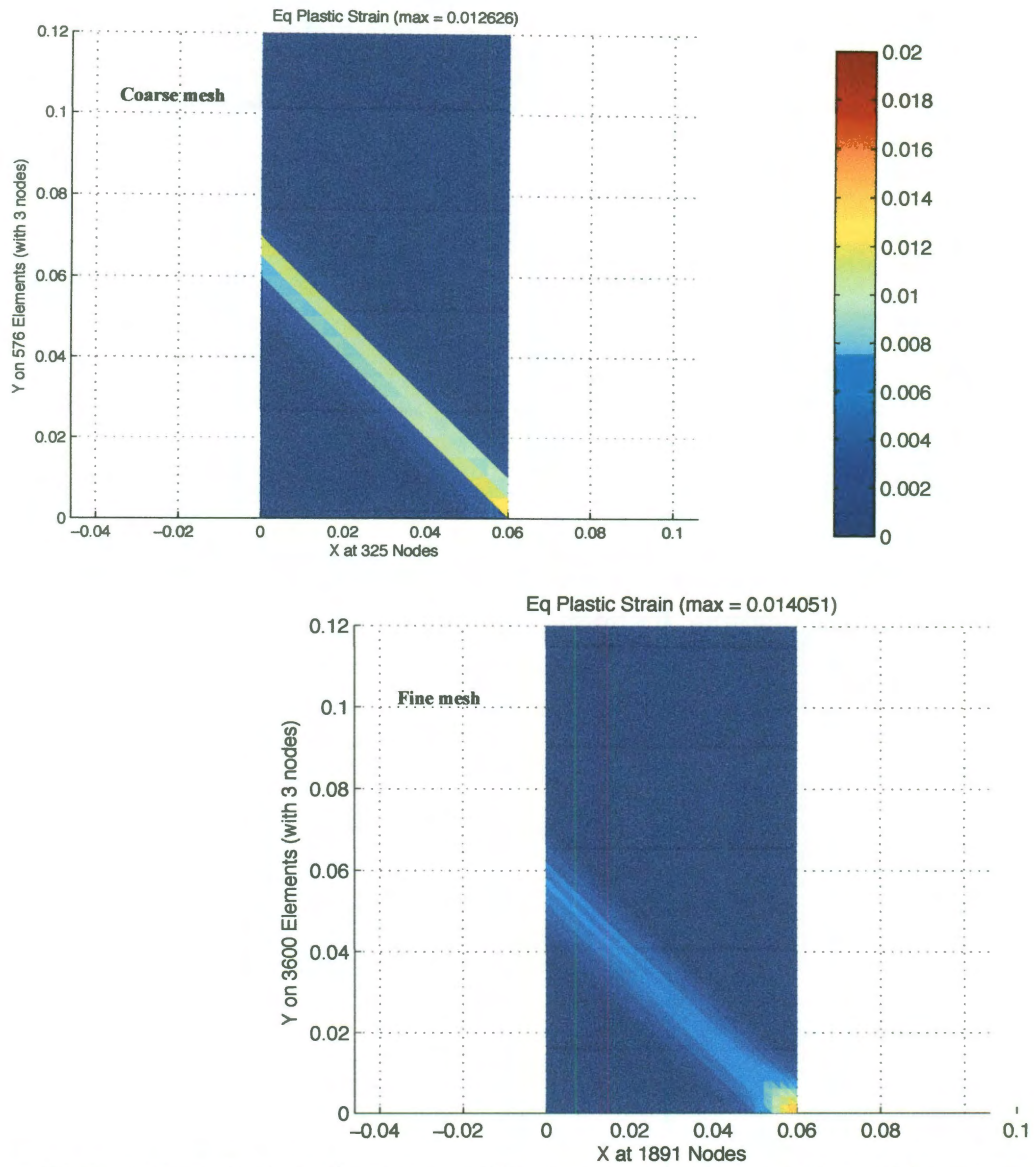**Figure 5.8 Equivalent plastic strain contour (Aifantis' model) by recovered by nodal averages (l = 5mm), coarse mesh (upper left) and fine mesh (lower right)**

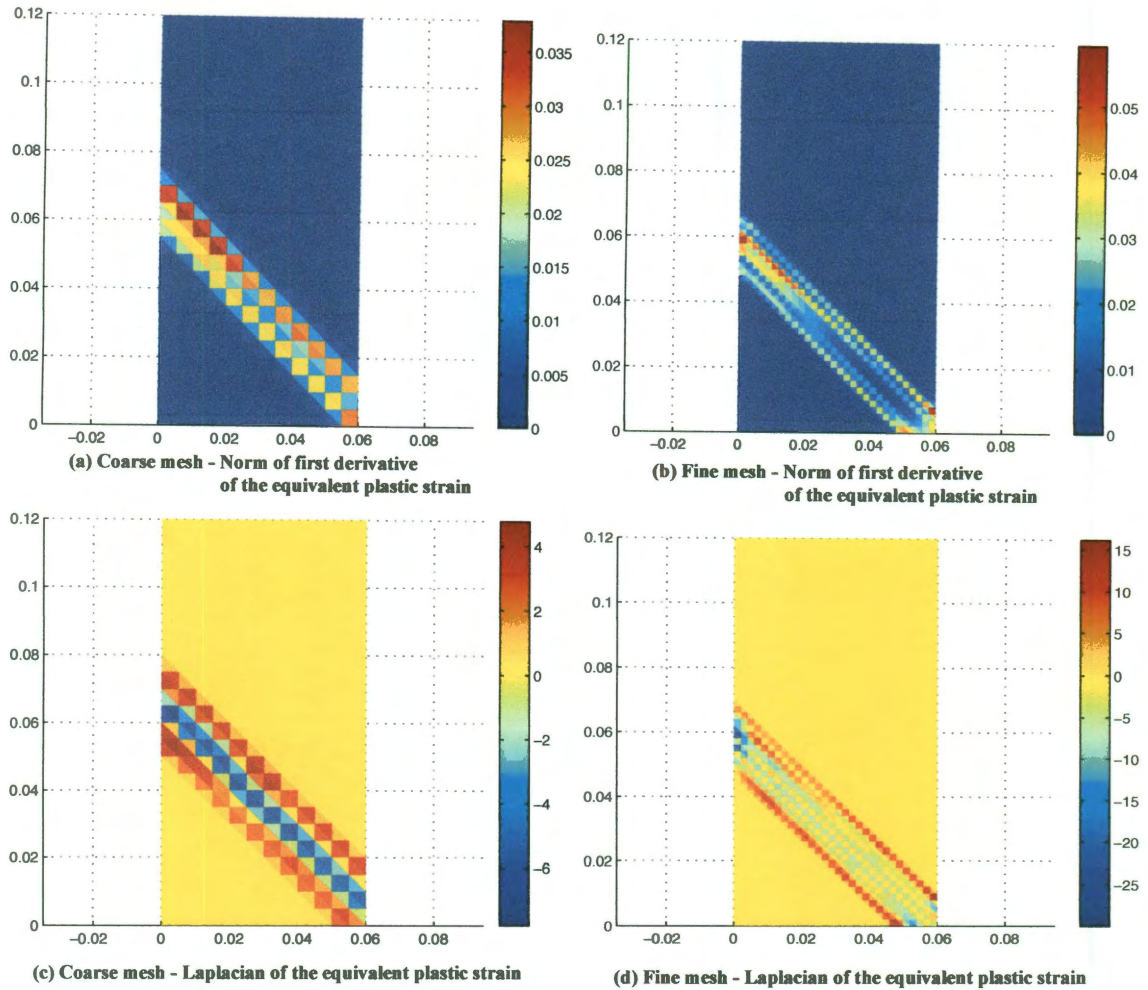(a) Coarse mesh – Norm of first derivative of the equivalent plastic strain

(b) Fine mesh – Norm of first derivative of the equivalent plastic strain

(c) Coarse mesh – Laplacian of the equivalent plastic strain

(d) Fine mesh – Laplacian of the equivalent plastic strain

Figure 5.9 Recovered norm of the first derivative and Laplacian of the equivalent plastic strain

## 5.3.2. Analysis with mixed quadratic C^0 elements

The numerical simulation of the shear band is repeated with the quadratic C^0 elements. Two types of unstructured meshes were created as shown in Figure 5.10. The first mesh contains only T6 elements, while the second mesh consists of a mixture of bi-quadratic Q8 and complete quadratic T6 elements. For Q8 elements, a 9-point quadrature rule is used. For T6 elements, a 4-point quadrature rule is used. The deformed
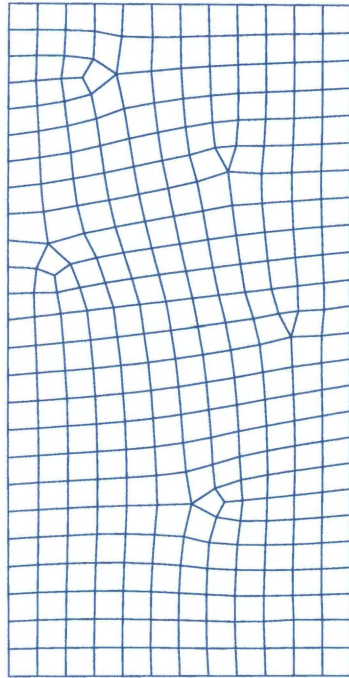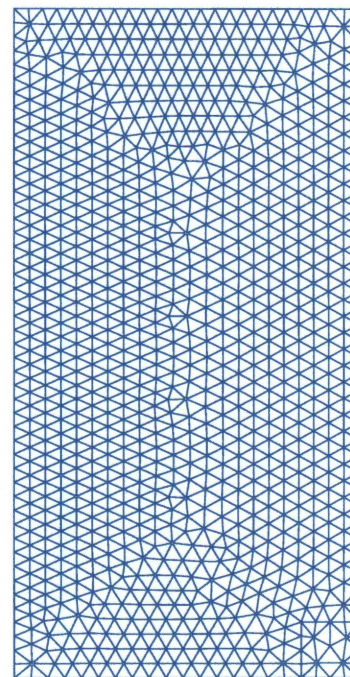
(a) Mixed T6 and Q8 coarse mesh:
297 Elements, 964 Nodes
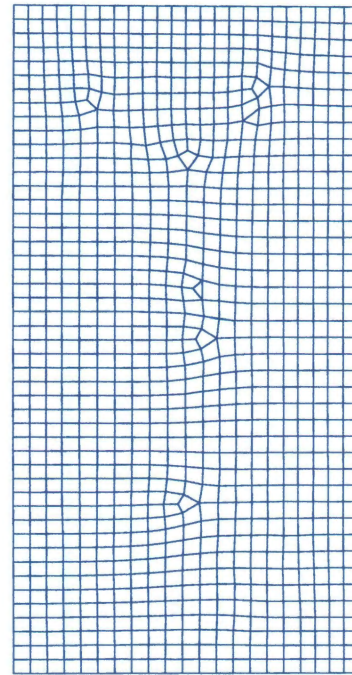
(b) Mixed T6 and Q8 fine mesh:
966 Elements, 3031 Nodes
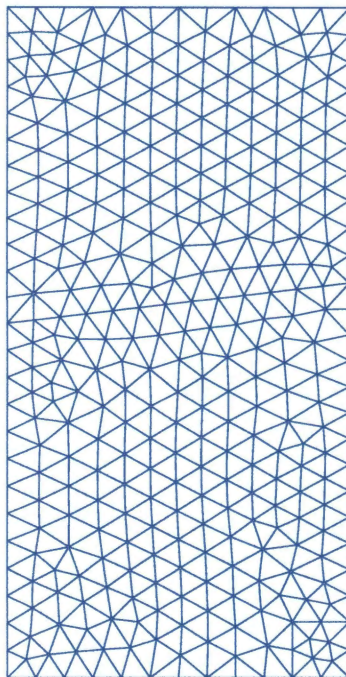
(c) T6 coarse mesh:
630 Elements, 1335 Nodes

(d) T6 fine mesh:
1904 Elements, 3943 Nodes

Figure 5.10 Meshes of quadratic elements

mesh obtained from a local model is plotted in Figure 5.11. With second order elements, the localization of a shear band is shown within a strip of elements initiated from the right bottom corner at an angle of about 45 degrees.
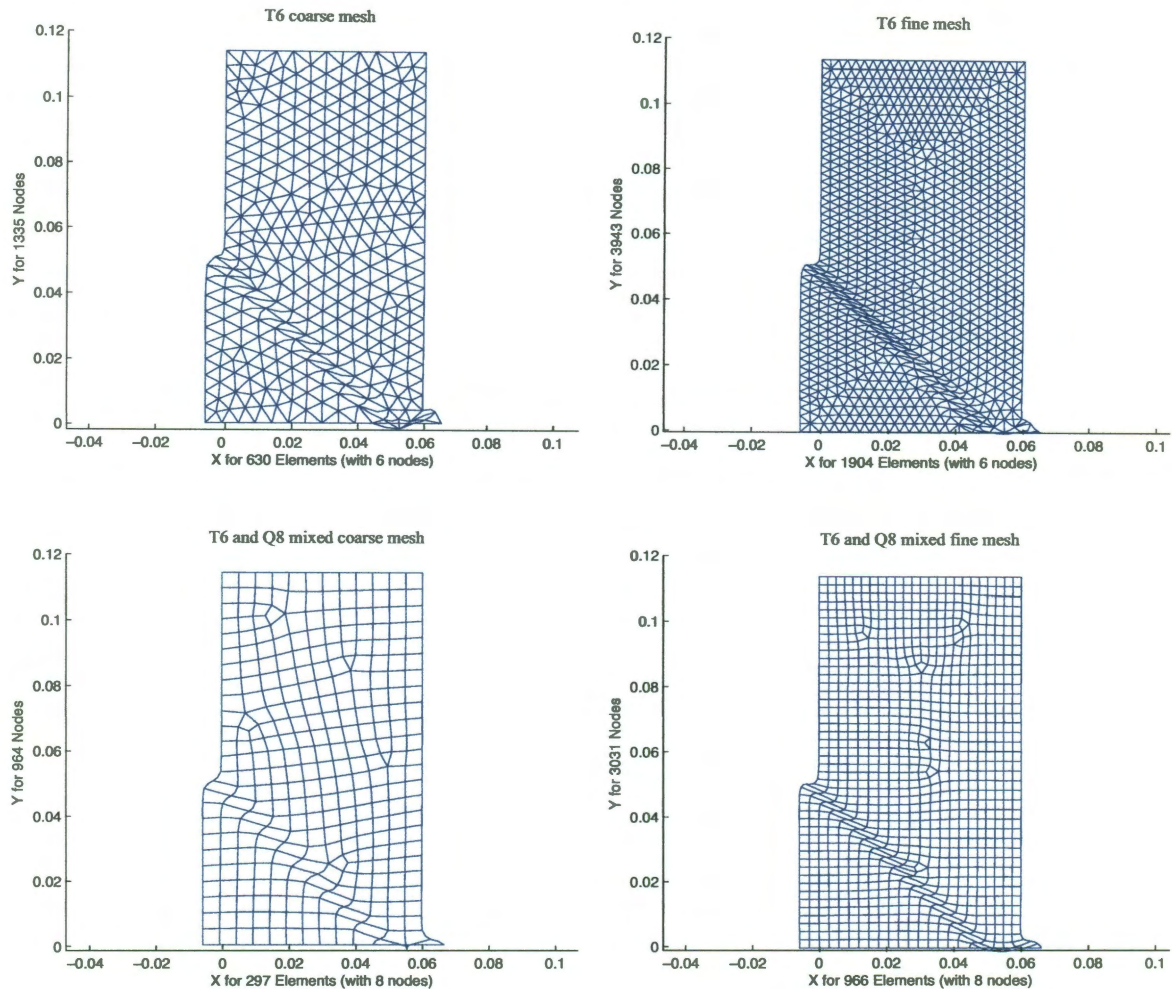

Figure 5.11 Deformed mesh from local model (Exaggerated)

Shear bands are next simulated with strain gradient plasticity models on the quadratic meshes in Figure 5.10. The material length scales used are kept as *5 mm* which is the same as used for linear meshes. De Borst's model is first utilized, the plastic strain contours obtained from their nodal averages are plotted in Figure 5.12. The right bottom corner of each mesh is where the shear band initiates. Therefore, those areas have the

most distorted elements where the maximum plastic strain occurs. Except in those areas, the plastic strain obtained from different meshes has very similar values and the bandwidth of different shear bands obtained are quite uniform. No oscillating behavior of the shear bands, as shown for linear element results (Figure 5.6), is observed in this case.

The Aifantis' model is also studied on the four meshes shown earlier in Figure 5.10. The plastic strain contours obtained from their nodal averages are displayed in Figure 5.13. Because of the norm of the first derivatives of the plastic strain is introduced in this method, the shear bands obtained are more constant than those from the de Borst model shown in Figure 5.12. Again, no oscillating shear band profiles are observed from the results.

The de Borst's and Aifantis' models are then repeated with the LSF recovery methods. The resultant plastic strain contours are plotted in Figure 5.14 and Figure 5.15, respectively. The bandwidth and the magnitudes of the shear bands obtained are very close to those obtained from the nodal averages option. Figure 5.14 shows a bandwidth difference within *22%* and an averaged plastic strain magnitude around *0.0030*. Figure 5.15 shows a bandwidth difference within *12%* and an averaged plastic strain magnitude around *0.0035*. The magnitude is measured at the center of the shear band except the lower right corner.

Next, the norm of the first derivatives and the Laplacian of the equivalent plastic strain obtained from the nodal averages are plotted in Figure 5.16 and Figure 5.17, respectively. For coarse meshes, the norm of the first derivatives recovered is more smooth than those recovered by the fine meshes. The Laplacian values also show the same behavior.
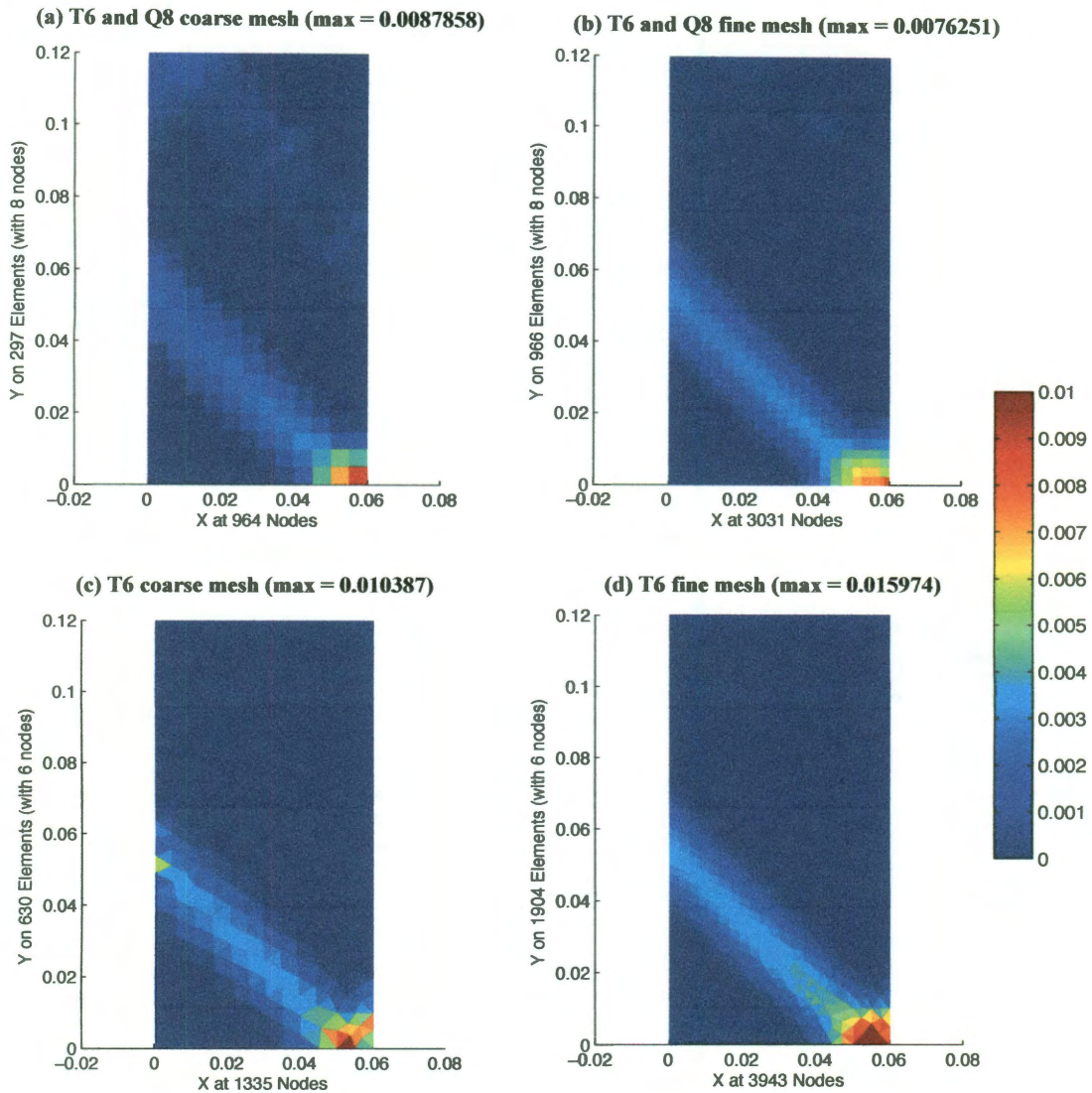
Figure 5.12 Plastic strain contour (l = 5mm), de Borst's model – Recovered by nodal averages

(a) T6 and Q8 coarse mesh (max = 0.010834)

(b) T6 and Q8 fine mesh (max = 0.011099)

(c) T6 coarse mesh (max = 0.020041)

(d) T6 fine mesh (max = 0.024822)
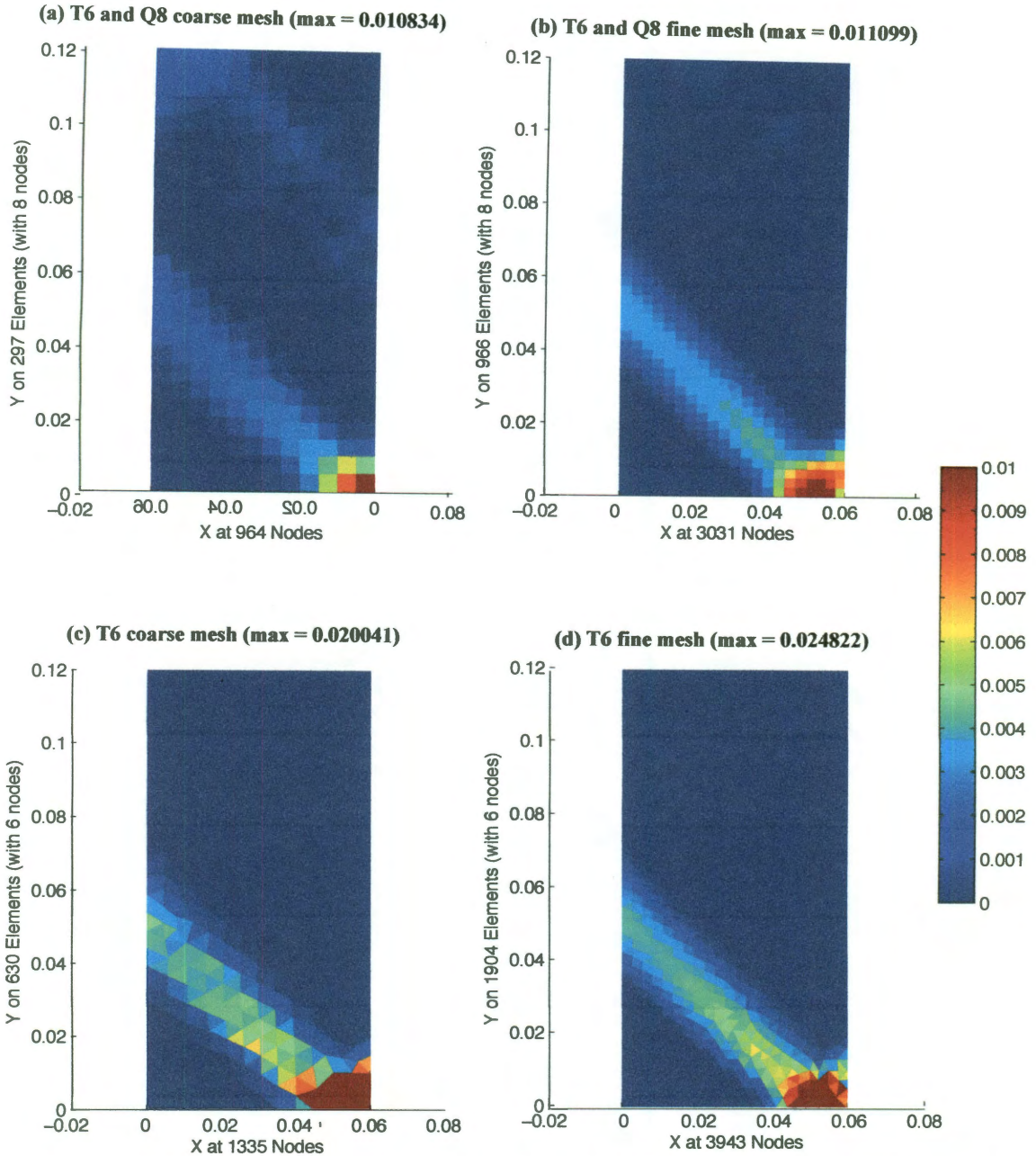
Figure 5.13 Plastic strain contour ($l = 5$mm), Aifantis' model – Recovered by nodal averages

(a) T6 and Q8 coase mesh (max = 0.0086873)

(b) T6 and Q8 fine mesh (max = 0.0079562)

(c) T6 coarse mesh (max = 0.011337)

(d) T6 fine mesh (max = 0.0073581)

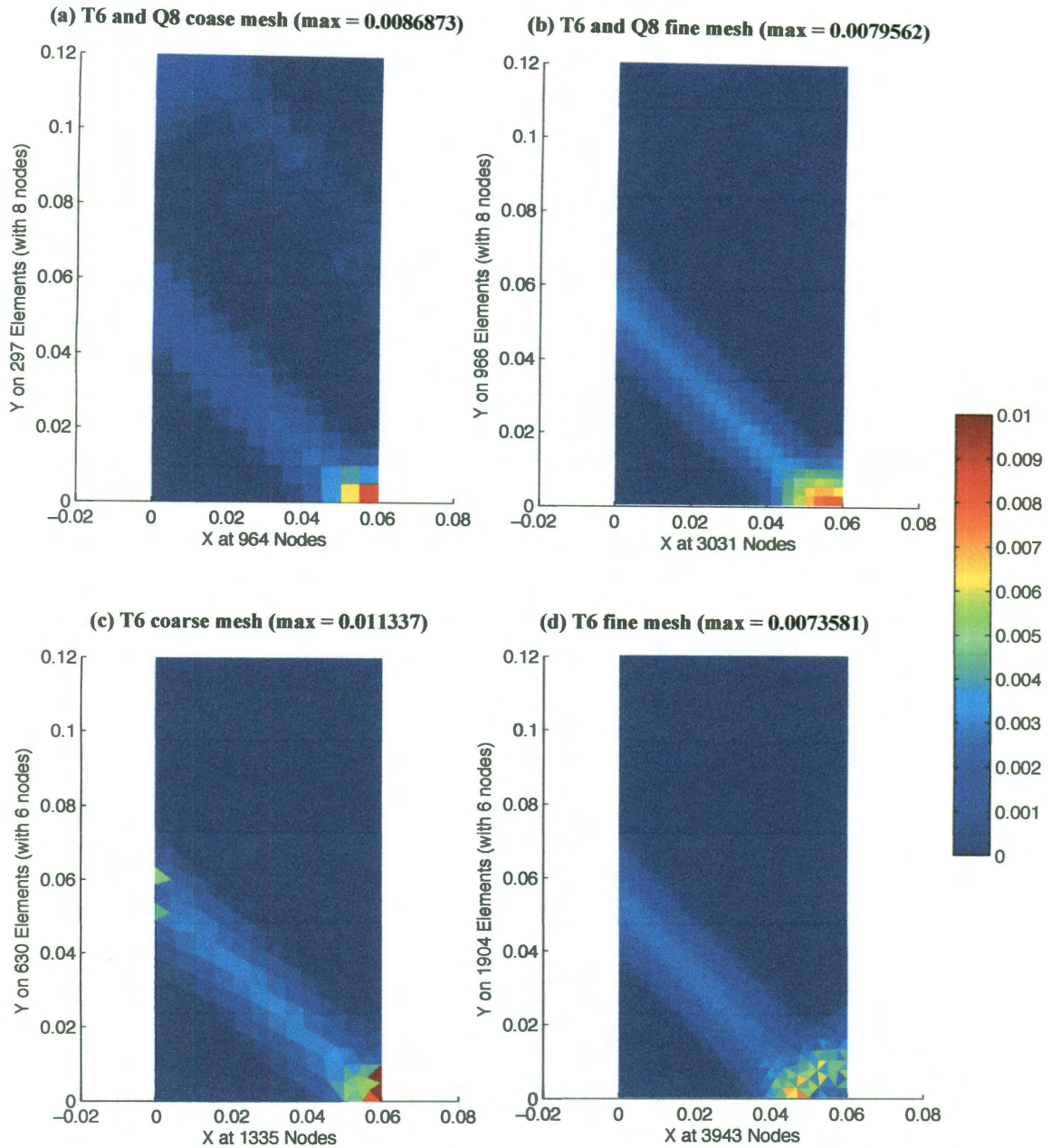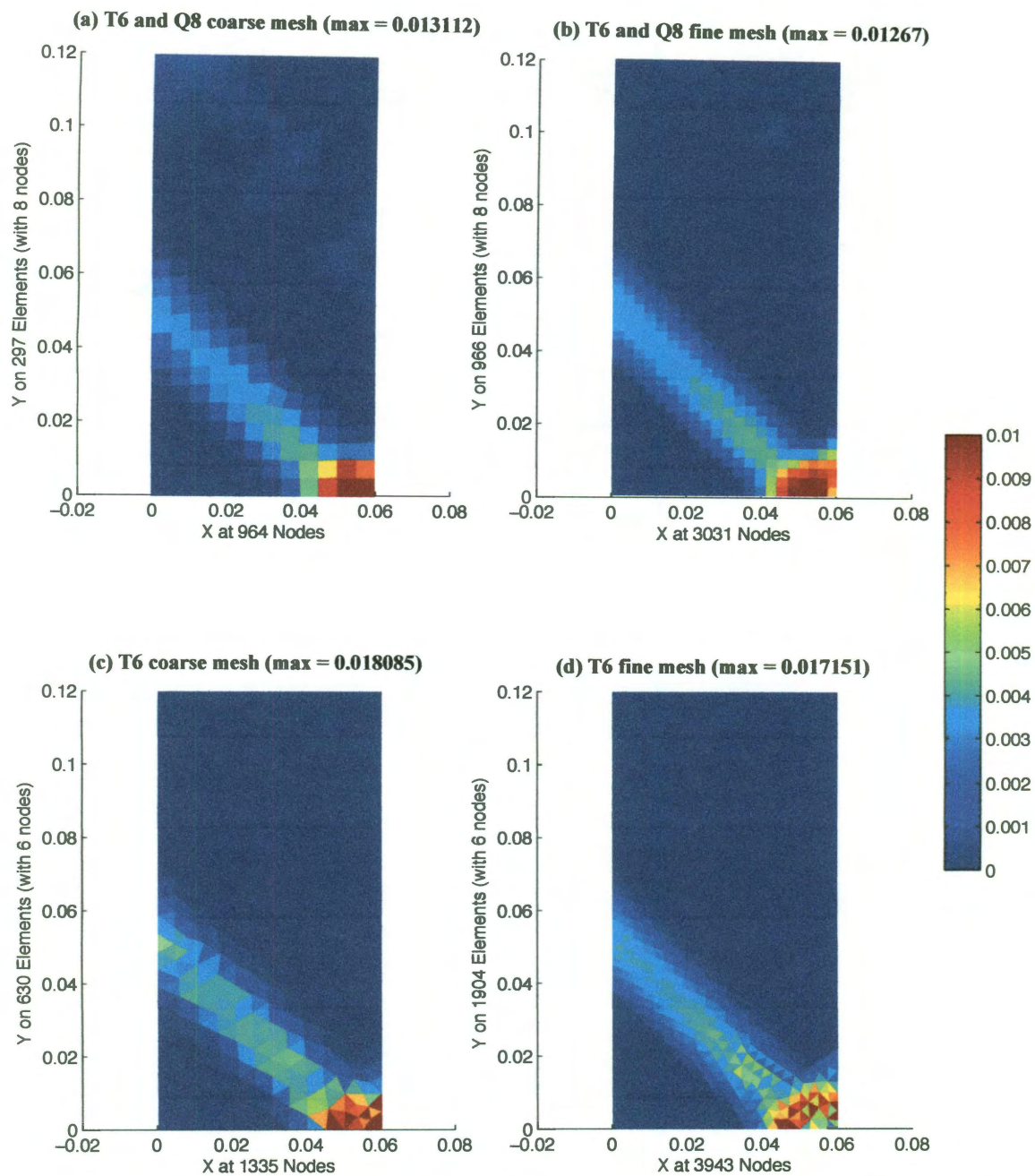**Figure 5.14 Plastic strain contour ($l = $ 5mm), de Borst method - Recovered by LSF method**

Figure 5.15 Plastic strain contour (l = 5mm), Aifantis' model – Recovered by LSF method
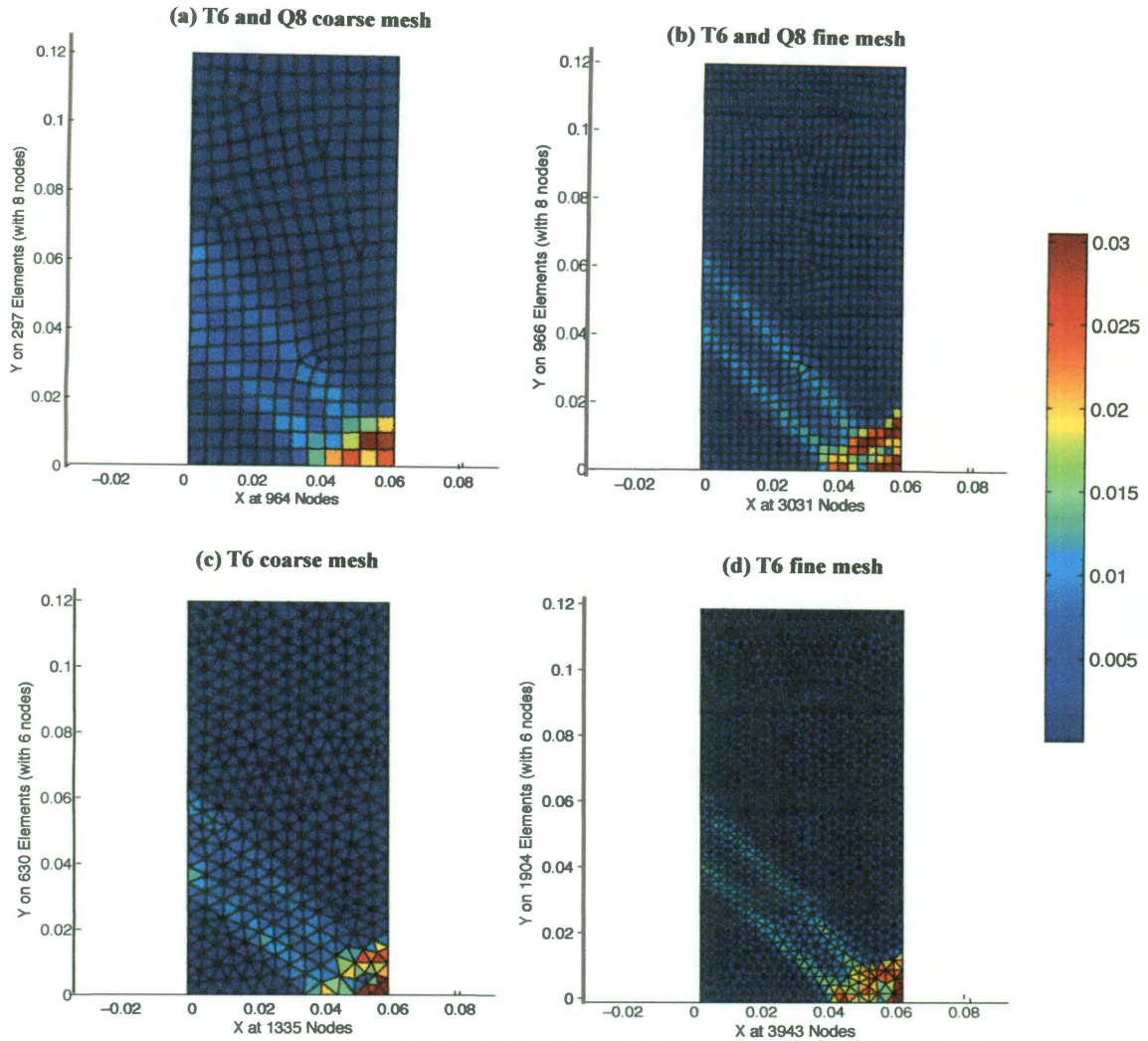
Figure 5.16 Norm of the first derivative of plastic strain

5.4. Discussion

The shear band simulation was conducted as a two-dimensional plain strain problem. Simulations have been conducted utilizing linear triangular T3 elements, quadratic triangular T6 elements, and bi-quadratic Q8 and triangular T6 elements. The Laplacian of the equivalent plastic strain recovered through nodal averages shows the expected oscillating behavior around the shear band area while those recovered through LSF methods do not.
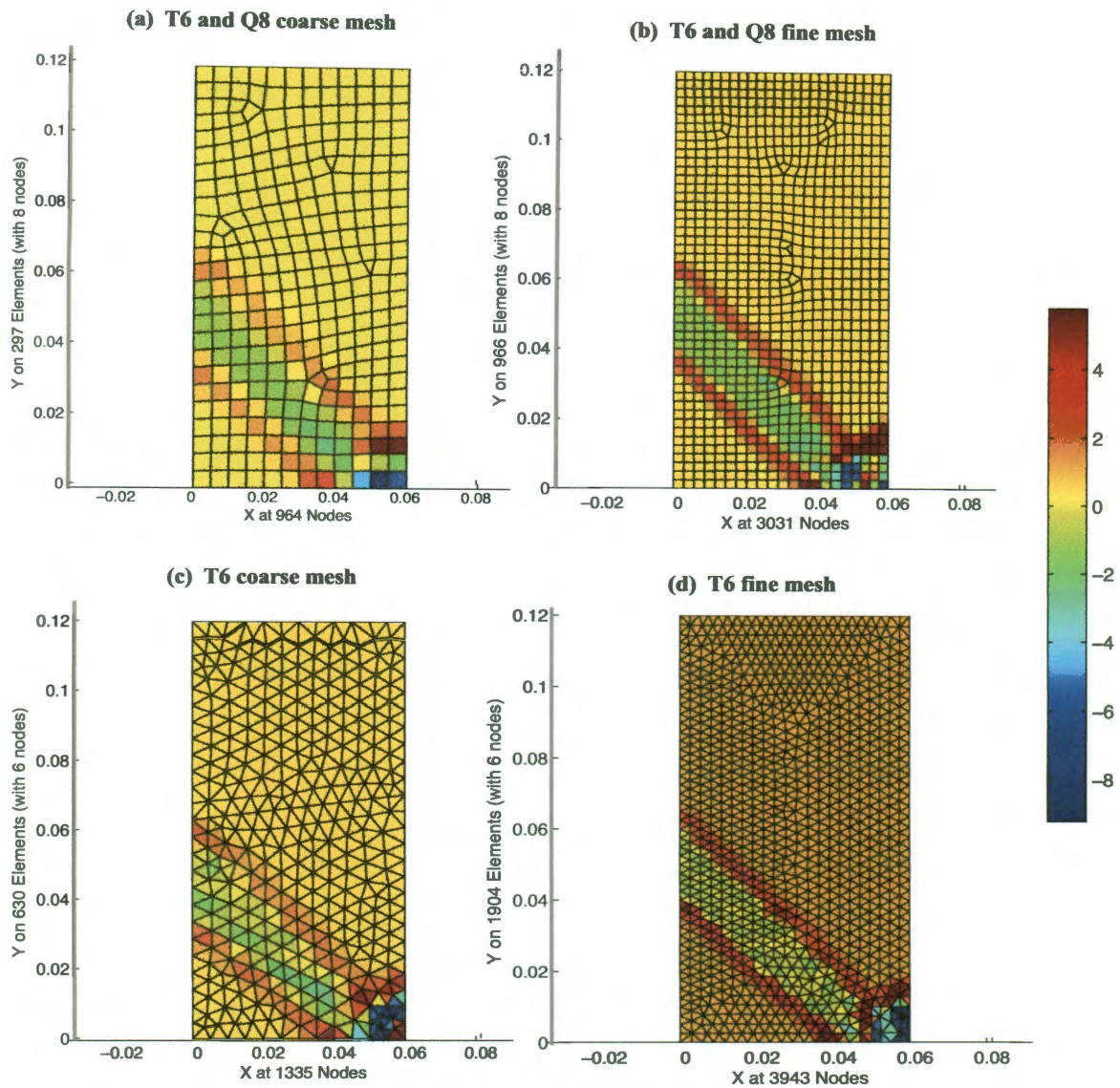
Figure 5.17 Laplacian of the plastic strain contour

For simulations using quadratic elements, the meshes were constructed in an unstructured way. Shear bands are successfully initiated and propagate properly. The LSF recovery method gives better shear band results as compared to the nodal averaged recovery method with regard to the elimination of the inappropriately initiated shear bands for

coarser meshes. To sum up, the strain gradient plasticity problems are simulated through the proposed nonlocal finite element approach. The shear bands recovered reflect the effects of the introduced length scale.

Chapter 6

Conclusions

This dissertation developed a nonlocal finite element technique based on the superconvergent patch recovery methods for second derivatives. The technique enables the recovery of the second derivative of the equivalent strain with the unstructured mesh only of C^0 elements. The idea of the element based patches is utilized for the recovery of the first and second derivatives (Laplacian) of the equivalent strain. A local least square fit process for the equivalent strain is conducted for each patch to recover a smoothed continuous field of the equivalent strain. Then the derivatives are recovered from the patch smoothed equivalent strain by two options. The first choice is to recover at the element nodes in the patch and is later averaged at each element node, named as the nodal averages recovery. The other choice is to recover the derivatives at the integration points of the parent element in each patch, named as the least square fits (LSF) recovery. Both recovery choices are tested and the results are compared.

Numerical simulations have been conducted on two famous nonlocal continuum mechanics problems. One is the nonlocal damage mechanics and the other is the strain gradient plasticity. The results show the efficiency and robustness of the newly developed finite element technique. The results are mesh independent and controllable with the length scales.

For the nonlocal damage mechanics, a three point beam bending test is simulated with linear quadrilateral C^0 elements. The resultant loading-displacement curves show a good match to both the experimental results and Jirasek's numerical results obtained from the integral type formula.

For the strain gradient plasticity problem, a benchmark shear band test is simulated based on two strain gradient theories. An extensive study on various mesh combinations of the C^0 elements is conducted for this example. For linear C^0 elements, the recovered nonlocal strain show oscillated behavior at the localized areas from the nodal averages recovery, however the oscillated behavior is not shown in LSF recovered results. For quadratic elements, the oscillated shear bands are not shown. For Aifantis' gradient enhanced plasticity model, the strain derivatives recovered from a direct least square fitted plastic strains at the integration points within the patch is more reliable than those recovered from the mesh nodal averages in terms of eliminating inappropriate initiation of the shear bands.

The numerical implementation of the nonlocal continuum mechanics is still an intriguing

topic. Following the work done in this thesis, future work may include extending the current two-dimensional cases to three-dimensional problems. The MODEL library already includes solid elements in the error estimator and second derivative recovery. Only the material constitutive law in the nonlocal mechanics and plasticity would need to be expanded to include additional components.

In conclusion, this thesis proposed and implemented a robust nonlocal finite element technique based on the superconvergent patch second derivative recovery methods. Numerical simulations are conducted and the results are discussed and evaluated. Further improvements are also pointed out.

References

[1] Abu Al-Rub R. and Voyiadjis G., 2005, A direct finite element implementation of the gradient-dependent theory, *Int. J. Numer. Meth. Eng.*, 63:603-629

[2] Abu Al-Rub R. and Voyiadjis G., 2006, A physically based gradient plasticity theory, *Int. J. Plasticity*, 22:654-684

[3] Abu Al-Rub R. and Voyiadjis G., 2009, Gradient-enhanced Coupled Plasticity-anisotropic damage model for concrete fracture: computational aspects and applications, *Int. J. Damage Mech.*, 18:115-154

[4] Addessi D., Marfia S., Sacco E., 2002, A plastic nonlocal damage model, *Comput. Methods Appl. Mech. Engrg.* 191:1291-1310

[5] Addessi D. and Ciampi V., 2006, A regularized force-based beam element with a damage-plastic section constitutive law, *Int. J. Numer. Meth. Eng.*, 70(5):610-629

[6] Aifantis E., 1984, On the microstructural origin of certain inelastic models, *J. Eng. Mater. Tech.*, 106:326-330

[7] Akin J. 2005, Finite element analysis with error estimators, Elsevier Butterworth-Heinemann, Burlington, MA, USA, ISBN-0750667222

[8] Askes H. and Sluys L., 2002, Explicit and implicit gradient series in damage mechanics, *Eur. J. Mech. A/Solids*, 21:379-390

[9] Askes H. and Aifantis E., 2002, Numerical modeling of size effects with gradient elasticity-formulation, meshless discretization and examples, *Int. J. Fracture*, 117:347-358

[10]   Bazant Z. and Chang T., 1987, Nonlocal finite element analysis of strain-softening solids, *J. Eng. Mech.*, 113:89-105

[11]   Bazant Z. and Lin F., 1988, Non-local yield limit degradation, *Int. J. Numer. Meth. Eng.*, 26:1805-1823

[12]   Bazant P. and Jirasek M., 2002, Nonlocal Integral Formulations of Plasticity and Damage: Survey of Progress, *J. Eng. Mech.*, 128(11):1119 – 1149

[13]   Begley M., Hutchinson J., 1998, The mechanics of size-dependent indentation, *J. Mech. Phys. Solids*, 46(10):2049-2068

[14]   Belytschko T. and Lasry D., 1989, A study of localization limiters for strain-softening in statics and dynamics, *Comput. Struct.*, 33(3):707-715

[15]   Belnoue J., Garnham B., Bache M., Korsunsky A., 2010, The use of coupled nonlocal damage-plasticity to predict crack growth in ductile metal plates, *Eng. Fract. Mech.*, in press

[16]   Bui Q., 2010, Initiation of damage with implicit gradient-enhanced damage models, *Int. J. Solids Struct.*, 47:2425-2435

[17]   Cesar de Sa J., Areias P., Zheng C., 2005, Damage modelling in metal forming problems using an implicit non-local gradient model, *Comput. Methods Appl. Mech. Engrg.* 195:6646-6660

[18]   Comi C. and Perego U., 2004, Criteria for mesh refinement in nonlocal damage finite element analyses, *Eur. J. Mech. A/Solids*, 23:615-632

[19]   De Borst R., 1992, Gradient-dependent plasticity: formulation and algorithmic aspects, *Int. J. Numer. Meth. Eng.*, 35:521-539

[20]   De Borst R. and Pamin J., 1996, Some novel developments in finite element procedures for gradient-dependent plasticity, *Int. J. Numer. Meth. Eng.*, 39:2477-2505

[21]   De Borst R. 2001, Some recent issues in computational failure mechanics, *Int. J. Numer. Meth. Eng.*, 52:63-95

[22]   De Vree J., Brekelmans W., van Gils M., 1995, Comparison of nonlocal approaches in continuum damage mechanics, *Comput. Struct.*, 55(4): 581-588

[23]   D'hers S. and Dvorkin E., 2011, On the modeling of shear bands formulation in J_2 materials with damage evolution, *Eng. Computation*, 28(2):130-153

[24]   Dorgan R. and Voyiadjis G., 2006, A mixed finite element implementation of a gradient-enhanced coupled damage-plasticity model, *Int. J. Damage Mech.*, 15:201-235

[25]   Dorgan R. 2006, A nonlocal model for coupled damage-plasticity incorporating gradients of internal state variables at multiscales, PhD dissertation, LSU

[26]   Engelen R., Geers M. and Baaijens F., 2003, Nonlocal implicit gradient-enhanced elasto-plasticity for the modelling of softening behaviour, *Int. J. Plasticity*, 19:403-433

[27]   Eringen A. and Edelen D., 1972, On nonlocal elasticity, *Int. J. Engng. Sci.*, 10:233-248

[28]   Eringen A. and Suhubi E., 1964a, Nonlinear theory of simple micro-elastic solids-I, *Int. J. Eng. Sci.*, 2(2):189-203

[29]   Eringen A. and Suhubi E., 1964b, Nonlinear theory of micro-elastic solids-II, *Int. J. Eng. Sci.*, 2(4):389-404

[30]   Gao H. and Huang Y., 2001, Taylor-based nonlocal theory of plasticity, *Int. J. Solids. Struct.*, 38:2615-2637

[31]   Gao H., Huang Y., Nix W., Hutchinson J., 1999, Mechanism-based strain gradient plasticity – I. theory, *J. Mech. Phys. Solids*, 47:1239-1263

[32]   Geers M., 2004, Finite strain logarithmic hyperelasto-plasticity with softening: a strongly non-local implicit gradient framework, *Comput. Methods Appl. Mech. Engrg.*, 193:3377-3401

[33]   Grassl P. and Jirasek M., 2006, Plastic model with non-local damage applied to concrete, *Int. J. Numer. Anal. Meth. Geomech.*, 30:71-90

[34]   Grassl P. and Jirasek M., 2006, Damage-plastic model for concrete failure, *Int. J. Solids Struct.*, 43:7166-7196

[35]   Gurtin M., 2002, A gradient theory of single-crystal viscoplasticity that accounts for geometrically necessary dislocations, *J. Mech. Phys. Solids*, 50:5-32

[36]   Gurtin M. and Anand L., 2005a, A theory of strain-gradient plasticity for isotropic, plastically irrotational materials. Part I: small deformations, *J. Mech. Phys. Solids*, 53:1624-1649

[37]   Gurtin M. and Anand L., 2005b, A theory of strain-gradient plasticity for isotropic, plastically irrotational materials. Part II: finite deformations, *Int. J. Plasticity*, 21:2297-2318

[38]   Han C., Ma A., Roters F. and Raabe D., 2007, A finite element approach with patch projection for strain gradient plasticity formulations, *Int. J. Plasticity*, 23:690-710

[39]   Huang Y., Gao H., Nix W., Hutchinson J., 2000, Mechanism-based strain gradient plasticity – II. analysis, *J. Mech. Phys. Solids*, 48:99-128

[40]   Jefferson C., 2001, Superconvergent second derivative recovery methods, MS thesis, Rice University, Houston, TX

[41]   Jirasek M. and Marfia S., 2005, Non-local damage model based on displacement averaging, *Int. J. Numer. Meth. Eng.*, 63:77-102

[42]   Jirasek M., 2007, Nonlocal damage mechanics, *Revue Europeenne de Genie Civil*, 11:993-1021

[43]   Jirasek M. and Grassl P., 2008, Evaluation of directional mesh bias in

concrete fracture simulations using continuum damage models, *Eng. Fract. Mech.*, 75:1921-1943

[44]   Jirasek M. and Rolshoven S., 2009a, Localization properties of strain-softening gradient plasticity models, Part I: Strain-gradient theories, *Int. J. Solids Struct.*, 46:2225-2238

[45]   Jirasek M. and Rolshoven S., 2009b, Localization properties of strain-softening gradient plasticity models, Part II: Theories with gradients of internal variables, *Int. J. Solids Struct.*, 46:2225-2238

[46]   Larsy D. and Belytschko T., 1988, Localization limiters in transient problems, *Int. J. Solids Struct.*, 24(6):581-597

[47]   Lloyd D., 1994, Particle reinforced aluminium and magnesium matrix composites, *Int. Mater. Rev.*, 39(1):1-23

[48]   Lou J., Shrotriya P., Allameh S., Buchheit T., Soboyejo W., 2006, Strain gradient plasticity length scale parameters for LIGA Ni MEMS thin films, *Mater. Sci. Eng. A-Struct.*, 441:299-307

[49]   Luzio G. and Bazant Z., 2005, Spectral analysis of localization in nonlocal and over-nonlocal materials with softening plasticity or damage, *Int. J. Solids Struct.*, 42:6071-6100

[50]   Mazar J., 1984, Application de la mécanique de l'endommagement au comportement non linearire et à la rupture du béton de structure, Thesis de Doctorate d'Etat, L.M.T – University Paris, 6, France, PhD Dissertation in French.

[51]   Mediavilla J., Peerlings R., Geers M., 2006, A nonlocal triaxiality-dependent ductile damage model for finite strain plasticity, *Comput. Methods Appl. Mech. Engrg.*, 195:4617-4634

[52]   Mindlin R., 1964, Micro-structures in linear elasticity, *Arch. Ration. Mech. Analysis*, 16(1):51-78

[53]   Needleman A., 1988, Material rate dependence and mesh sensitivity in localization problems, *Comput. Method. Appl. M.*, 67:69-85

[54]   Pamin J., 2005, Gradient plasticity and damage models: a short comparison, *Comp. Mater. Sci.*, 32:472-479

[55]   Pamin J., 1994, Gradient dependent plasticity in numerical simulation of localization phenomena, PhD dissertation, Delft University

[56]   Pamin J., Askes H. and de Borst R., 2003, Two gradient plasticity theories discretized with the element-free Galerkin method, *Comput. Methods Appl. Mech. Engrg.*, 192:2377-2403

[57]   Pan X. and Yuan H., 2009, Nonlocal damage modelling using the element-free Galerkin method in the frame of finite strains, , *Comput. Mater. Sci.*, 46:660-666

[58]   Pan X. and Yuan H., 2010, Computational algorithms and applications of element-free Galerkin methods for nonlocal damage models, *Eng. Fract. Mech.*, 77(14):2640-2653

[59]   Peerlings R., de Borst R., Brekelmans W. and De Vree J., 1996, Gradient enhanced damage for quasi-brittle materials, *Int. J. Numer. Meth. Eng.*, 39: 3391-3403

[60]   Peerlings R., 1999, Enhanced damage modelling for fracture and fatigue, PhD thesis, Technische Universiteit Eindinhoven

[61]   Peerlings R. 2006, On the role of moving elastic-plastic boundaries in strain gradient plasticity, *Modelling Simul. Mater. Sci. Eng.*, 15:S109-120, doi:10.1088/0965-0393/15/1/S10

[62]   Pisano A. Sofi A. and Fuschi P., 2009, Nonlocal integral elasticity: 2D finite element based solutions, *Int. J. Solids Struct.*, 46:3836-3849

[63]   Pijaudier-Cabot G. and Bazant Z., 1987, Nonlocal Damage Theory, *J. Eng.*

Mech., 113(10):1512 - 1533

[64]   Ramaswamy S. and Aravas N., 1998, Finite element implementation of gradient plasticity models Part I: Gradient dependent yield functions, *Comput. Methods Appl. Mech. Engrg.*, 163:11-32

[65]   Ricci S. and Brunig M., 2007, Numerical analysis of nonlocal anisotropic continuum damage, *Int. J. Damage Mech.*, 16:283-299

[66]   Rodriguez-Ferran A. and Huerta A., 2000, Error estimation and adaptivity for nonlocal damage models, *Int. J. Solids Struct.*, 37:7501-7528

[67]   Samal M., Seidenfuss M., Roos E., Dutta B. and Kushwaha H., 2008, Finite element formulation of a new nonlocal damage model, *Finite Elem. Anal. Des.*, 44:358-371

[68]   Simone A., Askes H., Peerlings R. and Sluys L., 2003, Interpolation requirements for implicit gradient-enhanced continuum damage models, *Commun. Numer. Meth. Engng.*, 19:563-572

[69]   Simone A., Askes H. and Sluys L., 2004, Incorrect initiation and propagation of failure in non-local and gradient-enhanced media, *Int. J. Solids Struct.*, 41:351-363

[70]   Stölken J., Evans A., 1998, A microbend test method for measuring the plasticity length scale, *Acta Mater.*, 46(14):5109-5115

[71]   Stromberg L. and Ristinmaa M., 1996, FE-formulation of a nonlocal plasticity theory, *Comput. Methods Appl. Mech. Engrg.*, 136:127-144

[72]   Wiberg N. and Abdulwahab F., 1993, Patch recovery based on superconvergent derivatives and equilibrium, *Int. J. Numer. Meth. Eng.*, 36:2703-2724

[73]   Wiberg N. and Li X., 1994, Superconvergent patch recovery of finite-element solution and a posteriori L2 norm error estimate, *Comm. Numer. Meth. Eng.*,

10:313-320

[74]   Wiberg N., Abdulwahab F. and Ziukas S., 1994, Enhanced Superconvergent Patch Recovery Incorporating Equilibrium and Boundary Conditions, *Int. J. Numer. Meth. Eng.*, 37:3417-3440

[75]   Zervos A., Papanastasiou P., Vardoulakis I., 2001, A finite element displacement formulation for gradient elastoplasticity, *Int. J. Numer. Meth. Eng.*, 50:1369-1388

[76]   Zienkiewicz O. and Zhu J., 1992a, The superconvergent patch recovery (SPR) and adaptive finite element refinement, *Comput. Methods. Appl. Mech. Engrg.*, 101:207-224

[77]   Zienkiewicz O. and Zhu J., 1992b, The superconvergent patch recovery and a posteriori error estimates. part 1: the recovery technique, *Int. J. Numer. Meth. Eng.*, 33: 1331-1364

[78]   Zienkiewicz O. and Zhu J., 1992c, The superconvergent patch recovery and a posteriori error estimates. part 2: error estimates and adaptivity, *Int. J. Numer. Meth. Eng.*, 33: 1365-1384

[79]   Zienkiewicz O., Taylor R. and Zhu J., 2005, The Finite Element Method: Its Basis and Fundamentals, Sixth Edition, Elsevier Butterworth-Heinemann, Burlington, MA, USA, ISBN- 0750663200

[80]   Zhu H., Zbib H., Aifantis E., 1997, Strain gradient and continuum modeling of size effect in metal matrix composites, *Acta Mech.*, 121:165-176